[AMERICAN JOURNAL OF SCIENCE, VOL. 288, JANUARY, 1988, P. 19–98]

CALCULATION OF THE THERMODYNAMIC AND TRANSPORT PROPERTIES OF AQUEOUS SPECIES AT HIGH PRESSURES AND TEMPERATURES: REVISED EQUATIONS OF STATE FOR THE STANDARD PARTIAL MOLAL PROPERTIES OF IONS AND ELECTROLYTES

JOHN C. TANGER IV and HAROLD C. HELGESON
Department of Geology and Geophysics,
University of California, Berkeley, California 94720

ABSTRACT. The Helgeson-Kirkham-Flowers (HKF) model for prediction of the standard partial molal properties of aqueous ions and electrolytes expands considerably the range of pressures and temperatures for which geochemical calculations can be carried out. However, combined empirical and theoretical analysis of experimental volumes, compressibilities, and heat capacities for a wide variety of aqueous electrolytes at temperatures below ~100°C indicates that the structural collapse contributions to the standard partial molal properties of electrolytes in the HKF model should be revised to be consistent with the temperature and pressure dependence of the solvent structure. Similiar analysis of experimental volumes and heat capacities of aqueous electrolytes at high temperatures indicates that the electrostatic solvation contributions to the standard partial molal properties of electrolytes in the HKF model should be modified to provide for the pressure and temperature dependence of the effective electrostatic radii of aqueous ions. The revised equations of state provide substantially improved accuracy in predictions of equilibrium constraints in geochemical processes at high pressures and temperatures.

INTRODUCTION

Accurate calculation of the standard partial molal thermodynamic properties of aqueous ions at high pressures and temperatures is a prerequisite for predicting the consequences of fluid-rock interactions in the Earth's crust. The equations of state developed by Helgeson and Kirkham (1976) and Helgeson, Kirkham, and Flowers (1981), hereinafter referred to as the HKF model, permit prediction of standard partial molal thermodynamic properties of aqueous ions to 600°C and 5 kb. However, comparisons of predicted values of standard partial molal volumes and heat capacities for aqueous electrolytes from the HKF model with corresponding experimental values reveal discrepancies in three specific regions of pressure and temperature.

Considerations of experimental volumes (Hilbert, 1979; Grant-Taylor, 1981; L'vov, Zarembo, and Gilyarov, 1981; Gates, 1985) and heat capacities (Puchkov, Styazhkin, and Fedorov, 1976; Smith-Magowan and Wood, 1981; Gates, 1985) of NaCl, KCl, LiCl, NaBr, $CaCl_2$, and $MgCl_2$ solutions indicates that solvation contributions to standard partial molal volumes and heat capacities predicted from the HKF model

become too large as temperatures and pressures approach the critical point of H_2O. Consideration of experimental volumes of NaCl solutions from Hilbert (1979) and Adams (1931) and experimental volumes of K_2SO_4 solutions from Adams (1932) indicates that at temperatures below ~100°C nonsolvation contributions to standard partial molal volumes predicted from the HKF model become increasingly too large as pressures rise above ~1 kb. Consideration of experimental heat capacities of NaCl, KCl, and NaBr solutions from Tanner and Lamb (1978) indicates that at 1 bar and temperatures below ~15°C nonsolvation contributions to standard partial molal heat capacities predicted from the HKF model are too small.

The purpose of the present study is to revise the HKF model so that more accurate predictions can be made of the standard partial molal thermodynamic properties of aqueous ions and electrolytes for temperatures to 450°C and pressures to 5 kb. Revised equation of state coefficients for 19 aqueous ions of geochemical interest are presented. Procedures for estimating the apparent standard partial molal Gibbs free energies of formation of aqueous ions and electrolytes for temperatures to 1000°C are also discussed.

STANDARD STATE CONVENTIONS AND THE ADDITIVITY PRINCIPLE

The standard state convention for aqueous ions and electrolytes adopted in the present study is one of unit activity of the aqueous solute in a hypothetical one molal solution referenced to infinite dilution at any pressure and temperature. The solvent standard state convention calls for unit activity of the pure solvent at any pressure and temperature. The relation between the absolute standard partial molal thermodynamic properties of the jth aqueous ions ($\bar{\Xi}_j^{\circ\,abs}$) and those of the kth aqueous electrolyte ($\bar{\Xi}_k^{\circ}$) can be expressed as

$$\bar{\Xi}_k^{\circ} = \sum_j \nu_{j,k}\, \bar{\Xi}_j^{\circ\,abs} \tag{1}$$

where $\nu_{j,k}$ represents the stoichiometric number of moles of the jth ion in one mole of the kth electrolyte. Because eq (1) is the basis for the additive relations among the standard partial molal properties of aqueous electrolytes that share common ions, it is commonly referred to as the additivity principle (Millero, 1972) or the additivity rule (Fortier, Leduc, and Desnoyers, 1974).

Conventional standard partial molal properties of the jth ion are defined by

$$\bar{\Xi}_j^{\circ} \equiv \bar{\Xi}_j^{\circ\,abs} - Z_j\, \bar{\Xi}_{H^+}^{\circ\,abs} \tag{2}$$

where $\bar{\Xi}_{H^+}^{\circ\,abs}$ refers to the absolute standard partial molal property of the hydrogen ion, and Z_j represents the charge of the jth aqueous ion. It follows from eqs (1) and (2) together with the requirement of electrical

neutrality of an aqueous electrolyte that $\overline{\Xi}_k^\circ$ is related to $\overline{\Xi}_j^\circ$ by

$$\overline{\Xi}_k^\circ = \sum_j \nu_{j,k} \overline{\Xi}_j^\circ \ . \tag{3}$$

The conventional standard partial molal properties of an aqueous anion (represented by A) are thus equal to the experimental values of $\overline{\Xi}_k^\circ$ for the acid electrolyte $H_{\nu_{H,k}}A$. Eq (3) permits calculation of the conventional standard partial molal properties of an aqueous cation (represented by C) from experimental values of $\overline{\Xi}_k^\circ$ for aqueous electrolytes represented by $H_{\nu_{H,k}}A$ and $C_{\nu_{C,k}}A_{\nu_{A,k}}$.

Although it is theoretically possible to calculate values of $\overline{\Xi}_j^{\circ\,abs}$ for aqueous ions, the equations of state for aqueous ions considered below are restricted to $\overline{\Xi}_j^\circ$. However, this does not impose any restrictions on geochemical calculations, because it follows from eq (2) and the definition of the apparent standard partial molal enthalpies and Gibbs free energies of formation (see below) that prediction of $\overline{\Xi}_j^\circ$ is sufficient for predicting the standard partial molal properties of aqueous ions in chemical reactions.

REVIEW OF THE HKF MODEL

General concepts.—Conceptual development of the HKF model begins with the commonly made assumption that for the jth aqueous ion, $\overline{\Xi}_j^{\circ\,abs}$ can be regarded as the sum of an intrinsic property ($\overline{\Xi}_{i,j}^{\circ\,abs}$) and an electrostriction contribution ($\Delta\overline{\Xi}_{e,j}^{\circ\,abs}$); that is

$$\overline{\Xi}_j^{\circ\,abs} = \overline{\Xi}_{i,j}^{\circ\,abs} + \Delta\overline{\Xi}_{e,j}^{\circ\,abs}. \tag{4}$$

Intrinsic properties are attributed solely to the ion, but the electrostriction contributions arise from ion-solvent interaction. Electrostriction is assumed to be a consequence of the sum of structural collapse ($\Delta\overline{\Xi}_{c,j}^{\circ\,abs}$) and solvation ($\Delta\overline{\Xi}_{s,j}^{\circ\,abs}$) contributions, which can be written as

$$\Delta\overline{\Xi}_{e,j}^{\circ\,abs} = \Delta\overline{\Xi}_{c,j}^{\circ\,abs} + \Delta\overline{\Xi}_{s,j}^{\circ\,abs} \tag{5}$$

Electrostriction collapse accounts for structural changes in the solvent caused by the ion, but electrostriction solvation arises from electrostatic ion-solvent interactions.

The HKF model involves consideration of the combined contribution from intrinsic and collapse terms. As a consequence, it is convenient to define a nonsolvation contribution ($\Delta\overline{\Xi}_{n,j}^{\circ\,abs}$) given by

$$\Delta\overline{\Xi}_{n,j}^{\circ\,abs} \equiv \overline{\Xi}_{i,j}^{\circ\,abs} + \Delta\overline{\Xi}_{c,j}^{\circ\,abs}. \tag{6}$$

Eqs (4) through (6) can be combined to give

$$\overline{\Xi}_j^{\circ\,abs} = \overline{\Xi}_{n,j}^{\circ\,abs} + \Delta\overline{\Xi}_{s,j}^{\circ\,abs}.$$

Eqs (4) through (7) can also be expressed in terms of the conventional standard partial molal properties of aqueous ions represented by $\overline{\Xi}_{i,j}^\circ$, $\Delta\overline{\Xi}_{e,j}^\circ$, $\Delta\overline{\Xi}_{c,j}^\circ$, and $\Delta\overline{\Xi}_{s,j}^\circ$ by first defining these contributions in terms of

equations analogous to eq (2). Consequently, it follows from eqs (1) and (3) through (7) that appropriate analogs of the additivity relations given by eqs (1) and (3) also apply to $\overline{\Xi}^\circ_{i,k}$, $\Delta\overline{\Xi}^\circ_{e,k}$, $\Delta\overline{\Xi}^\circ_{c,k}$, $\Delta\overline{\Xi}^\circ_{s,k}$, and $\Delta\overline{\Xi}^\circ_{n,k}$. The additivity relations for standard partial molal nonsolvation and solvation contributions given by

$$\Delta\overline{\Xi}^\circ_{n,k} = \sum_j \nu_{j,k}\,\Delta\overline{\Xi}^{\circ\,abs}_{n,j} = \sum_j \nu_{j,k}\,\Delta\overline{\Xi}^\circ_{n,j} \tag{8}$$

and

$$\Delta\overline{\Xi}^\circ_{s,k} = \sum_j \nu_{j,k}\,\Delta\overline{\Xi}^{\circ\,abs}_{s,j} = \sum_j \nu_{j,k}\,\Delta\overline{\Xi}^\circ_{s,j} \tag{9}$$

are of particular interest in the following discussion of the HKF model.

Development of the HKF model proceeds from the above conceptual framework by using eqs (1), (7), (8), and (9) to represent the standard partial molal properties of aqueous electrolytes as

$$\overline{\Xi}^\circ_k = \Delta\overline{\Xi}^\circ_{n,k} + \Delta\overline{\Xi}^\circ_{s,k}. \tag{10}$$

The Born equation was used to derive theoretical expressions for $\Delta\overline{\Xi}^\circ_{s,k}$. Regression procedures were used to determine semiempirical expressions for $\Delta\overline{\Xi}^\circ_{n,k}$ as well as a predictive equation for the ion radius term in the Born equation.

Equations for solvation contributions($\Delta\overline{\Xi}^\circ_s$).—The Born equation (Born, 1920) is used to represent the absolute standard partial molal Gibbs free energy of solvation for the jth aqueous ion. The Born equation can be expressed as

$$\Delta\overline{G}^{\circ\,abs}_{s,j} = \omega^{abs}_j = \left(\frac{1}{\epsilon} - 1\right) \tag{11}$$

where ϵ represents the dielectric constant of H_2O and ω^{abs}_j refers to the absolute Born coefficient for the jth aqueous ion, which is defined by

$$\omega^{abs}_j \equiv \frac{N^\circ e^2 Z_j^2}{2r_{e,j}} = \frac{\eta Z_j^2}{r_{e,j}} \tag{12}$$

where η is equal to 1.66027×10^5 Å cal mole^{-1}, N° stands for Avogadro's number, e designates elementary charge (4.80298×10^{-10} cm$^{3/2}$g$^{1/2}$s^{-1}), and Z_j and $r_{e,j}$ correspond to the charge and the effective electrostatic radius of the jth aqueous ion. The conventional analog of eq (11) is given by

$$\Delta\overline{G}^\circ_{s,j} = \omega_j\left(\frac{1}{\epsilon} - 1\right) \tag{13}$$

where the conventional Born coefficient of the jth aqueous ion (ω_j) is defined by

$$\omega_j \equiv \omega^{abs}_j - Z_j\omega^{abs}_{H^+} \tag{14}$$

where $\omega^{abs}_{H^+}$ refers to the absolute Born coefficient of the hydrogen ion. The standard partial molal Gibbs free energy of the kth aqueous electrolyte ($\Delta\overline{G}^{\circ}_{s,k}$) is related to $\Delta\overline{G}^{\circ\,abs}_{s,j}$ and $\Delta\overline{G}^{\circ}_{s,j}$ by eq (9). Consequently, it follows from eqs (11), (12), and (13) that we can write

$$\omega_k = \sum_j \nu_{j,k}\omega^{abs}_j = \sum_j \frac{\nu_{j,k}\,\eta Z_j^2}{r_{e,j}} = \sum_j \nu_{j,k}\,\omega_j \tag{15}$$

which permits $\Delta\overline{G}^{\circ}_{s,k}$ to be expressed as

$$\Delta\overline{G}^{\circ}_{s,k} = \omega_k\left(\frac{1}{\epsilon} - 1\right). \tag{16}$$

Because the effective electrostatic radii of aqueous ions are taken to be independent of temperature and pressure in the HKF model, ω^{abs}_j, ω_j, and ω_k are constants. Note that it follows from eq (15) that expressions for the standard partial molal solvation properties of aqueous ions ($\Delta\overline{\Xi}^{\circ\,abs}_{s,j}$ and $\Delta\overline{\Xi}^{\circ}_{s,j}$) and electrolytes ($\Delta\overline{\Xi}^{\circ}_{s,k}$) derived from $\Delta\overline{G}^{\circ}_{s}$ and eqs (11), (13), and (16) are consistent with the additivity principle represented by eq (9).

It follows from eq (16) that the standard partial molal volume ($\overline{V}^{\circ}$), compressibility ($\overline{\kappa}^{\circ}$), and isobaric heat capacity ($\overline{C}^{\circ}_{P}$) of solvation for the kth aqueous electrolyte can be expressed as

$$\Delta\overline{V}^{\circ}_{s,k} = \left(\frac{\partial\Delta\overline{G}^{\circ}_{s,k}}{\partial P}\right)_T = -\omega_k\,Q, \tag{17}$$

$$-\Delta\overline{\kappa}^{\circ}_{s,k} = \left(\frac{\partial^2\Delta\overline{G}^{\circ}_{s,k}}{\partial P^2}\right)_T = -\omega_k\,N, \tag{18}$$

and

$$\Delta\overline{C}^{\circ}_{Ps,k} = -T\left(\frac{\partial^2\Delta\overline{G}^{\circ}_{s,k}}{\partial T^2}\right)_P = \omega_k\,TX \tag{19}$$

where Q, N, and X denote Born functions defined by eqs (D-2), (D-3), and (D-4) in app. D, P stands for pressure in bars, and T stands for temperature in kelvins. Expressions analogous to eqs (17), (18), and (19) for $\Delta\overline{V}^{\circ\,abs}_{s,j}$, $\Delta\overline{V}^{\circ}_{s,j}$, $-\Delta\overline{\kappa}^{\circ\,abs}_{s,j}$, $-\Delta\overline{\kappa}^{\circ}_{s,j}$, $\Delta\overline{C}^{\circ\,abs}_{Ps,j}$, and $\Delta\overline{C}^{\circ}_{Ps,j}$ of the jth aqueous ion can be derived from eqs (11) and (13). Regression analysis of experimental values of $\overline{V}^{\circ}_{k}$, $-\overline{\kappa}^{\circ}_{k}$ and $\overline{C}^{\circ}_{Pk}$ for a wide variety of aqueous electrolytes at pressures close to vapor-liquid saturation for H_2O and temperatures from 0° to 200°C was used to determine semiempirical expressions in the HKF model for $\Delta\overline{V}^{\circ}_{n,k}$, $-\overline{\kappa}^{\circ}_{n,k}$, and $\Delta\overline{C}^{\circ}_{P,n,k}$, as well as values for ω_k in eqs (17) through (19). Subsequently, the regression values of ω_k were fit to eq (15) using

$$r_{e,j} = r_{x,j} + |Z_j|\,\Gamma_Z \tag{20}$$

where $r_{x,j}$ stands for the crystallographic radius of the jth aqueous ion in angstroms (see caption of table 3) and Γ_Z represents an empirical

parameter characteristic of either cations or anions. The values of the Γ_Z parameter (in Å) are given by

$$\Gamma_Z = 0.94 \text{ for } \textit{cations}; \tag{21A}$$

$$\Gamma_Z = 0.0 \text{ for } \textit{anions}. \tag{21B}$$

It is assumed in the HKF model that calculation of $r_{e,j}$ from eqs (20) and (21A and B) permits accurate prediction of ω_j^{abs}, ω_j, ω_k, $\Delta\bar{\Xi}^{\circ abs}_{s,j}$, $\Delta\bar{\Xi}^{\circ}_{s,j}$, and $\bar{\Xi}^{\circ}_{s,k}$ for all aqueous ions and electrolytes.

Equations for nonsolvation contributions($\Delta\bar{\Xi}^{\circ}_n$).—The nonsolvation contributions to the standard partial molal volumes, compressibilities, and isobaric heat capacities of aqueous electrolytes in the HKF model are given by

$$\Delta\bar{V}^{\circ}_{n,k} = a_{1,k} + a_{2,k} f(P) + a_{3,k} f(T) + a_{4,k} f(P) f(T), \tag{22}$$

$$-\Delta\bar{\kappa}^{\circ}_{n,k} \equiv \left(\frac{\partial \Delta\bar{V}^{\circ}_{n,k}}{\partial P}\right)_T = (a_{2,k} + a_{4,k} f(T)) \left(\frac{\partial f(P)}{\partial P}\right)_T, \tag{23}$$

and

$$\Delta\bar{C}^{\circ}_{P,n,k} = c_{1,k} + c_{2,k} f(T), \tag{24}$$

where $a_{1,k}$, $a_{2,k}$, $a_{3,k}$, $a_{4,k}$, $c_{1,k}$, $c_{2,k}$, and Θ_k stand for constants characteristic of the kth electrolyte, P_r denotes the reference pressure of 1 bar,

$$f(T) = \frac{T}{T - \Theta_k} = 1 + \Theta_k \left(\frac{1}{T - \Theta_k}\right) \tag{25}$$

and

$$f(P) = P \tag{26}$$

Regression of experimental values of $\bar{V}^{\circ}_k$ at constant pressures close to 1 bar with eqs (17) and (22) indicated that representation of $f(T)$ with eq (25) affords accurate description of the data. The values of Θ_k generated in the regression calculations were subsequently used to regress experimental $\bar{C}^{\circ}_{P,k}$ values with eqs (19), (24), and (25). The latter calculation indicated that the experimental heat capacity data could be described accurately with these equations at temperatures above ~15 °C, but slight discrepancies were observed at lower temperatures. Combination of eq (18) with eqs (23) and (25) permits accurate representation of experimental values of $-\bar{\kappa}^{\circ}_k$ at 1 bar. This required provision for the terms containing $f(P)$ in the equation for $\Delta\bar{V}^{\circ}_{n,k}$ (eq 22). Eq (26) was accepted for representation of $f(P)$ because substitution of eq (26) in eq (22), if used in combination with eqs (17) and (25), resulted in accurate prediction of experimental values of $\bar{V}^{\circ}_k$ for NaCl at pressures up to 1000 bars at 25 °C.

Analogous statements of eqs (22) through (26) are used in the HKF model for representation of $\Delta\bar{V}^{\circ}_{n,j} - \Delta\bar{\kappa}^{\circ}_{n,j}$, and $\Delta\bar{C}^{\circ}_{P,n,j}$ for the jth aqueous

ion. However, because the equation of state coefficients Θ_k and Θ_j are solute-dependent, the ion coefficients $a_{1,j}$, $a_{2,j}$, $a_{3,j}$, $a_{4,j}$, $c_{1,j}$, and $c_{2,j}$ cannot be calculated from the additivity relation represented by eq (8) using the corresponding coefficients for aqueous electrolytes. Nevertheless, the regression procedures used to obtain the ion equation of state coefficients in the HKF model permit close approximation of the additivity relations given by eq (8) at temperatures above 0 °C.

The standard molal intrinsic volume ($\overline{V}_i^\circ$) and heat capacity ($\overline{C}_{P,i}^\circ$) of an aqueous ion or electrolyte are assumed in the HKF model to be essentially independent of pressure and temperature, which requires $\overline{\kappa}_i^\circ \sim 0$. It follows that $a_1 \sim \overline{V}_i^\circ$ and $c_1 \sim \overline{C}_{P,i}^\circ$. The temperature and pressure dependence of the nonsolvation contributions ($\Delta\overline{V}_n^\circ$, $\Delta\overline{\kappa}_n^\circ$, and $\Delta\overline{C}_{P,n}^\circ$) to $\overline{V}^\circ$, $\overline{\kappa}^\circ$, and $\overline{C}_P^\circ$ are thus controlled in the HKF model solely by the structural collapse contributions, $\Delta\overline{V}_c^\circ$, $\Delta\overline{\kappa}_c^\circ$, and $\Delta\overline{C}_{P,c}^\circ$.

REVISION OF THE HKF MODEL

Solvent structure as a function of temperature.—Striking parallels exist between the HKF model and current theoretical and predictive models of water properties at supercooled temperatures. In his reviews of the properties of supercooled water, Angell (1982, 1983) attributed the rapid changes in these properties with decreasing temperature to the increasing structure of water. According to several theories, the increase in water structure eventually causes some properties of supercooled water to approach $\pm\infty$ at a singular temperature, T_s. Similarly, predicted values of the structural collapse contributions ($\Delta\overline{V}_{c,k}^\circ$, $\Delta\overline{\kappa}_{c,k}^\circ$, and $\Delta\overline{C}_{P,c,k}^\circ$) to $\overline{V}_k^\circ$, $\overline{\kappa}_k^\circ$, and $\overline{C}_{P,k}^\circ$ for an aqueous electrolyte in the HKF model increase with decreasing temperature, and at supercooled temperatures they approach $-\infty$ at a singular temperature. However, the singular temperatures in the HKF model (Θ_k in eq 25) depend on the identity of the electrolyte and have values that lie both above and below the value of the singular temperature for the supercooled solvent proposed by Angell (T_s = 228 K). As shown below the assumed solute dependence of Θ in the HKF model is not required.

A singular temperature for supercooled water of 228 ± 3 K is indicated by regression of experimental thermodynamic, transport, and relaxation properties at 1 bar and supercooled temperatures with the scaling law for critical-type phase transitions (Angell, 1982, 1983). Following Angell's notation, the scaling law is given by

$$y = A_y\left(\frac{T}{T_s} - 1\right)^{-\lambda_y} = A_y T_s^{\lambda_y}\left(\frac{1}{T - T_s}\right)^{\lambda_y} \qquad (27)$$

where y represents a thermodynamic, transport, or relaxation property of supercooled water, which approaches infinity as temperature approaches the singular temperature (T_s), A_y denotes a proportionality constant characteristic of the property, and λ_y refers to a property-dependent exponent, which is termed a critical exponent if eq (27) is used for critical phenomena. As emphasized by Angell, theoretical

interpretation of λ_y exponents requires application of eq (27) at temperatures significantly remote from T_s to be restricted to description of the "anomalous" component or structural properties of supercooled water. In his review of various approaches to extract structural properties from bulk properties of supercooled water, Angell reports that in every case regression of calculated structural properties at 1 bar with the scaling law is consistent with a singular temperature of 228 K.

By analogy with their approach to $-\infty$ as temperature increases toward the critical point of H_2O, it seems reasonable to us that $\overline{V}^\circ_k$, $\overline{\kappa}^\circ_k$, and $\overline{C}^\circ_{P,k}$ for aqueous electrolytes should approach $-\infty$ as the temperature nears a singular temperature for the supercooled solvent (T_s). Calculations for binary mixtures using a lattice-gas model reported by Wheeler (1972) predict that the standard partial molal volumes and enthalpies of solutes approach $\pm\infty$ at the critical point of the solvent. Consistent with Wheeler's results, predicted values of $\overline{V}^\circ$, $\overline{\kappa}^\circ$, and $\overline{C}^\circ_P$ for aqueous electrolytes from the Born equation approach $\pm\infty$ at the critical point of H_2O (Helgeson and Kirham, 1976; Helgeson, Kirkham, and Flowers, 1981; Gates, Wood, and Quint, 1982; Wood and others, 1983). These predicted limits of $\pm\infty$ for electrolytes are supported by experimental data (Gates, Wood, and Quint, 1982; Wood and others, 1983). Electrostatic ion-solvent interactions cause large changes in $\overline{V}^\circ_k$, $\overline{\kappa}^\circ_k$, and $\overline{C}^\circ_{P,k}$ in the vicinity of the critical point of H_2O. By analogy, it seems highly probable that structural modification of the solvent by aqueous ions would lead to large changes in $\overline{V}^\circ_k$, $\overline{\kappa}^\circ_k$, and $\overline{C}^\circ_{P,k}$ in the vicinity of T_s.

The structural collapse contributions to $\overline{V}^\circ_k$, $\overline{\kappa}^\circ_k$, and $\overline{C}^\circ_{P,k}$, ($\Delta\overline{V}^\circ_{c,k}$, $\Delta\overline{\kappa}^\circ_{c,k}$, and $\Delta\overline{C}^\circ_{P,c,k}$, respectively) in the HKF model are asymptotic functions of temperature. They approach nearly constant values at high temperatures but rapidly become more negative as temperature drops below -50°C. Helgeson and Kirkham (1976) argue that the asymptotic decrease in the structural collapse contributions with increasing temperature is a consequence of decreasing water structure. If this is the case, the fact that the temperature dependence of the structural properties of supercooled water can be described with the scaling law (eq 27) suggests that the temperature terms on the right sides of the second equalities in eqs (25) and (27) should be closely related. Comparison of these terms indicates that the HKF model can be revised to be consistent with the scaling law by incorporating in eq (25) the property-dependent exponents ($\lambda_{\overline{y}^\circ}$) and identifying Θ_k for all electrolytes as T_s. Under these circumstances, $f(T)$ in eq (25) becomes $f_{\overline{y}^\circ}(T)$ in the revised HKF model.

Consideration of experimental uncertainties in the standard partial molal properties of aqueous electrolytes with respect to the covariance of the equation of state coefficients in the HKF model indicates that it is not possible to determine unambiguously a singular temperature (T_s) by regression of experimental $\overline{V}^\circ_k$ values for aqueous electrolytes at 1 bar and temperatures above 0°C. However, the vast majority of the regressin values of Θ_k reported by Helgeson and Kirkham (1976) fall within the range of 228 ± 30 K. These considerations suggest that regression of $\overline{V}^\circ_k$ data forcing a value of 228 K for Θ and a value of unity for $\lambda_{\overline{v}^\circ}$ should

provide accurate description of the experimental data. Similar considerations suggest that $\bar{\kappa}^\circ$ data can be described accurately with $\Theta = 228$ K and $\lambda_{\bar{\kappa}^\circ} = 1$. In contrast, observed differences between predicted values of $\bar{C}^\circ_{P,k}$ and experimental values at temperatures below ~15°C (Helgeson, Kirkham, and Flowers, 1981) are greater than the corresponding experimental uncertainties, which suggests that the value of $\lambda_{\bar{C}^\circ_P}$ differs significantly from unity.

Regression calculations summarized below confirm that experimental values of $\bar{V}^\circ_k$, $\bar{\kappa}^\circ_k$, and $\bar{C}^\circ_{P,k}$ can be described accurately using $\Theta = 228$ K, $\lambda_{\bar{V}^\circ} = 1$, $\lambda_{\bar{\kappa}^\circ} = 1$, and $\lambda_{\bar{C}^\circ_P} = 2$. Under these circumstances the revised temperature dependence of the structural contributions to $\bar{V}^\circ_k$, $\bar{\kappa}^\circ_k$, and $\bar{C}^\circ_{P,k}$ can be expressed as

$$f_{\bar{V}^\circ}(T) = \left(\frac{1}{T - \Theta}\right), \tag{28A}$$

$$f_{\bar{\kappa}^\circ}(T) = \left(\frac{1}{T - \Theta}\right), \tag{28B}$$

and

$$f_{\bar{C}^\circ_P}(T) = \left(\frac{1}{T - \Theta}\right)^2. \tag{28C}$$

There are two practical advantages to these revisions of the HKF model: (1) the number of solute-dependent fit parameters in the model is reduced by setting Θ_k (electrolytes) and Θ_j (ions) to $\Theta = T_s = 228$ K, and (2) the revised $f_{\bar{y}^\circ}(T)$ functions convert eqs (22), (23), and (24) for $\Delta\bar{V}^\circ_n$, $\Delta\bar{\kappa}^\circ_n$, and $\Delta\bar{C}^\circ_{P,n}$ into linear equations with additive coefficients. Consequently, the additivity relations for nonsolvation contributions ($\Delta\bar{\Xi}^\circ_n$) represented by eq (8) are exact equalities, and the equation of state coefficients for $\Delta\bar{\Xi}^\circ_{n,j}$ for the jth aqueous ion can be calculated from regression values of corresponding coefficients for the kth aqueous electrolyte using the relation,

$$\Omega_k = \sum_j \nu_{j,k}\Omega_j \tag{29}$$

where Ω stands for equation of state coefficients a_1, a_2, a_3, a_4, c_1, or c_2.

Solvent structure as a function of pressure.—Despite arguments to the contrary (Helgeson, 1982), comparison of predicted values of $\Delta\bar{V}^\circ_{n,\mathrm{NaCl}}$ and $\Delta\bar{V}^\circ_{n,\mathrm{K_2SO_4}}$ with values calculated from the experimental data reported by Adams (1931, 1932) at 25°C and pressures to 10 kb indicates to us that the pressure dependence of the nonsolvation volumes in the HKF model should be revised. Predicted values of $\Delta\bar{V}^\circ_{n,k}$ for NaCl and K_2SO_4 from the HKF model are represented by the curves in figures 1 and 2. The slopes of these curves correspond to $-\Delta\bar{\kappa}^\circ_{n,k}$, which is taken to be independent of pressure in the HKF model. The symbols in figures 1 and 2 represent values of $\Delta\bar{V}^\circ_{n,k}$ calculated from the volume analog of eq

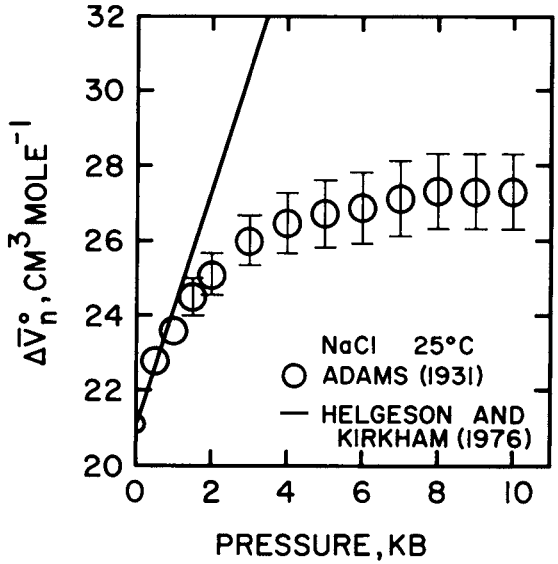

Fig. 1. Nonsolvation contribution to the standard partial molal volume ($\Delta\bar{V}^\circ_n$) of NaCl as a function of pressure at 25°C (see text). The symbols represent experimental data, but the curves correspond to predicted values from the HKF model.

(10) using predicted values of $\Delta\bar{V}^\circ_{s,k}$ (eq 17) and values of $\bar{V}^\circ_k$ generated by regression of experimental apparent molal volumes ($\Phi_{V,k}$) with the $\Phi_{V,k}$ equation given by Helgeson, Kirkham, and Flowers (1981). Uncertainties in the experimental values of $\Delta\bar{V}^\circ_{n,NaCl}$ and $\Delta\bar{V}^\circ_{n,K_2SO_4}$ were estimated by analysis of (1) uncertainties in $\Delta\bar{V}^\circ_{s,k}$ values due to predictive uncertainties in Q (eq D-2 in app. D) and (2) uncertainties in values of $\bar{V}^\circ_k$ generated from the experimental volume data due to experimental uncertainties in $\Phi_{V,k}$ and predictive uncertainties in the Debye-Hückel contributions to $\Phi_{V,k}$. These estimated uncertainties are indicated by the lengths of the vertical bars through the symbols in figures 1 and 2.

The discrepancies between the predicted and experimental values of $\Delta\bar{V}^\circ_{k,n}$ in figures 1 and 2 indicate that accurate prediction of $\Delta\bar{V}^\circ_{n,k}$ and $-\Delta\bar{\kappa}^\circ_{n,k}$ at high pressures with eqs (20) and (21) requires revision of eq (26) for f(P). It can be seen in figures 1 and 2 that the experimental values of $\Delta\bar{V}^\circ_{n,k}$ at 25°C exhibit asymptotic configurations that require $-\Delta\bar{\kappa}^\circ_{n,k}$ to decrease from a maximum value at the vapor-liquid saturation pressure for H_2O to a near zero value at the ICE VI-water equilibrium pressure (9630 bars). These observations suggest that f(P) is an asymptotic function which decreases and approaches zero with increasing pressure.

It is well established that increasing pressure and temperature have a similar effect on the structural state of water (Angell, 1982, 1983). The "structural component" of the partial molal volume of H_2O ($\bar{V}_{struc,H_2O}$) apparently decreases asymptotically and approaches zero with increas-

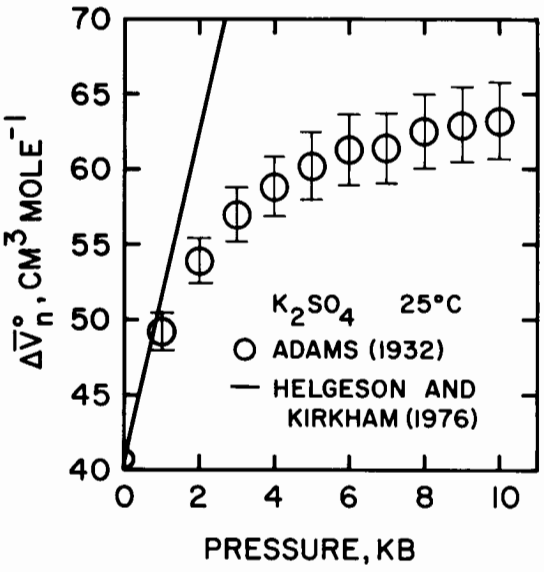

Fig. 2. Nonsolvation contribution to the standard partial molal volume ($\Delta\bar{V}_n^\circ$) of K_2SO_4 as a function of pressure at 25°C (see text and caption of fig. 1).

ing pressure. It follows by analogy with the temperature dependence of $\Delta\bar{V}_{c,k}^\circ$ in the revised HKF model that the pressure dependence of $\Delta\bar{V}_{c,k}^\circ$ should be a function of the pressure dependence of $\bar{V}_{struc,H_2O}$. These considerations lead to the proposition that $f(P)$ represents a characteristic function of the solvent structure. It should be noted that this interpretation of $f(P)$ is consistent with the additivity relation for nonsolvation contributions (eq 8), as well as the additive relation between equation of state coefficients for ions and electrolytes (eq 29).

The proposition that $f(P)$ is characteristic of the solvent and independent of the identity of the electrolyte is supported by the Tait-Tammann-Gibson (TTG) equation of state (Gibson, 1938), which Gibson (1934) used successfully to predict the high pressure volume data reported by Adams (1931, 1932). As in the HKF model, the expression for the standard partial molal volume of an aqueous electrolyte in the TTG model corresponds to $\bar{V}_k^\circ$ as the sum of an intrinsic contribution by the electrolyte and a second term which can be interpreted conceptually as an electrostriction contribution ($\Delta\bar{V}_{e,k}^\circ$). The pressure dependence of $\Delta\bar{V}_{e,k}^\circ$ in the TTG model is given by $1/(B + P)$, where B denotes the Tait-Tammann (Tammann, 1895) coefficient for the solvent. Similarly, the pressure dependence of $\Delta\bar{V}_{e,k}^\circ$ in the revised HKF model is described by the asymptotic solvent functions Q and $f(P)$, the latter of which can be expressed as

$$f(P) = \frac{1}{\Psi + P} \tag{30}$$

where Ψ represents a constant characteristic of H_2O. It follows from eqs (23) and (30) that the pressure dependence of $-\Delta\bar{\kappa}^\circ_{n,k}$ is given by

$$\left(\frac{\partial f(P)}{\partial P}\right)_T = \frac{-1}{(\Psi + P)^2}. \tag{31}$$

Revised equations for the nonsolvation contributions to the standard partial molal volumes, compressibilities, expansibilities, heat capacities, entropies, enthalpies, and Gibbs free energies that are consistent with the revised equations for $f(P)$ (eq 30) and $f_{\bar{y}^\circ}(T)$ (eqs 28A, B, and C) are given in app. F.

Solvent contributions to $r_{e,j}$.—Comparison of predicted and experimental high-temperature values of $\bar{V}^\circ_k$ and $\bar{C}^\circ_{P,k}$ for several aqueous

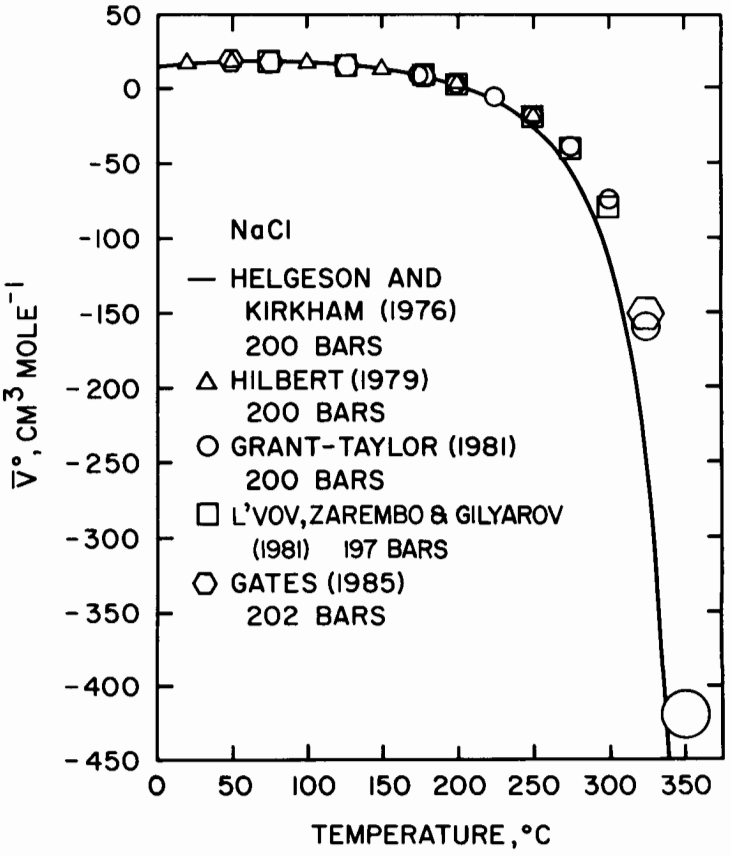

Fig. 3. Standard partial molal volume ($\bar{V}^\circ$) of NaCl as a function of temperature at ~200 bars (see caption of fig. 1).

electrolytes at pressures close to the critical pressure of H_2O (P_{c,H_2O}) indicates that the predicted values become increasingly too negative at temperatures approaching the critical temperature of H_2O (T_{c,H_2O}). As discussed previously (Helgeson and Kirkham, 1976), $\Delta\overline{V}^\circ_{n,k}$ and $\Delta\overline{C}^\circ_{P,n,k}$ are relatively insignificant contributions to $\overline{V}^\circ_k$ and $\overline{C}^\circ_{P_k}$ compared to $\Delta\overline{V}^\circ_{s,k}$ and $\Delta\overline{C}^\circ_{P,s,k}$, respectively, at high temperatures and $P \sim P_{c,H_2O}$. It follows that the solvation contributions ($\Delta\overline{\Xi}^\circ_s$) in the HKF model are responsible for the discrepancies between the predicted and experimental values of $\overline{V}^\circ_k$ and $\overline{C}^\circ_{P,k}$ at temperatures and pressures approaching T_{c,H_2O} and P_{c,H_2O}.

Experimental values of $\overline{V}^\circ_k$ and $\overline{C}^\circ_{P,k}$ at temperatures from 0° to 350°C and pressures from 172 to 206 bars are represented by the symbols in figures 3 through 6. Predicted values from the HKF model correspond to the curves in these figures. The experimental values of $\overline{V}^\circ_k$

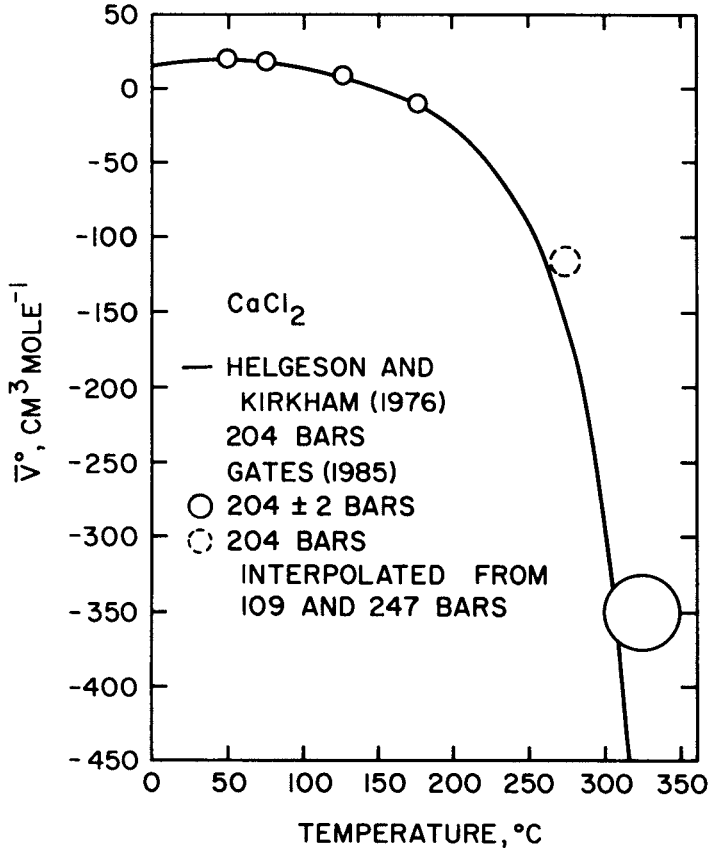

Fig. 4. Standard partial molal volume ($\overline{V}^\circ$) of $CaCl_2$ as a function of temperature at ~204 bars (see caption of fig. 1).

and $\overline{C}^{\circ}_{P,k}$ were obtained by regression of experimental apparent molal properties ($\Phi_{V,k}$ and $\Phi_{C_P,k}$) using the equations for $\Phi_{V,k}$ and $\Phi_{C_P,k}$ given by Helgeson, Kirkham, and Flowers (1981). The sources of the experimental data used in the regression calculations are given in the figures. It can be seen in figures 3 through 6 that the predicted values of $\overline{V}^{\circ}_{k}$ and $\overline{C}^{\circ}_{P,k}$ at temperatures >200°C depart systematically to an increasing degree from the experimental values with increasing temperature. These discrepancies can be attributed to errors arising from the electrostatic Born term in the HKF model.

The systematic departures of the curves from the symbols in figures 3 through 6 suggest that the constant Born coefficients adopted in the HKF model (ω) should instead be considered to be pressure- and temperature-dependent. Trial regression calculations indicated that representation of ω_{NaCl} with an orthogonal temperature-density function permits accurate description of all the experimental values of $\overline{V}^{\circ}_{NaCl}$ and $\overline{C}^{\circ}_{P,NaCl}$ shown in figures 3 and 5. Revised equations for solvation contributions to the standard partial molal volume, compressibility,

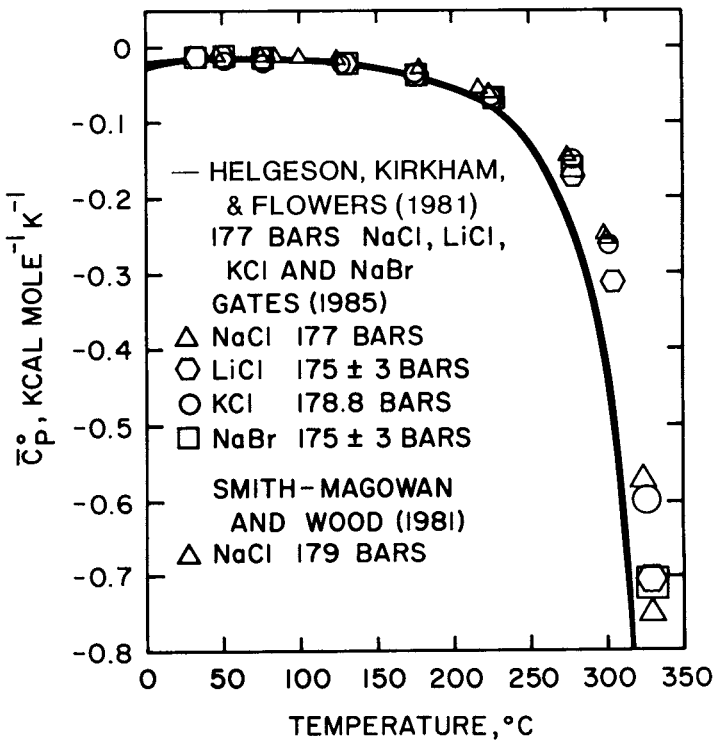

Fig. 5. Standard partial molal isobaric heat capacities ($\overline{C}^{\circ}_{P}$) of NaCl, KCl, LiCl, and NaBr as functions of temperature at ~177 bars (see caption of fig. 1).

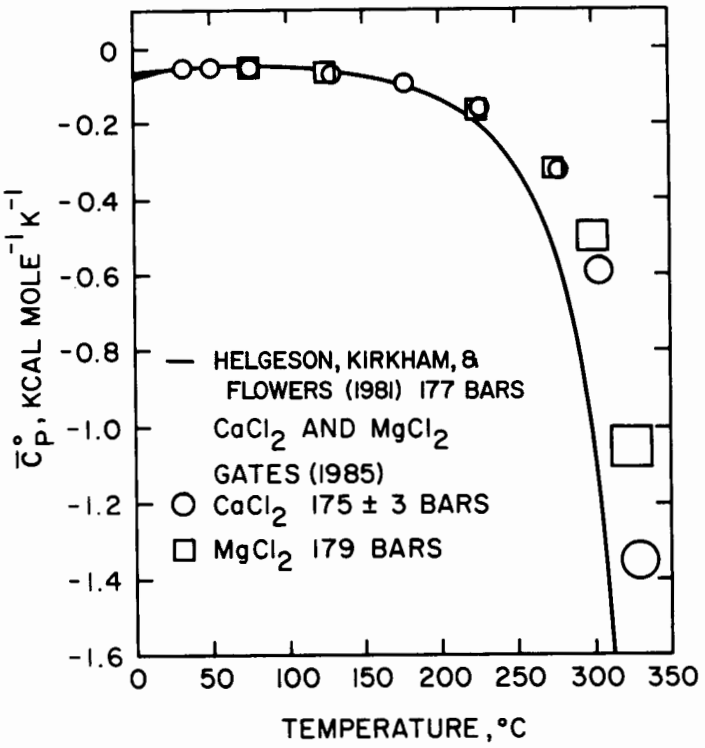

Fig. 6. Standard partial molal isobaric heat capacities ($\bar{C}_P^\circ$) of $CaCl_2$ and $MgCl_2$ as functions of temperature at ~177 bars (see caption of fig. 1).

expansibility, heat capacity, entropy, and enthalpy that are consistent with the pressure- and temperature-dependent Born coefficients are given in app. G.

It follows from the observations summarized above and the definition of the Born coefficient of an aqueous ion (eq 12) that the effective electrostatic radius of an aqueous ion ($r_{e,j}$) also changes from a constant to a function of pressure and temperature with increasing temperature. The revised HKF equation for $r_{e,j}$ (eq 20) can be expressed as

$$r_{e,j} = r_{x,j} + |Z_j| k_Z + h_j \tag{32}$$

where k_Z stands for the low-temperature Γ_Z constants in eqs (21A) and (21B) and h_j represents a function of pressure and temperature characteristic of the aqueous ion. As a first approximation, h_j in eq (32) can be expressed as

$$h_j = D_j g \tag{33}$$

where D_j denotes a constant characteristic of the charge and/or crystallographic radius of an aqueous ion and g represents a function of pressure and temperature independent of the identity of the ion. It should be noted that revision of the equation for $r_{e,j}$ by incorporating the g function is consistent with additivity relations (eq 9). The g function in the revised equation for $r_{e,j}$ provides implicitly for the pressure and temperature-dependence of the higher-order solvent contributions to $\Delta\overline{G}^\circ_{s,k}$ (Frank, 1955), such as dielectric saturation (Booth, 1951) and the compressibility of the solvent (Wood and others, 1981), neither of which is explicitly accounted for in the Born equation. Consequently, the g function can be regarded as a solvent contribution to $r_{e,j}$.

Alternate expressions for D_j were used to calculate values of g from experimental values of $\overline{V}^\circ_k$ and $\overline{C}^\circ_{P,k}$ for NaCl at various pressures and temperatures using the regression procedures discussed below. Because g and its pressure and temperature derivatives can be used to predict $\Delta\overline{V}^\circ_{s,k}$ and $\Delta\overline{C}^\circ_{P,s,k}$ for any aqueous electrolyte, the alternate expressions for D_j could be evaluated by comparison of predicted values of $\overline{V}^\circ_k$ and $\overline{C}^\circ_{P,k}$ with the experimental values in figures 4, 5, and 6. Such comparisons indicate that $D_j = |Z_j|$ affords accurate prediction of $\overline{V}^\circ_k$ and $\overline{C}^\circ_{P,k}$ at high temperatures and low pressures. It follows that the revised equation for $r_{e,j}$ is given by

$$r_{e,j} = r_{x,j} + |Z_j|\,\Gamma_Z \tag{34}$$

where Γ_Z is redefined as

$$\Gamma_Z \equiv k_z + g. \tag{35}$$

If $g = 0$, eqs (34) and (35), together with the revised equations for ω and $\Delta\overline{\Xi}^\circ_s$ in apps. B and G, respectively, reduced to the corresponding equations in the HKF model.

Trial regression calculations for ω_{NaCl} (see above) indicated that the functional dependence of g on temperature and pressure can be expressed as

$$g = 0.5\,(-b + \sqrt{b^2 - 4c}) \tag{36A}$$

where

$$b = 3.72 - 2\eta\left(\sum_{i=-1}^{4}\sum_{j=0}^{4} a_{ij}\,T^i\rho^j\right)^{-1} \tag{36B}$$

and

$$c = 3.4571 - 3.72\,\eta\left(\sum_{i=-1}^{4}\sum_{j=0}^{4} a_{ij}\,T^i\rho^j\right)^{-1} \tag{36C}$$

where ρ represents the specific density of H_2O and a_{ij} stands for an array of fit coefficients. The regression calculations discussed below confirm

that eq (36A, B, and C) permits accurate representation of g. Expressions for the partial derivatives of g with respect to pressure and temperature that are consistent with eq (36A, B, and C) are given in app. C.

REGRESSION CALCULATIONS

Retrieval of parameters and coefficients for the revised nonsolvation contributions.—Because regression values of the parameters $\lambda_{\bar{V}}^{\circ}$, $\lambda_{\bar{\kappa}}^{\circ}$, and $\lambda_{\bar{C}_P^{\circ}}$ are most sensitive to the temperature dependence of $\overline{V}_k^{\circ}$, $\bar{\kappa}_k^{\circ}$, and $\overline{C}_{P,k}^{\circ}$ at 1 bar and temperatures below 100°C, the extensive low-temperature experimental data for electrolytes at 1 bar were regressed to retrieve values of these parameters. As indicated above, the regression calculations confirmed that the revised HKF model affords accurate description of the experimental values of $\overline{V}_k^{\circ}$, $\bar{\kappa}_k^{\circ}$, and $\overline{C}_{P,k}^{\circ}$ using $\Theta = 228$ K and $\lambda_{\bar{V}}^{\circ} = 1$. $\lambda_{\bar{\kappa}}^{\circ} = 1$, and $\lambda_{\bar{C}_P^{\circ}} = 2$.

To facilitate regression analysis, the temperature-independent terms in the revised HKF equation for $\Delta\overline{V}_n^{\circ}$ (eq F-1 in app. F) were combined into two isobaric fit parameters denoted by σ and ξ, which can be expressed as

$$\sigma \equiv a_1 + \frac{a_2}{\Psi + P} \tag{37}$$

and

$$\xi \equiv a_3 + \frac{a_4}{\Psi + P}. \tag{38}$$

Substitution of eqs (37) and (38) in eq (F-1) in app. F leads to

$$\Delta\overline{V}_n^{\circ} = \sigma + \xi\left(\frac{1}{T - \Theta}\right)^{\lambda_V^{\circ}}. \tag{39}$$

It follows from eqs (37), (38), and (F-2) that

$$-\Delta\bar{\kappa}_n^{\circ} = \left(\frac{\partial\sigma}{\partial P}\right)_T + \left(\frac{\partial\xi}{\partial P}\right)_T \left(\frac{1}{T - \Theta}\right)^{\lambda_{\bar{\kappa}}^{\circ}} \tag{40}$$

where $(\partial\sigma/\partial P)_T$ and $(\partial\xi/\partial P)_T$ are given by

$$\left(\frac{\partial\sigma}{\partial P}\right)_T = \frac{-a_2}{(\Psi + P)^2} \tag{41}$$

and

$$\left(\frac{\partial\xi}{\partial P}\right)_T = \frac{-a_4}{(\Psi + P)^2}. \tag{42}$$

Taking account of eq (8), statements of eqs (37) through (42) can be written either for the kth electrolyte or the jth aqueous ion. Conse-

quently, the isobaric fit parameters σ_k, ξ_k, $(\partial\sigma_k/\partial P)_T$, and $(\partial\xi_k/\partial P)_T$ for the kth electrolyte are related to the corresponding parameters for the jth ion by eq (29). It follows from eqs (24) and (28c) that at 1 bar

$$\Delta\bar{C}^\circ_{P,n,k} = c_{1,k} + c_{2,k}\left(\frac{1}{T-\Theta}\right)\lambda_{\bar{C}^\circ_P}. \tag{43}$$

Eqs (39), (40), and (43) were used to generate the curves in figures 7 through 11, which represent regression values of $\Delta\bar{V}^\circ_{n,k}$, $-\Delta\bar{\kappa}^\circ_{n,k}$, and $\Delta\bar{C}^\circ_{P,n,k}$ at 1 bar consistent with $\Theta = 228$ K, $\lambda_{\bar{V}^\circ} = 1$, $\lambda_{\bar{\kappa}^\circ} = 1$, and $\lambda_{\bar{C}^\circ_P} = 2$. The regression parameters σ_k, ξ_k, $(\partial\sigma_k/\partial P)_T$, and $(\partial\xi_k/\partial P)_T$ for aqueous electrolytes at 1 bar are given in table 1. The symbols in figures 7 through 11 represent values of $\Delta\bar{V}^\circ_{n,k}$, $-\Delta\bar{\kappa}^\circ_{n,k}$, and $\Delta\bar{C}^\circ_{P,n,k}$ computed from eq (10) using experimental values of $\bar{V}^\circ_k$, $-\bar{\kappa}^\circ_k$ and $\bar{C}^\circ_{P,k}$ and values of $\Delta\bar{V}^\circ_{s,k}$, $-\Delta\bar{\kappa}^\circ_{s,k}$ and $\Delta\bar{C}^\circ_{P,s,k}$ calculated from eqs (17), (18), and (19). The latter equations were used in lieu of their revised analogs (eqs G-1, G-2, and G-4 in app. G) because at 1 bar and $T < 150$ °C, $g = 0$ in eq 35, and the Born coefficients of aqueous electrolytes (ω_k) are thus constant in this temperature range. The experimental values of $\bar{V}^\circ_k$, $-\bar{\kappa}^\circ_k$, and $\bar{C}^\circ_{P,k}$ were generated using the regression procedures and equations described above (Helgeson, Kirkham, and Flowers, 1981) together with experimental data reported in the sources shown in figures 7 through 11. The values of $\Delta\bar{V}^\circ_{n,k}$, $-\Delta\bar{\kappa}^\circ_{n,k}$, and $\Delta\bar{C}^\circ_{P,n,k}$ derived from experimental data at 20 bars or pressures corresponding to vapor-liquid saturation for H_2O were regarded within their uncertainties as 1 bar values in the regression calculations.

It can be seen in figures 7 through 11 that the curves representing eqs (39), (40), and (43) with $\Theta = 228$, $\lambda_{\bar{V}^\circ} = 1$, $\lambda_{\bar{\kappa}^\circ} = 1$, $\lambda_{\bar{C}^\circ_P} = 2$ are in close agreement with the distribution of all the experimental data represented by the symbols. It can be shown that calculated values of $\bar{V}^\circ$, $\bar{\kappa}^\circ$, and $\bar{C}^\circ_P$, respectively, for NaCl from the revised HKF model at 1 bar and temperatures from 0° to 100 °C also compare favorably with $\bar{V}^\circ$ values reported by Lo Surdo, Alzola, and Millero (1982) and Rogers and Pitzer (1982), $\bar{\kappa}^\circ$ values generated by Millero, Ricco, and Schreiber (1982) and Rogers and Pitzer (1982), and $\bar{C}^\circ_P$, values given by Pitzer, Peiper, and Busey (1984) and Clarke and Glew (1985). The accuracy of the revised HKF model is equivalent to that achieved in these studies, which is not true of the HKF model itself. For example, Helgeson, Kirkham, and Flowers (1981) observed discrepancies between values of $\bar{C}^\circ_P$ for NaCl and a number of other electrolytes calculated from the HKF model and corresponding experimental values at temperatures below ~15 °C. These discrepanacies do not occur if the revised HKF model is used.

Values of the equation of state coefficients $c_{1,j}$ and $c_{2,j}$ as well as the parameters σ_j, ξ_j, $(\partial\sigma_j/\partial P)_T$, and $(\partial\xi_j/\partial P)_T$ for aqueous ions at 1 bar are given in table 2. Unless indicated otherwise in the footnotes to table 2, these parameters and coefficients were calculated from eq (29) and the corresponding parameters and coefficients for aqueous electrolytes

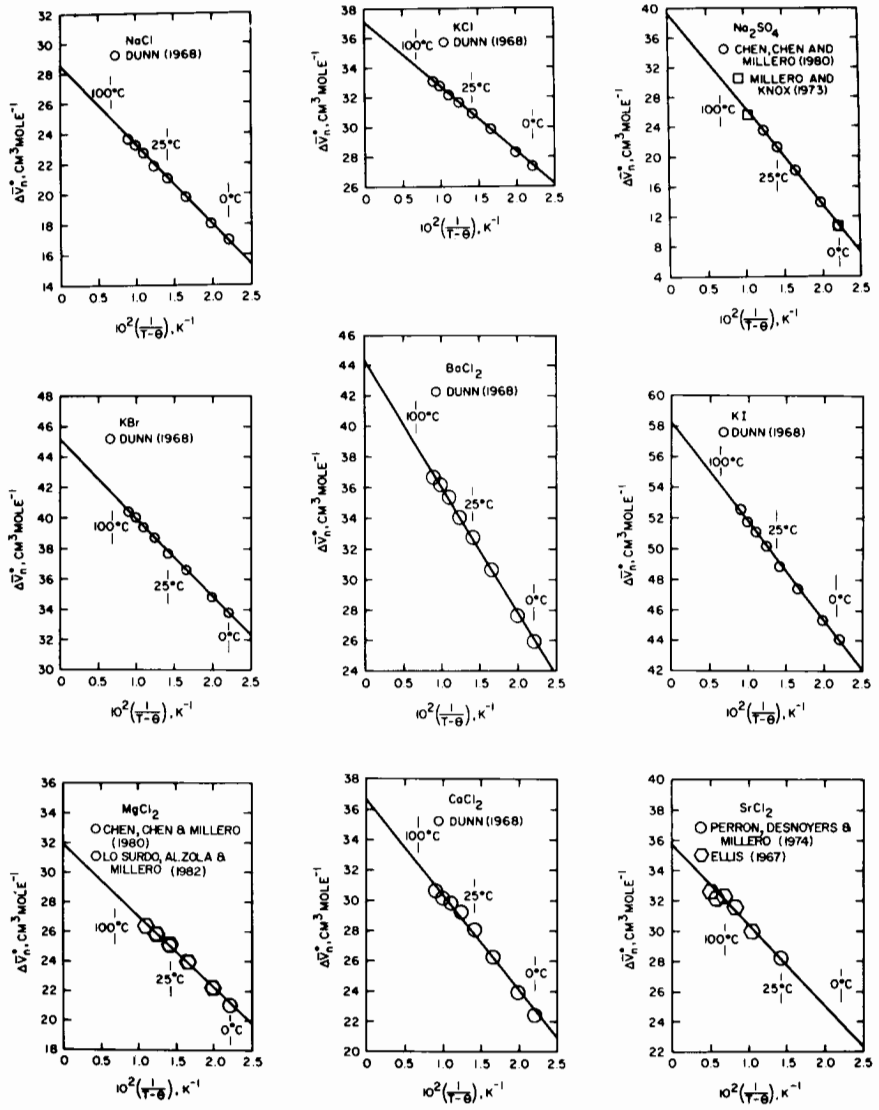

Fig. 7. Graphic representation of eq (39) for the nonsolvation contributions to the standard partial molal volumes ($\Delta\bar{V}_n^\circ$) of aqueous electrolytes at 1 bar (see table 1). The symbols represent experimental data, but the curves correspond to regression values (see text).

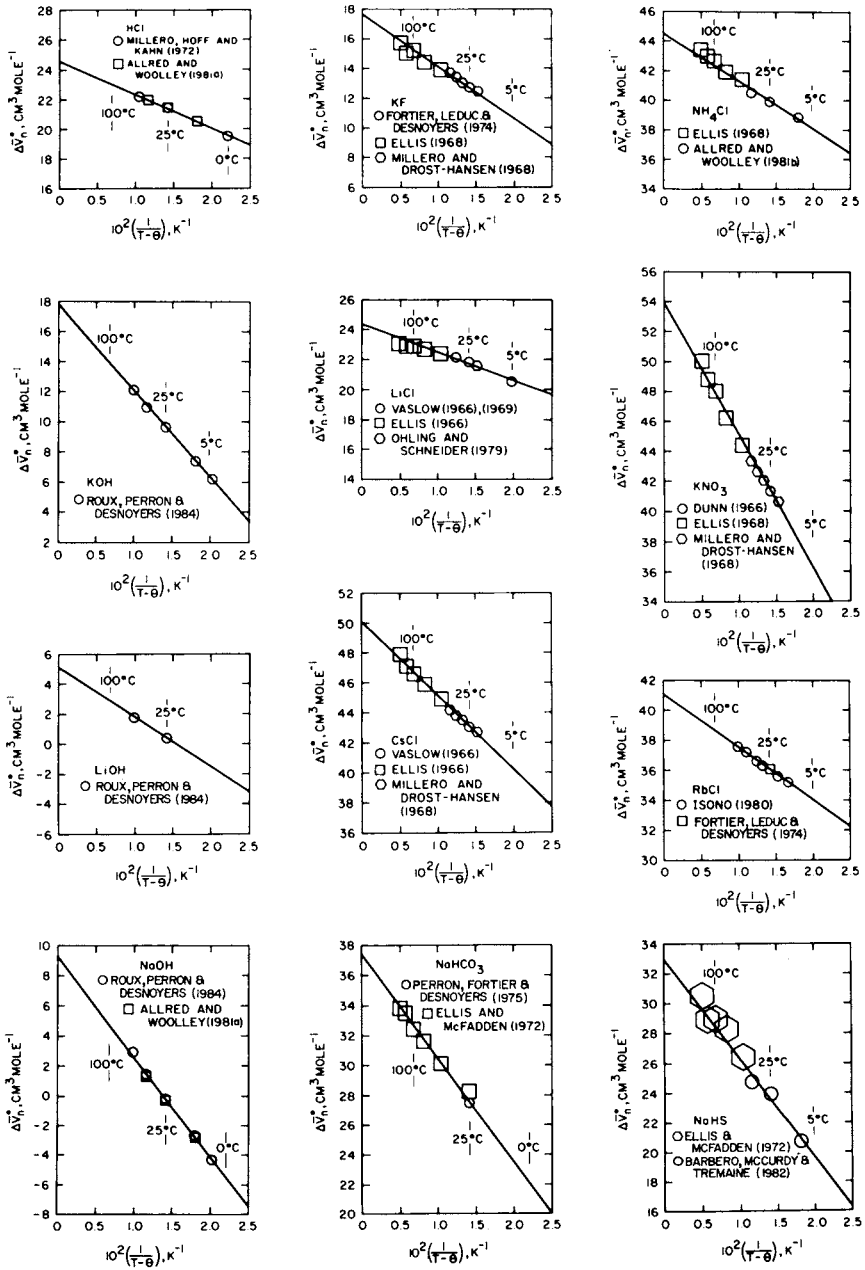

Fig. 8. Graphic representation of eq (39) for the nonsolvation contributions to the standard partial molal volumes ($\Delta\bar{V}_n^\circ$) of aqueous electrolytes at 1 bar (see table 1 and the caption of fig. 7).

given in table 1. It follows from eqs (37), (38), (41), and (42) that values of the equation of state coefficients for aqueous ions represented by $a_{1,j}$, $a_{2,j}$, $a_{3,j}$, and $a_{4,j}$ can be calculated from the values of σ_j, ξ_j, $(\partial\sigma_j/\partial P)_T$, and $(\partial\xi_j/\partial P)_T$ at 1 bar given in table 2. However, these calculations require a value of the solvent parameter Ψ, which can be retrieved from experimental values of $\bar{V}_k^\circ$ at high pressures.

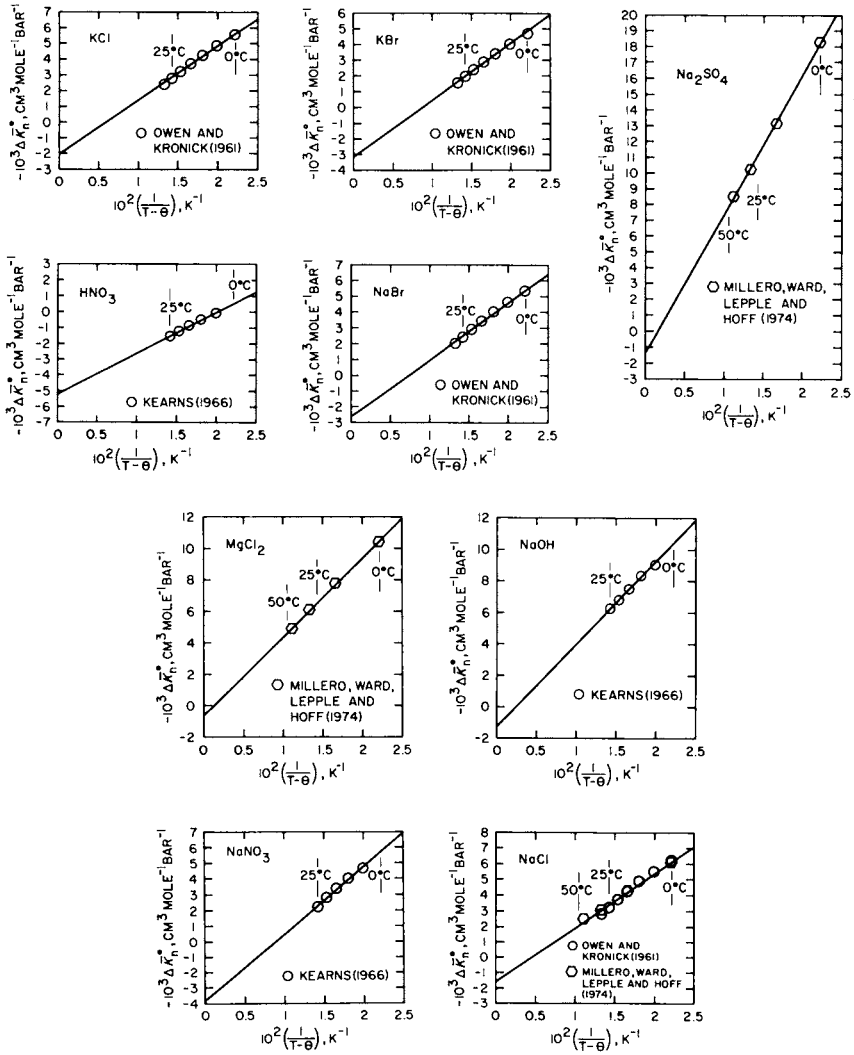

Fig. 9. Graphic representation of eq (40) for the nonsolvation contributions to the standard partial molal isothermal compressibilities ($\Delta\bar{K}_n^\circ$) of aqueous electrolytes at 1 bar (see table 1 and the caption of fig. 7).

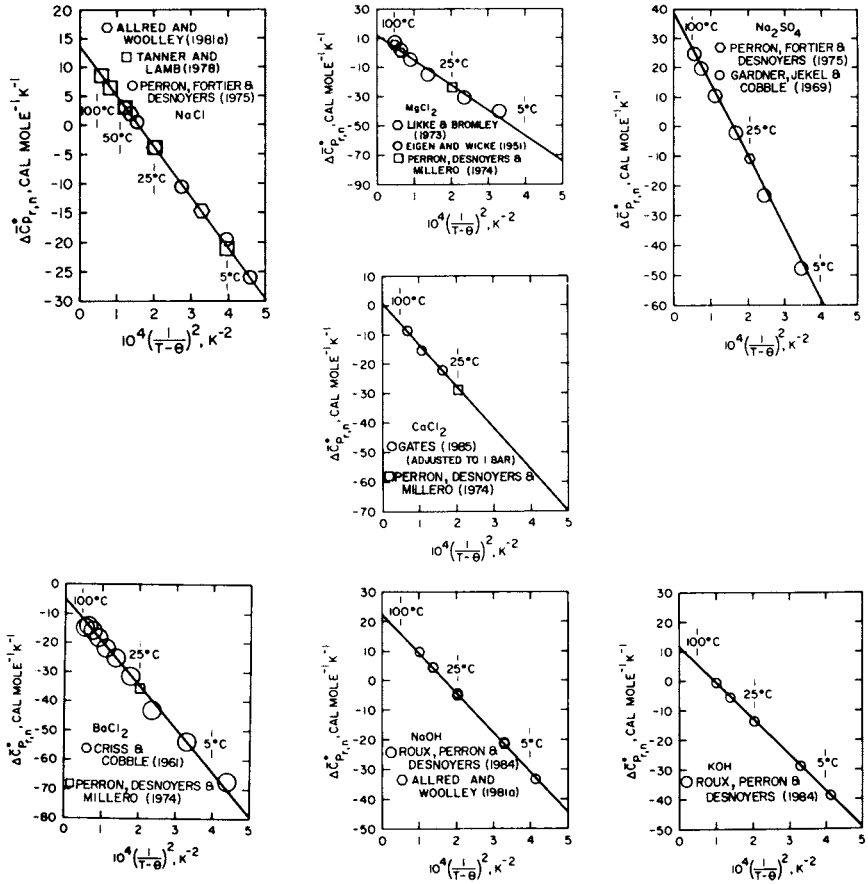

Fig. 10. Graphic representation of eq (43) for the nonsolvation contributions to the standard partial molal isobaric heat capacities ($\Delta\bar{C}^\circ_{Prn}$) of aqueous electrolytes at 1 bar (see table 1 and the caption of fig. 7). The values represented by the circles for $CaCl_2$ were obtained by adjusting the experimental values at higher pressures to 1 bar using eq (F-4) in app. F together with coefficients taken from table 3.

Experimental values of V_k° for NaCl and K_2SO_2 extrapolated from data reported by Adams (1931, 1932) at 25°C and pressures to 10 kb were selected for evaluation of Ψ. These data were chosen because the sensitivity of calculated values of Ψ to uncertainties in high-pressure values of $\bar{V}_k^\circ$ minimizes at low temperatures and decreases with increasing pressure. It follows from eqs (F-1) and (F-2) in app. F that Ψ can be calculated from

$$\Psi = \frac{P\,(\Delta_{k,P,T} - 1) + 1}{P - \Delta_{k,P,T} - 1} \tag{44}$$

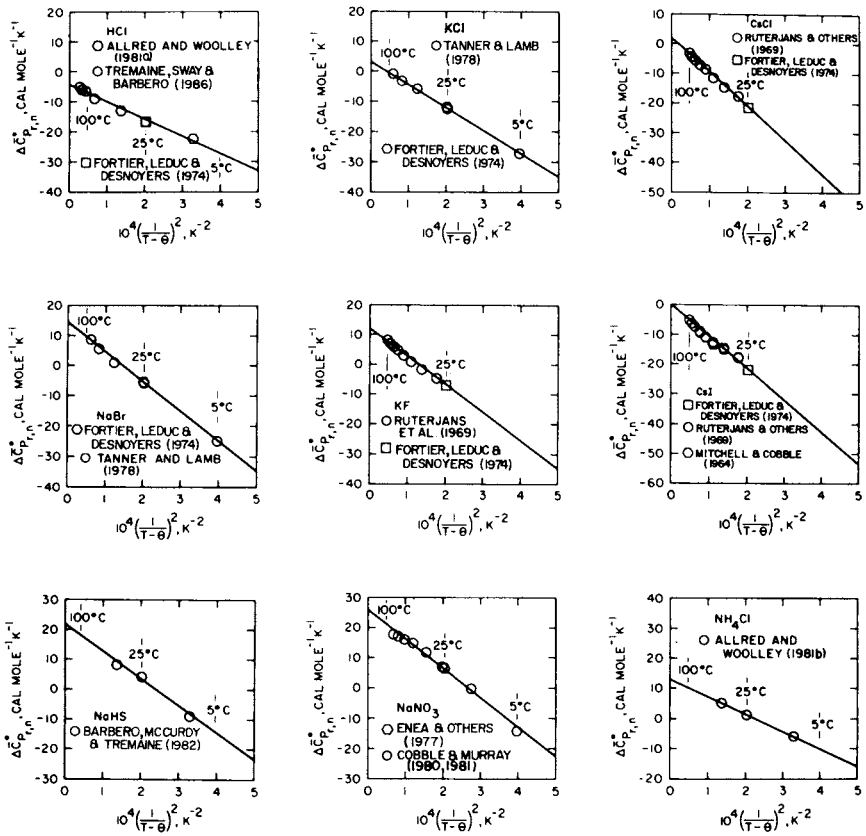

Fig. 11. Graphic representation of eq (43) for the nonsolvation contributions to the standard partial molal isobaric heat capacities ($\Delta\bar{C}^\circ_{P,n}$) of aqueous electrolytes at 1 bar (see table 1 and the caption of fig. 7).

where $\Delta_{k,P,T}$ is given by

$$\Delta_{k,P,T} = \frac{\Delta\bar{V}^\circ_{n,k,P,T} - \Delta\bar{V}^\circ_{n,k,P_r,T}}{-\Delta\bar{K}^\circ_{n,k,P_r,T}}. \tag{45}$$

Values of Ψ generated from eqs (44) and (45) using the high-pressure values of $\Delta\bar{V}^\circ_{n,k,P,T}$ represented by the symbols in figures 1 and 2 are shown in figure 12. The values of $\Delta\bar{V}^\circ_{n,k,P_r,T}$ and $-\Delta\bar{K}^\circ_{n,k,P_r,T}$ at T = 25°C and P_r = 1 bar were computed from eqs (29), (39), and (40) using the parameters for Na^+, Cl^-, K^+, and SO_4^{--} given in table 2.

The calculated values of Ψ obtained from the values of $\Delta\bar{V}^\circ_{n,k,P,T}$ for NaCl and K_2O_4 represented by the circles in figures 1 and 2 are designated by the circles and hexagons in figure 12. Uncertainty ranges

TABLE 1

Summary of the nonsolvation parameters and equation of state coefficients generated by regression of standard partial molal volume, isothermal compressibility, and isobaric heat capacity data for aqueous electrolytes as a function of temperature at 1 bar (figs. 7 through 11) with eqs (17), (18), (19), (39), (40), and (43), values of Q, N, and X in table H-1 in app. H, and Born coefficients (ω_k) computed from eqs (15), (20), and (21A and B) using values of the crystallographic radii of ions ($r_{x,j}$) given in table 3

Species	σ_k [a]	$10^{-2}\xi_k$ [b]	$10^3\left[\frac{\partial\sigma_k}{\partial P}\right]_T$ [c]	$\left[\frac{\partial\xi_k}{\partial P}\right]_T$ [d]	$c_{1,k}$ [e]	$10^{-4}c_{2,k}$ [f]
HCl	24.59	-2.253			-4.40	-5.714
LiCl	24.38	-1.875				
NaCl	28.61	-5.276	-1.556	0.3447	13.78	-8.695
KCl	37.11	-4.341	-2.058	0.3438	3.00	-7.505
CsCl	50.10	-4.953			1.87	-11.45
RbCl	41.10	-3.529				
NH_4Cl	44.58	-3.243			13.05	-5.735
NaBr			-2.665	0.3630	14.38	-9.792
KBr	45.17	-5.159	-3.167	0.3621		
KF	17.58	-3.468			11.86	-9.279
KI	58.31	-6.501				
CsI					0.00	-10.68
$NaHCO_3$	37.51	-7.001				
HNO_3			-5.228	0.2600		
KNO_3	54.04	-8.916				
$NaNO_3$			-3.815	0.4286	25.88	-9.706
NaHS	33.00	-6.680			21.59	-9.027
NaOH	9.38	-6.721	-1.275	0.5259	22.33	-13.327
KOH	17.88	-5.786			11.55	-12.137
LiOH	5.15	-3.320				
$MgCl_2$	31.91	-4.840	-0.620	0.5000	12.00	-17.32
$CaCl_2$	36.70	-6.272			0.20	-13.95
$SrCl_2$	35.81	-5.366				
$BaCl_2$	44.46	-8.322			-5.00	-14.878
Na_2SO_4	39.58	-12.90	-1.372	0.8824	38.00	-23.96

[a] $cm^3\,mole^{-1}$. [b] $cm^3\,K\,mole^{-1}$. [c] $cm^3\,mole^{-1}\,bar^{-1}$. [d] $cm^3\,K\,mole^{-1}\,bar^{-1}$.
[e] $cal\,mole^{-1}\,K^{-1}$. [f] $cal\,K\,mole^{-1}$.

for Ψ consistent with the estimated uncertainties in the values of $\Delta\overline{V}^\circ_{n,k,P,T}$ shown in figures 1 and 2 are also shown in figure 12. At all pressures, the maximum calculated value of Ψ was generated from the maximum value of $\Delta\overline{V}^\circ_{n,k,P,T}$ for K_2SO_4 and the minimum value of Ψ was obtained from the minimum value of $\Delta\overline{V}^\circ_{n,k,P,T}$ for NaCl. These maximum and minimum values are indicated by the brackets in figure 12. Uncertainty ranges for Ψ consistent with the experimental values and uncertainties

TABLE 2

Summary of the nonsolvation parameters and equation of state coefficients at 1 bar for the standard partial molal volumes, isothermal compressibilities, and isobaric heat capacities of aqueous ions computed from eqs (3) and (29) using values of σ_k, ξ_k, $(\partial\rho_k/\partial P)_T$, $(\partial\xi_k/\partial P)_T$, $c_{1,k}$ and $c_{2,k}$ for aqueous electrolytes given in table 1 or estimated in the manner described in the footnotes to the table

Ions	σ_j [a]	$10^{-2}\xi_j$ [b]	$10^3\left(\frac{\partial\sigma_j}{\partial P}\right)_T$ [c]	$\left(\frac{\partial\xi_j}{\partial P}\right)_T$ [d]	$c_{1,j}$ [e]	$10^{-4}c_{2,j}$ [f]
Li^+	-0.21	0.378	0.092[g]	0.1682[i]		
Na^+	4.02	-3.023	1.413	0.1686	18.18	-2.981
K^+	12.52	-2.088	0.911	0.1677	7.40	-1.791
Rb^+	16.51	-1.276	0.582[g]	0.1682[i]	6.06[j]	-3.764[k]
Cs^+	25.51	-2.700	0.132[g]	0.1682[i]	6.27	-5.736
NH_4^+	19.99	-0.990	-1.338[g]	0.1682[i]	17.45	-0.021
Mg^{++}	-17.27	-0.334	5.318	0.1478	20.80	-5.892
Ca^{++}	-12.48	-1.766	4.563[g]	0.1478[i]	9.00	-2.522
Sr^{++}	-13.37	-0.860	6.253[g]	0.1478[i]	6.49[j]	-2.986[k]
Ba^{++}	-4.72	-3.816	6.193[g]	0.1478[i]	3.80	-3.450
F^-	5.06	-1.380	-0.850[g]	0.1761[i]	4.46	-7.488
Cl^-	24.59	-2.253	-2.969	0.1761	-4.40	-5.714
Br^-	32.65	-3.071	-4.078	0.1944	-3.80	-6.811
I^-	45.79	-4.413	-5.131[g]	0.1944[i]	-6.27	-4.944
OH^-	5.36	-3.698	-2.688	0.3573	4.15	-10.346
NO_3^-	41.52	-6.828	-5.228	0.2600	7.70	-6.725
HCO_3^-	33.49	-3.978	-1.011[g]	0.1944[i]		
HS^-	28.98	-3.657	-2.960[h]	0.1761[i]	3.41	-6.046
SO_4^{--}	31.54	-6.854	-4.198	0.5452	1.64	-17.998

[a] $cm^3\,mole^{-1}$. [b] $cm^3\,K\,mole^{-1}$. [c] $cm^3\,mole^{-1}\,bar^{-1}$. [d] $cm^3\,K\,mole^{-1}\,bar^{-1}$. [e] $cal\,mole^{-1}\,K^{-1}$. [f] $cal\,K\,mole^{-1}$. [g] Calculated from eqs. (3), (10), (18) and (40) using experimental values of $\bar{\kappa}^\circ_j$ at 1 bar and 25°C reported by Millero (1982) together with values of $(\partial\xi_j/\partial P)_T$ shown above, ω_j from eqs. (14) and (20), $r_{x,j}$ from table 3, and $N = -1.819 \times 10^{-10}$. [h] Calculated in the manner described in footnote g assuming $\bar{\kappa}^\circ_{HS^-,P_r,T_r} = \bar{\kappa}^\circ_{Cl^-,P_r,T_r} = -0.649 \times 10^{-3}\ cm^{-3}\,mole^{-1}\ bar^{-1}$. [i] Estimated from calculated values of $(\partial\xi_j/\partial P)_T$ for ions of similar charge and radius assuming $(\partial\xi_j/\partial P)_T$ for Li^+, Rb^+, Cs^+, and NH_4^+, to be equal to the average of those for Na^+ and K^+, and $(\partial\xi_j/\partial P)_T$ for the ions in the following groups to be equal to each other: Ca^{++}, Sr^{++}, Ba^{++}, Mg^{++}; F^-, HS^-, Cl^-; I^-, HCO_3^-, Br^-. [j] Calculated from eqs. (3), (10), (19) and (43) using values of $\bar{C}^\circ_{P,k}$ for RbCl and $SrCl_2$ at 1 bar and 25°C generated by Helgeson, Kirkham, and Flowers (1981) from experimental data given by Fortier, Leduc, and Desnoyers (1974) for RbCl, and Perron, Fortier, and Desnoyers (1974) for $SrCl_2$, together with $\bar{C}^\circ_{P,Cl^-,P_r,T_r} = -29.42$, values of $c_{2,j}$ shown above, ω_j calculated from eqs. (14) and (20), $r_{x,j}$ taken from table 3, and $X = -3.09 \times 10^{-7}$. [k] Estimated from calculated values of $c_{2,j}$ for ions of similar charge and radius assuming c_2 for Rb^+ to be the average of those for Cs^+ and K^+, and Sr^{++} to be the average of those for Ca^{++} and Ba^{++}.

TABLE 3

Summary of the conventional standard partial molal Gibbs free energies of formation ($\Delta\bar{G}^\circ_{f,j}$), enthalpies of formation ($\Delta\bar{H}^\circ_{f,j}$), and entropies ($\bar{S}^\circ_{j,P_r,T_r}$) of aqueous ions ($j$) at 1 bar and 25°C, together with the crystallographic radii of ions ($r_{x,j}$) and the revised equation of state coefficients ($a_{1,j}$, $a_{2,j}$, $a_{3,j}$, $a_{4,j}$, $c_{1,j}$ and $c_{2,j}$) required to calculate the conventional standard partial molal properties of aqueous ions at high pressures and temperatures from the revised HKF model using Θ = 228 K and Ψ = 2600 bars

Ion	$\Delta\bar{G}^\circ_{f,j}$ [a,g]	$\Delta\bar{H}^\circ_{f,j}$ [a,h]	$\bar{S}^\circ_{j,P_r,T_r}$ [b,h]	$10a_{1,j}$ [c,i]	$10^{-2}a_{2,j}$ [a,j]
H^+	0.	0.	0.0	0.0	0.
Li^+	-69933.	-66552.	2.7	0.0070	-0.1488
Na^+	-62603.	-57433.	14.0	1.8390	-2.2850
K^+	-67527.	-60270.	24.2	3.5590	-1.4730
Rb^+	-67786.	-60019.	28.8	4.3080	-0.9411
Cs^+	-69732.	-61673.	31.8	6.1790	-0.2134
NH_4^+	-19000.	-31850.	26.6	3.9460	2.1630
Mg^{++}	-108502.	-111367.[o]	-33.0[u]	-0.8217	-8.5990
Ca^{++}	-132118.	-129804.	-13.5	-0.1462	-7.3780
Sr^{++}	-134766.	-131668.[p]	-7.5[p]	0.6917	10.1100
Ba^{++}	-133023.	-127510.[q]	2.3[u]	2.7220	-10.0140
F^-	-67325.	-80151.	-3.2	0.6810	1.3740
Cl^-	-31394.	-39933.	13.6	4.0320	4.8010
Br^-	-24868.	-29039.	19.8	5.2690	6.5940
I^-	-12412.	-13599.	25.5	7.7540	8.2970
OH^-	-37595.	-54977.	-2.6	-0.3899	4.3460
NO_3^-	-26504.	-49429.[r]	35.1	6.6740	8.4530
HCO_3^-	-140277.	-164898.[s]	23.5[s]	7.3760	1.6350
HS^-	2878.	-3848.[t]	16.3[t]	5.0860	4.7860
SO_4^{--}	-177934.	-217400.	4.5	4.9290	6.7880

[a] Cal mole^{-1}. [b] Cal mole^{-1} K^{-1}. [c] Cal mole^{-1}bar^{-1}. [d] Cal K mole^{-1}bar^{-1}. [e] Cal K mole^{-1}. [f] Å. [g] Computed from the values of $\Delta\bar{H}^\circ_{f,j}$ and $\bar{S}^\circ_{j,P_r,T_r}$ shown above using standard partial molal entropies of the elements taken from the source in footnote h, except for Sr and Ba which were taken from the sources in footnotes p and u, respectively. Owing to round-off differences, these values differ slightly from those given by Helgeson, Kirkham, and Flowers (1981). [h] CODATA (1978), except where indicated otherwise. [i] Calculated from eq. (37) using values of σ_j given in table 2 together with those of $a_{2,j}$ shown above and the conversion factor 41.8393 cm^3 bar cal^{-1}. [j] Calculated from eq. (41) and values of $(\partial\sigma_j/\partial P)_T$ given in table 2. [k] Computed from eq. (38) using values of ξ_j given in table 2 and those of $a_{4,j}$ shown above. [l] Calculated from eq. (42) and values of $(\partial\xi_j/\partial P)_T$ given in table 2.

TABLE 3
(Continued)

Ion	$a_{3,j}$ [d,k]	$10^{-4}a_{4,j}$ [e,l]	$c_{1,j}$ [b,m]	$10^{-4}c_{2,j}$ [e,m]	$r_{x,j}$ [f,n]
H^+	0.0	0.0	0.0	0.0	2.142[v]
Li^+	11.3600	-2.72			0.68
Na^+	3.2560	-2.726	18.18	-2.981	0.97
K^+	5.4350	-2.712	7.40	-1.791	1.33
Rb^+	7.4070	-2.72	6.06	-3.764	1.47
Cs^+	4.0030	-2.72	6.27	-5.736	1.67
NH_4^+	8.0900	-2.72	17.45	-0.021	1.37[w]
Mg^{++}	8.3900	-2.390	20.80	-5.892	0.66
Ca^{++}	4.9670	-2.390	9.00	-2.522	0.99
Sr^{++}	7.1330	-2.390	6.49	-2.986	1.12
Ba^{++}	0.0676	-2.390	3.80	-3.450	1.34
F^-	7.6490	-2.847	4.46	-7.488	1.33
Cl^-	5.5630	-2.847	-4.40	-5.714	1.81
Br^-	4.7450	-3.143	-3.80	-6.811	1.96
I^-	1.5380	-3.143	-6.27	-4.944	2.20
OH^-	13.3700	-5.777	4.15	-10.346	1.40[x]
NO_3^-	-0.1563	-4.204	7.70	-6.725	2.81[w]
HCO_3^-	2.5770	-3.143			2.17[w]
HS^-	2.2070	-2.847	3.41	-6.046	1.84[x]
SO_4^{--}	17.5100	-8.816	1.64	-17.998	3.14[w]

[m] From table 2. [n] Ahrens (1952), except where indicated otherwise. [o] Shin and Criss (1979). [p] Busenburg, Plummer, and Parker (1984). [q] Morss and Williams (1983). [r] Cox, Harrop, and Head (1979). [s] Berg and Vanderzee (1978). [t] Barbero, McCurdy, and Tremaine (1982). [u] Wagman et al. (1982). [v] Computed from eqs. (15), (20) and (21a and b) using the regression value of $\omega_{HCl} = 1.4560 \times 10^5$ cal mole^{-1} reported by Helgeson and Kirkham (1976) and the value of r_{x,Cl^-} shown above. [w] Computed from eqs. (20) and (21a, and b) using values of $\bar{S}°_{j,P_r,T_r}$ shown above and the $r_{e,j}$ estimation correlation with $\bar{S}°_{j,P_r,T_r}$ given by Helgeson and Kirkham (1976). [x] Assuming $r_{x,OH^-} = r_{x,O^{--}}$ and $r_{x,HS^-} = r_{x,S^{--}}$ using radii taken from Pauling (1927).

of $\Delta\bar{V}°_{n,k,P,T}$ for both NaCl and K_2SO_4 are indicated by the vertical bars in figure 12.

If only the circles and hexagons in figure 12 are considered, Ψ would appear to be a function of both pressure and the identity of the aqueous electrolyte. However, it can be seen that a constant value of Ψ = 2600 bars falls within the uncertainty range represented by the vertical bars at all pressures. The values of the equation of state coefficients $a_{1,j}$, $a_{2,j}$, $a_{3,j}$, and $a_{4,j}$ for aqueous ions given in table 3 were calculated from eqs (37), (38), (41), and (42) using Ψ = 2600 bars and the values of the nonsolvation parameters σ_j, ξ_j, $(\partial\sigma_j/\partial P)_T$, and $(\partial\xi_j/\partial P)_T$ for 1 bar shown in table 2. The equation of state coefficients given in table 3, together with eqs (17), (29), and (F-1) in app. F permit prediction of $\bar{V}°_k$ for aqueous electrolytes at high pressures. Curves representing predicted

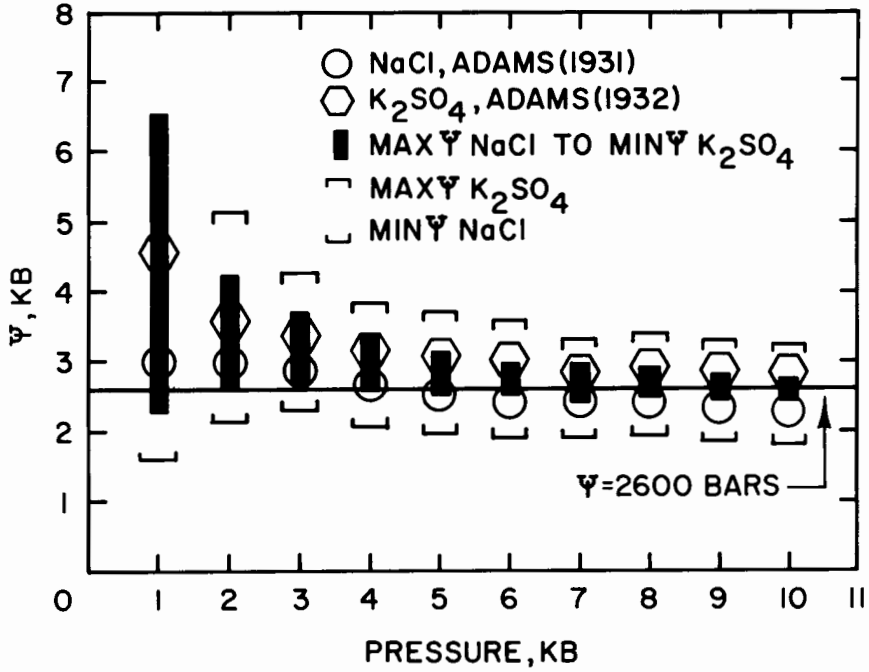

Fig. 12. Computed values of the Ψ parameter from eqs (44) and (45) as a function of pressure at 25°C—see text.

values of $\overline{V}_k^\circ$ for KCL, Na_2SO_4, K_2SO_4, $MgCl_2$, and NaCl at high pressures and temperatures can be compared with their experimental counterparts represented by symbols in figures 13 through 18. The close agreement of the predicted values of $\overline{V}_k^\circ$ and the experimental data shown in figures 13 through 18 supports the functional form of the pressure dependence of $\overline{V}^\circ$ in the revised HKF model, as well as the value of 2600 bars for the solvent parameter Ψ. The correspondence of the curves and symbols shown in figure 18 also indicates that even at temperatures as high as 400°C, the solvation contribution $\Delta\overline{V}_s^\circ$ from the HKF model eq (17) combined with the nonsolvation contribution $\Delta\overline{V}_s^\circ$ from the revised HKF model (eq F-1 in app. F) permits close approximation of $\overline{V}_k^\circ$ at high pressures. These observations constrain the pressure and temperature region in which Born coefficients and effective electrostatic radii of aqueous ions must be regarded as functions of pressure and temperature.

Retrieval of fit coefficients for g.—Because more experimental volumes and heat capacities at high temperatures and low pressures are available for NaCl solutions than for other electrolytes, values of $\overline{V}^\circ$ and $\overline{C}_p^\circ$ generated from these data were selected for regression retrieval of the array of coefficients a_{ij} in eqs (36A, B, and C). The Born coefficient of

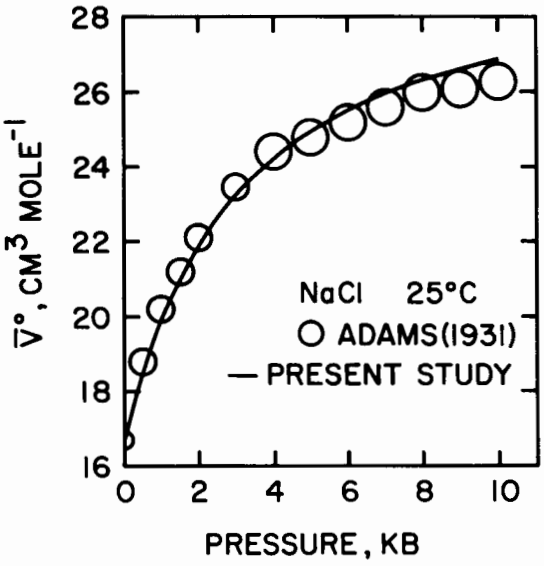

Fig. 13. Standard partial molal volume ($\bar{V}^\circ$) of NaCl as a function of pressure at 25°C (see text). The symbols represent experimental data, but the curves correspond to independently predicted values using the revised HKF model with Ψ = 2600 bars for $\Delta\bar{V}_n^\circ$ and the original HKF model for $\Delta\bar{V}_s^\circ$(eq 17).

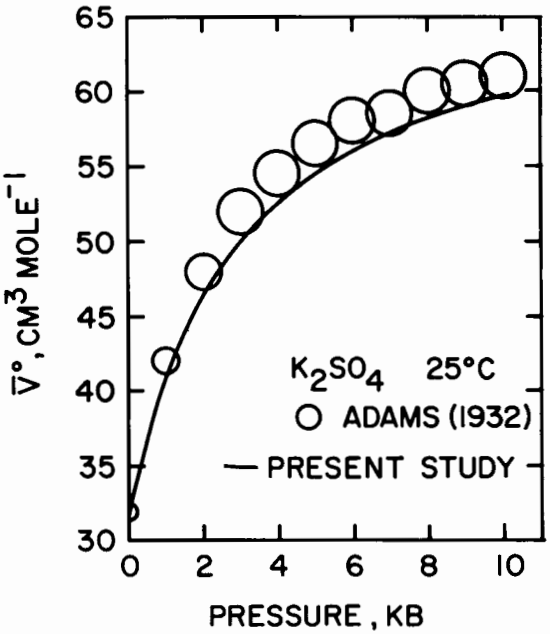

Fig. 14. Standard partial molal volume ($\bar{V}^\circ$) of K_2SO_4 as a function of pressure at 25°C (see text and the caption of fig. 13).

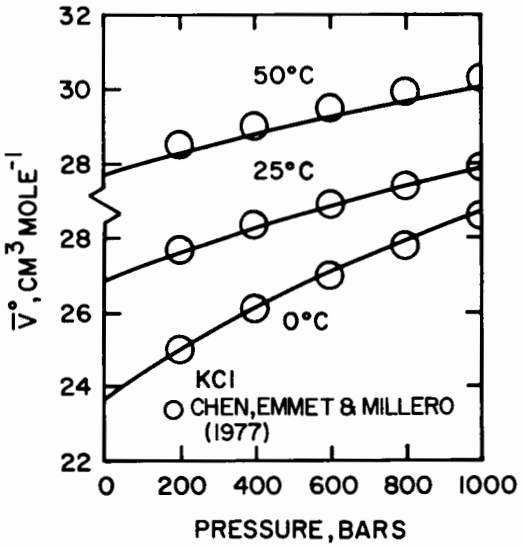

Fig. 15. Standard partial molal volume ($\bar{V}^\circ$) of KCl as a function of pressure at 0°, 25°, and 50°C (see text and the caption of fig. 13).

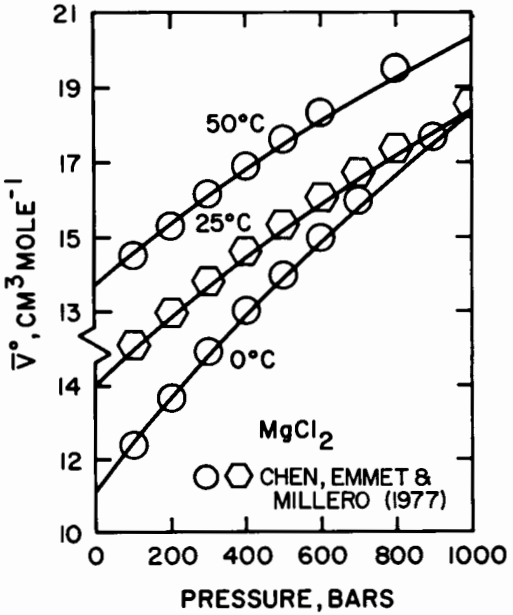

Fig. 16. Standard partial molal volume ($\bar{V}^\circ$) of $MgCl_2$ as a function of pressure at 0°, 25°, and 50°C (see text and the caption of fig. 13).

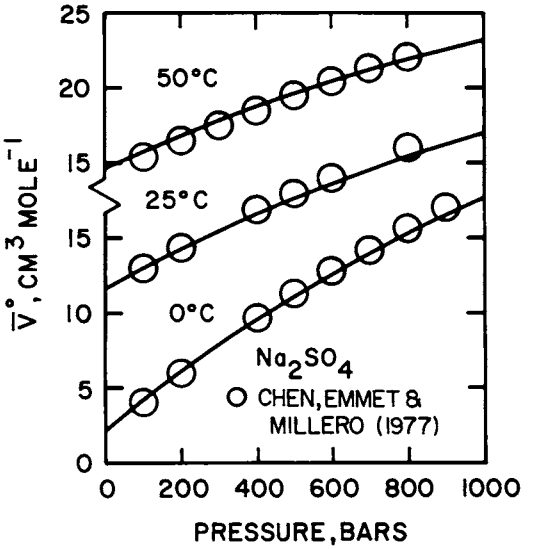

Fig. 17. Standard partial molal volume ($\bar{V}^\circ$) of Na_2SO_4 as a function of pressure at 0°, 25°, and 50°C (see text and the caption of fig. 13).

an aqueous electrolyte and its pressure and temperature derivatives are expressed in terms of g and its pressure and temperature derivatives in the equations given in app. B. Substitution of app. B eqs (B-1), (B-2), (B-4), and (B-6) in eqs (G-1) and (G-4) in app. G leads to

$$\Delta\bar{V}^\circ_{s,k} = -\eta[(1.91 + g)^{-1} + (1.81 + g)^{-1}]\,Q + \left(\frac{\partial g}{\partial P}\right)_T X_1 \left(\frac{1}{\epsilon} - 1\right) \quad (46)$$

and

$$\Delta\bar{C}^\circ_{P,s,k} = -\eta\,[(1.91 + g)^{-1} + (1.81 + g)^{-1}]TX + 2TY\left(\frac{\partial g}{\partial T}\right)_P X_1 - T\left(\frac{1}{\epsilon} - 1\right)\left[\left(\frac{\partial g}{\partial T}\right)^2_P X_2 + \left(\frac{\partial^2 g}{\partial T^2}\right)_P X_1\right], \quad (47)$$

where X_1 and X_2 are given by eqs (B-7) and (B-8) in app. B. Expressions for $(\partial g/\partial P)_T$, $(\partial g/\partial T)_P$, and $(\partial^2 g/\partial T^2)_P$ in terms of the a_{ij} coefficients are given by eqs (C-2), (C-3), and (C-5) in app. C, respectively. These equations, together with eqs (36A, B, and C), (46), and (47) permit regression of experimental values of $\Delta\bar{V}^\circ_{s,k}$ and $\Delta\bar{C}^\circ_{P,s,k}$ to retrieve values of the a_{ij} coefficients.

The values of $\Delta\bar{V}^\circ_{s,k}$ and $\Delta\bar{C}^\circ_{P,s,k}$ for NaCl used in the regression calculations described above were computed from the experimental values of $\bar{V}^\circ_{NaCl}$ and $\bar{C}^\circ_{P,NaCl}$ given in tables 4 and 5 using eqs (10), (29), (F-1), and (F-4) in app. F and the equation of state coefficients for Na^+

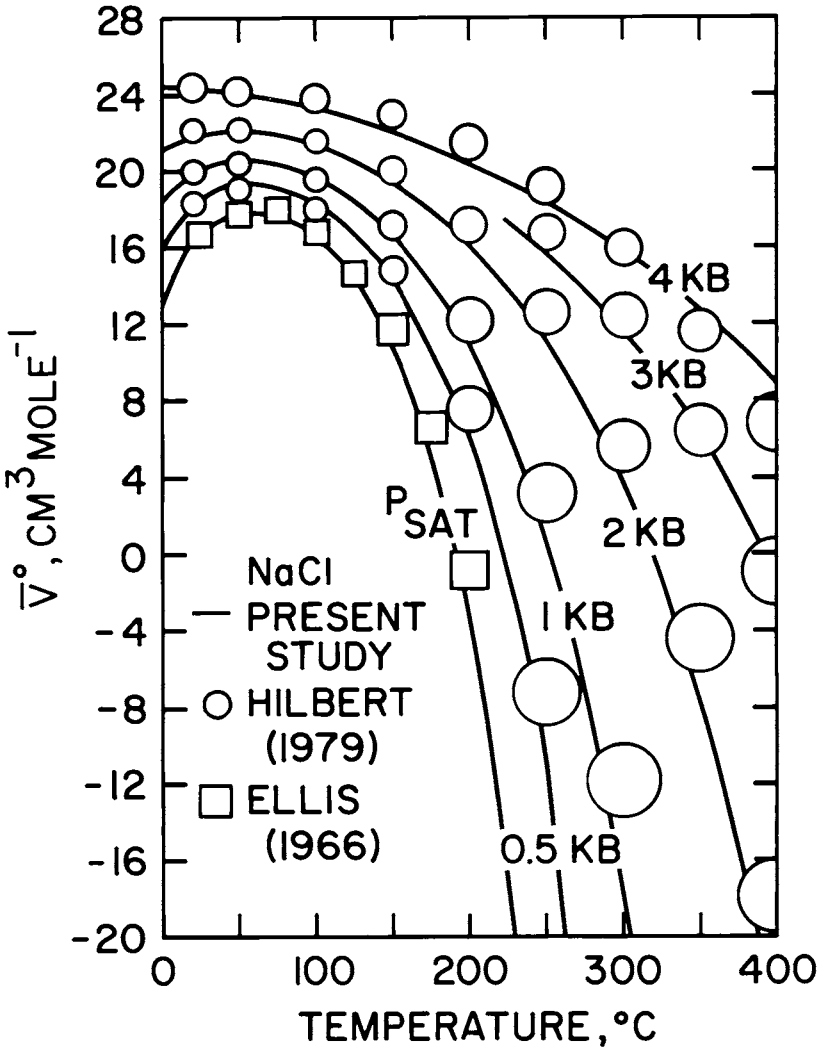

Fig. 18. Standard partial molal volume ($\overline{V}^\circ$) of NaCl as a function of temperature at P_{SAT} and constant pressures. P_{SAT} refers to liquid-vapor saturation pressures for H_2O (see text and the caption of fig. 13).

and Cl^- shown in table 3. Comparison of predicted values of $\overline{V}_k^\circ$ and $\overline{C}_{P,k}^\circ$ with their experimental counterparts in figures 3 through 6 and 13 through 18 suggest that g is negligible and Born coefficients are therefore essentially constant at higher pressures or lower temperatures than those represented by the dashed curve in figure 19. Consequently, g, $(\partial g/\partial P)_T$, $(\partial g/\partial T)_P$, and $(\partial^2 g/\partial T^2)_P$ were taken to be zero at these

TABLE 4

Experimental (Exp.) and calculated (Calc.) high temperature/pressure values of the standard partial molal volume ($\bar{V}°$) of NaCl in cm^3 $mole^{-1}$.

T (°C)	P (Bars)	$\bar{V}°$[a] Exp.	$\bar{V}°$[b] Calc.	T (°C)	P (Bars)	$\bar{V}°$[a] Exp.	$\bar{V}°$[b] Calc.
225.0	200.0	-6.0[c]	-6.4	250.0	99.2	-25.5[e]	-26.0
250.0	200.0	-18.5[c]	-19.2	250.0	197.4	-19.0[e]	-19.4
275.0	200.0	-39.0[c]	-39.6	250.0	492.0	-7.5[e]	-7.7
300.0	200.0	-75.0[c]	-75.3	250.0	786.5	0.0[e]	-1.5
325.0	200.0	-153.0[c]	-152.7	274.9	99.2	-51.5[e]	-52.7
350.0	200.0	-420.0[c]	-420.4	274.9	197.4	-39.5[e]	-39.7
274.9	109.3	-48.5[d]	-51.1	274.9	492.0	-18.0[e]	-19.6
274.9	245.8	-33.0[d]	-35.0	274.9	786.5	-8.0[e]	-9.9
274.9	371.3	-24.0[d]	-25.8	300.0	99.2	-107.5[e]	-107.7
324.3	206.5	-147.0[d]	-145.2	300.0	197.4	-78.5[e]	-76.0
324.3	387.8	-81.0[d]	-80.1	300.0	492.0	-37.0[e]	-37.0
				300.0	786.5	-19.5[e]	-21.3

[a] Generated by regression of experimental apparent molal volumes (Φ_V) of NaCl solutions reported by the sources in footnotes c, d, and e with the Φ_V equation given by Helgeson and Kirkham (1976). [b] Computed from eqn (46), and eqns (C-1a, b, and c), (C-2), (C-7), (D-2), (E-1), (E-2) and (F-1) in apps. C, D, and E using coefficients given in tables 3, C-1 and E-1. [c] Grant-Taylor (1981). [d] Gates (1985). [e] L'vov, Zarembo, and Gilyarov (1981).

TABLE 5

Experimental (Exp.) and calculated (Calc.) high temperature/pressure values of the standard partial molal isobaric heat capacity ($\bar{C}_P^o$) of NaCl in cal $mole^{-1}$ K^{-1}

T (°C)	P (Bars)	$\bar{C}_P^{o}$[a] Exp.	$\bar{C}_P^{o}$[b] Calc.	T (°C)	P (Bars)	$\bar{C}_P^{o}$[a] Exp.	$\bar{C}_P^{o}$[b] Calc.
180.0	10.0	-42.0[c,d]	-43.1	217.9	177.0	-56.0[f]	-57.5
200.0	15.5	-54.5[c,e]	-55.4	224.6	177.0	-61.5[f]	-62.9
250.0	39.7	-122.0[e]	-120.0	276.0	177.0	-143.0[f]	-146.
300.0	85.8	-365.0[e]	-385.0	299.0	177.0	-246.0[f]	-247.
350.0	165.2	-4450.0[e]	-4444.0	330.2	177.0	-748.0[f]	-745.
225.6	49.6	-78.0[f]	-76.6	225.6	179.0	-61.0[g]	-63.6
225.6	101.0	-71.0[f]	-70.9	275.9	179.0	-146.0[g]	-145.
275.9	101.0	-183.0[f]	-178.0	300.3	179.0	-254.0[g]	-254.
299.0	100.0	-341.0[g]	-344.0	324.7	179.0	-570.0[g]	-571.

[a] Generated by regression of experimental apparent molal isobaric heat capacities (Φ_{C_P}) of NaCl solutions reported by the sources shown in footnotes c, d, e, f and g with the Φ_{C_P} equation given by Helgeson, Kirkham, and Flowers (1981). [b] Computed from eq. (47), and eqs. (C-1a, b, and c), (C-3), (C-5), (C-7), (C-8), (D-1), (D-4), (E-1), (E-3), (E-5) and (F-4) in apps. C, D, E, and F using coefficients taken from tables 3, C-1 and E-1. [c] Likke and Bromley (1973). [d] Cobble and Murray (1981). [e] Puchkov, Styazhkin, and Fedorov (1976). [f] Gates (1985). [g] Smith-Magowan and Wood (1981).

pressures and temperatures as well as at selected pressures and temperatures along the dashed curve in figure 19. These values were then regressed simultaneously with the experimental values of $\Delta\overline{V}^{\circ}_{s,NaCl}$ and $\Delta\overline{C}^{\circ}_{P,s,NaCl}$ which generated the a_{ij} coefficients given in table C-1 in app. C. It should be emphasized that the values of g apply only to the shaded pressure-temperature region shown in figure 19.

The pressures and temperatures in the shaded area of figure 19 are bounded by eqs (C-9) and (C-10) in app. C. The dashed curve in figure 19 was chosen to minimize discontinuities in $\overline{V}^{\circ}_{k}$ and $\Delta\overline{C}^{\circ}_{P,k}$ of electrolytes along the curve. However, values of g computed from eq (C-1A, B, and C) in app. C for pressures and temperatures slightly below the dashed curve in figure 19 may be positive. These small positive values should be regarded as zero.

Values of $\overline{V}^{\circ}_{NaCl}$ and $\overline{C}^{\circ}_{P,NaCl}$ computed from the revised HKF model using the a_{ij} coefficients in table C-1 compare favorably with their experimental counterparts. For example, it can be seen in table 4 that the maximum absolute difference between the calculated and experimental values of $\overline{V}^{\circ}_{NaCl}$ is 2.6 cm^3mole^{-1}, and most of the differences are within ± 1.5 cm^3mole^{-1}. Similarly, the majority of the calculated values of $\overline{C}^{\circ}_{P,NaCl}$ in table 4 are within ~2 cal $mole^{-1}K^{-1}$ of the experimental values. Modification of the empirical equation for g (eq 36A, B, and C) to reduce the differences between the calculated and experimental values shown in tables 3 and 4 was not attempted, because the differences are not systematic and all the differences are less than the likely uncertainties in the experimental values.

Values of $\overline{V}^{\circ}_{k}$ and $\overline{C}^{\circ}_{Pk}$ at high temperatures and low pressures predicted from the revised HKF model can be compared with their

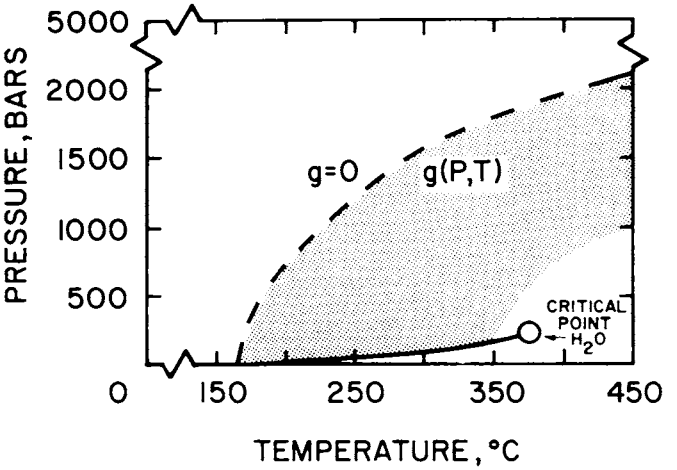

Fig. 19. Pressure and temperature region (shaded) in which the value of g is non-zero and consistent with eqs (36A, B, and C).

experimental counterparts in figures 20 through 23. The close agreement of the predicted curves with the symbols representing the experimental values strongly supports the revised equations for the effective electrostatic radius of aqueous ions (eqs 34 and 35), as well as the functional form of the empirical equation for g (eq 36A, B, and C or C-1A, B, and C).

Values of g and its pressure and temperature derivatives generated from the equations and coefficients given in app. C are represented by the isobaric and isothermal curves in figures 24 and 25. Uncertainties in the derivatives of g increase rapidly as pressures and temperatures approach the boundary of the shaded region in figure 19 which is closest to the critical point of H_2O. Consequently, eqs (C-2) through (C-8) in app. C should not be used outside the shaded pressure/temperature

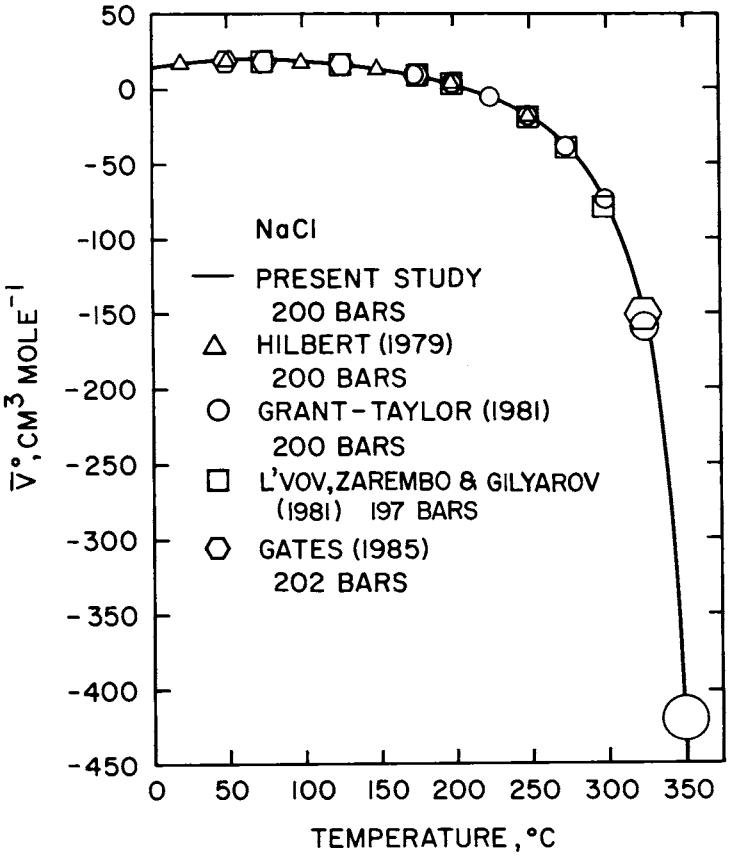

Fig. 20. Standard partial molal volume ($\bar{V}°$) of NaCl as a function of temperature at ~200 bars. The symbols represent experimental data, but the curves correspond to independently predicted values from the revised HKF model (see text).

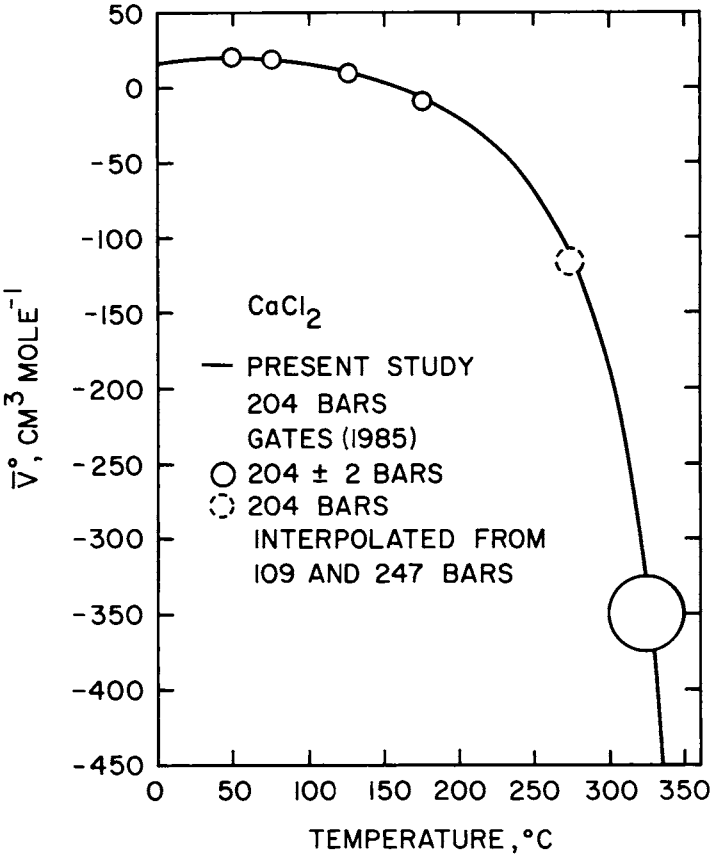

Fig. 21. Standard partial molal volume ($\bar{V}^\circ$) of $CaCl_2$ as a function of temperature at ~204 bars (see caption of fig. 20).

region in figure 19. Because the calculated values of g and its pressure and temperature derivatives are not necessarily identical to zero at the pressures and temperatures corresponding to the dashed curve in figure 19, predicted values of the standard partial molal properties of aqueous species from the revised HKF model may exhibit small discontinuities at the pressures and temperatures represented by this curve. These discontinuities should have a negligible effect on most geochemical calculations.

As indicated above, eqs (36A, B, and C or C-1A, B, and C) cannot be used to estimate reliable values of g at temperatures higher than those indicated by the shaded region in figure 19. However, because many geochemical processes occur at pressures and temperatures in the critical region of H_2O, values of g have been graphically extrapolated into this region. These values are represented by the dashed curves in

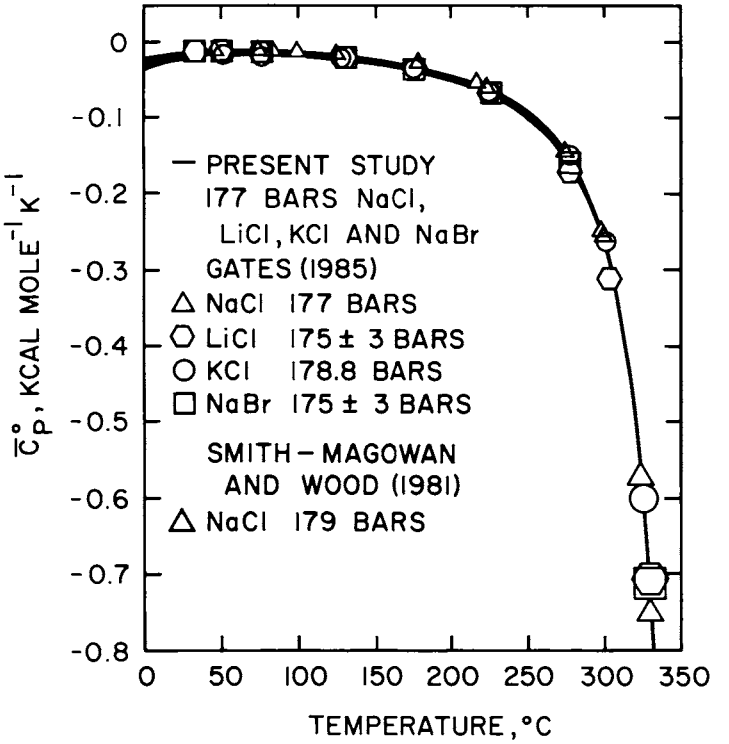

Fig. 22. Standard partial molal isobaric heat capacities ($\overline{C}^{\circ}_P$) of NaCl, KCl, LiCl, and NaBr as functions of temperature at ~177 bars (see caption of fig. 20).

figure 26. Values of the dielectric constant of H_2O (ϵ) at temperatures greater than 450°C calculated from the equations given by Pitzer (1983) are given in table 6. The dashed curves shown in figure 26 can be used together with the values of ϵ given in table 6 to calculate rough estimates of $\Delta\overline{G}^{\circ}$ for aqueous ions and electrolytes to temperatures of 1000°C. It should be emphasized in this regard that the partial derivatives of the dashed curves in figure 26 are not reliable.

SUMMARY OF THE REVISED EQUATIONS OF STATE

Revised expressions for the nonsolvation ($\Delta\overline{\Xi}^{\circ}_n$) and solvation ($\Delta\overline{\Xi}^{\circ}_s$) contributions to the standard partial molal properties ($\overline{\Xi}^{\circ}$) of aqueous species are given in apps. F and G, respectively. These equations permit derivation of the revised expressions for the standard partial molal volume ($\overline{V}^{\circ}$), isothermal compressibility ($\overline{\kappa}^{\circ}$), expansibility ($\overline{E}^{\circ}_x$), isobaric heat capacity ($\overline{C}^{\circ}_P$), and entropy ($\overline{S}^{\circ}$) of the kth aqueous electrolyte or the jth ion, which are given in app. A (eqs A-1 through A-5). The revised equations for the change in the standard partial molal enthalpy ($\overline{H}^{\circ} - \overline{H}^{\circ}_{P_r,T_r}$) and Gibbs free energy ($\overline{G}^{\circ} - \overline{G}^{\circ}_{P_r,T_r}$) from the reference pressure

(P_r) and temperature (T_r) of 1 bar and 298.15 K to the pressure and temperature of interest correspond to eqs (A-6) and (A-7). Calculation of the apparent standard partial molal enthalpy of formation ($\Delta\overline{H}°$) and the apparent standard partial molal Gibbs free energy of formation ($\Delta\overline{G}°$) of an ion or electrolyte can be carried out by combining eqs (A-6) and (A-7) with

$$\Delta\overline{H}° \equiv \Delta\overline{H}^{\circ}_{f} + (\overline{H}° - \overline{H}^{\circ}_{P_r,T_r}) \tag{48}$$

and

$$\Delta\overline{G}° \equiv \Delta\overline{G}^{\circ}_{f} + (\overline{G}° - \overline{G}^{\circ}_{P_r,T_r}) \tag{48}$$

where $\Delta\overline{H}^{\circ}_{f}$ and $\Delta\overline{G}^{\circ}_{f}$ denote the standard partial molal enthalpy and Gibbs free energy of formation from the elements of the aqueous ion or electrolyte at P_r and T_r.

Values of the equation of state coefficients for the jth aqueous ion represented by $a_{1,j}$, $a_{2,j}$, $a_{3,j}$, $a_{4,j}$, $c_{1,j}$, and $c_{2,j}$, together with the

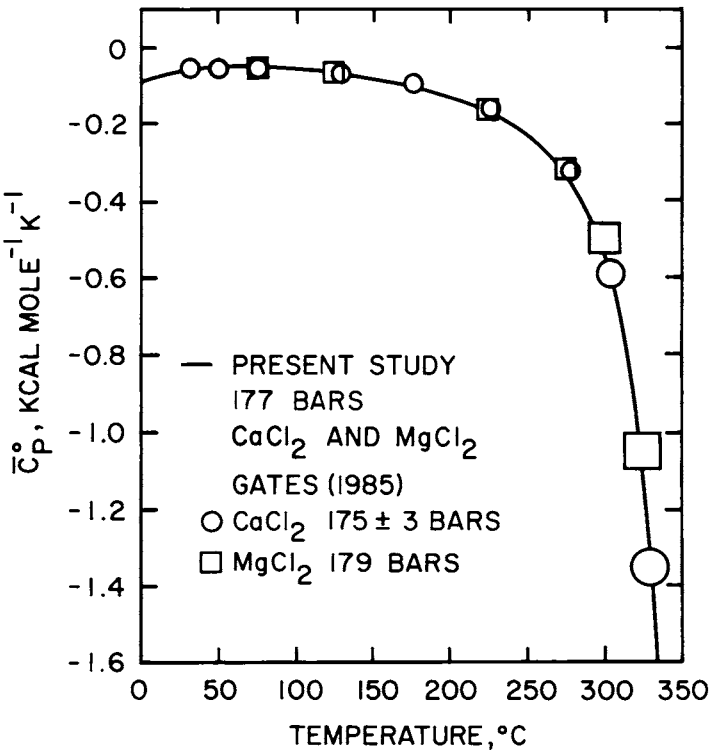

Fig. 23. Standard partial molal isobaric heat capacities ($\overline{C}^{\circ}_{P}$) of $CaCl_2$ and $MgCl_2$ as functions of temperature at ~177 bars (see caption of fig. 20).

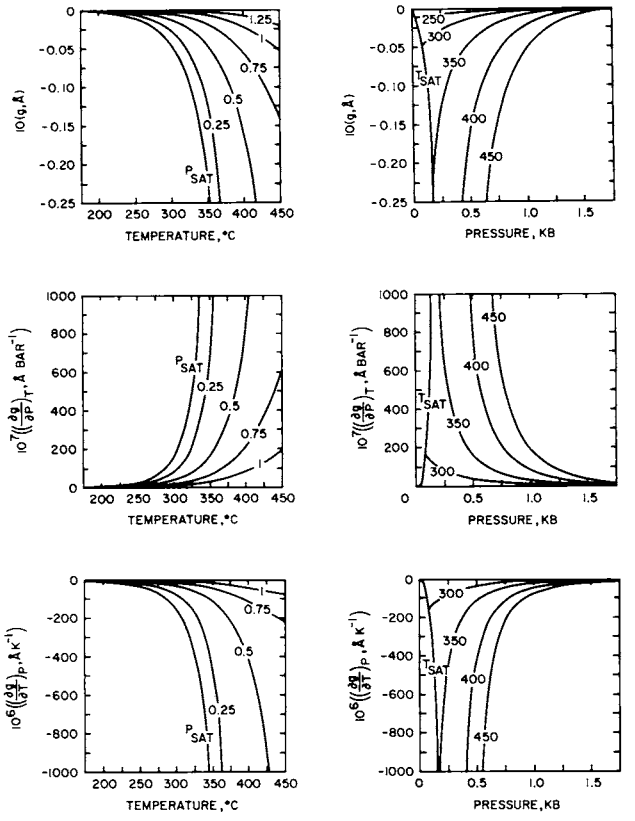

Fig. 24. Solvent function g and its first derivatives as functions of pressure and temperature computed using equations and coefficients given in app. C.

crystallographic radii ($r_{x,j}$) and the conventional standard partial molal entropies ($\bar{S}^{\circ}_{j,P_r,T_r}$), enthalpies of formation ($\Delta\bar{H}^{\circ}_{f,j}$), and Gibbs free energies of formation ($\Delta\bar{G}^{\circ}_{f,j}$) at P_r and T_r are given in table 3. The coefficients and thermodynamic data for the ions given in table 3 permit calculation of $a_{1,k}$, $a_{2,k}$, $a_{3,k}$, $a_{4,k}$, $c_{1,k}$, and $c_{2,k}$ for the kth aqueous electrolyte from eq (29) and $\bar{S}^{\circ}_{k,P_r,T_r}$, $\Delta\bar{H}^{\circ}_{f,k}$, and $\Delta\bar{G}^{\circ}_{f,k}$ from eq (3).

The Born coefficient of the kth aqueous electrolyte (ω_k) or the jth aqueous ion (ω_j), together with their pressure and temperature derivatives are given by eqs (B-1) through (B-11) in app. B. The values of g and its pressure and temperature derivatives required to evaluate eqs (B-1) through (B-11) can be calculated from eqs (C-1) through (C-8) and the coefficients given in table C-1 in app. C. The Born functions represented by Y, Q, N, X, and U are expressed in terms of the dielectric constant of H_2O (ϵ) and its pressure and temperature derivatives in eqs (D-1) through (D-5) in app. D. At temperatures below 100°C and pressures

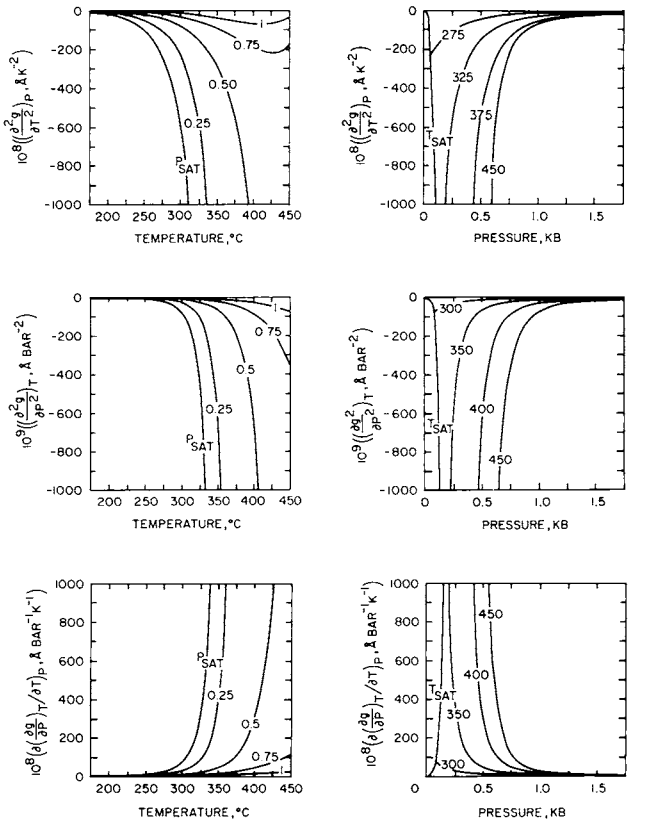

Fig. 25. Second derivatives and the cross-derivative of g as functions of pressure and temperature computed using equations and coefficients given in app. C.

above 1 kb, the values of ϵ and its pressure and temperature derivatives used in the present study were generated by extrapolating equations given by Bradley and Pitzer (1979). At all other pressures and temperatures, the values of ϵ and its pressure and temperature derivatives were calculated using equations and coefficeints taken from Helgeson and Kirkham (1974) which are given in app. E. At the boundary of the pressure and temperature regions in which these two equations for ϵ are valid, slight discontinuities occur in the predicted standard partial molal properties of aqueous species. These discrepancies are small enough that they should have a negligible effect on geochemical calculations.

To facilitate application of the revised HKF equations to geochemical calculations, values of ϵ, Y, Q, N, X, U, g, and the pressure and temperature derivatives of g are given in app. H for various pressures and temperatures of geologic interest. These values, combined with the

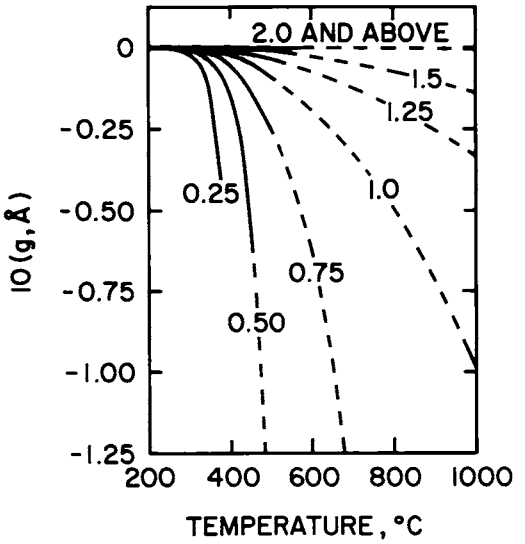

Fig. 26. Graphically extrapolated values of the solvent fraction g to 1000°C at pressures from 0.25 to 2 kb (see text).

coefficients given in table 3 and the equations summarized in apps. A and B permit calculation of the standard partial molal properties of aqueous ions and electrolytes at pressures from those corresponding to vapor-liquid saturation for H_2O to 5 kb and temperatures from 0° to 450°C.

TABLE 6

Values of the dielectric constant of H_2O at temperatures from 475° to 1000°C and pressures from 0.5 to 5 kb computed from the equations given by Pitzer (1983) and Haar, Gallagher, and Kell (1980)

T	PRESSURE, KB								
(°C)	0.5	0.75	1.0	1.25	1.5	2	3	4	5
475	4.89	8.76	10.90	12.34	13.44	15.10	17.40	19.02	20.27
500	3.76	7.17	9.45	10.98	12.14	13.86	16.20	17.82	19.05
550	2.73	4.91	7.03	8.64	9.87	11.69	14.09	15.72	16.94
600	2.26	3.68	5.34	6.81	8.03	9.87	12.31	13.95	15.16
650	1.99	3.00	4.24	5.48	6.58	8.36	10.79	12.44	13.65
700	1.82	2.58	3.52	4.53	5.49	7.14	9.51	11.14	12.34
750	1.69	2.29	3.04	3.85	4.67	6.16	8.42	10.01	11.21
800	1.60	2.09	2.69	3.36	4.05	5.37	7.49	9.04	10.22
850	1.52	1.93	2.43	3.00	3.58	4.74	6.71	8.20	9.35
900	1.47	1.82	2.24	2.71	3.22	4.24	6.04	7.47	8.59
950	1.42	1.72	2.08	2.49	2.93	3.83	5.48	6.83	7.91
1000	1.38	1.64	1.96	2.32	2.70	3.49	5.00	6.27	7.31

HIGH PRESSURE AND TEMPERATURE PREDICTIONS
FROM THE REVISED EQUATIONS OF STATE

Comparison of predicted and experimental dissociation constants for H_2O.—Few experimental studies of the standard partial molal properties of aqueous electrolyes have been carried out over extensive ranges of temperature and pressure. Among those that have not already been considered above, experimental dissociation constants for H_2O at temperatures to 300°C and pressures to 5 kb can be compared in detail to independently predicted values to evaluate the efficacy of the revised HKF model.

Differences (δ log K_w) between experimental (Sweeton, Mesmer, and Baes, 1974) and predicted values of log K_w (δ log K_w = the experimental log K_w − the predicted log K_w) at 1 bar for temperatures below 100°C and at vapor-liquid saturation pressures for H_2O at temperatures from 100° to 300°C are given in table 7. Corresponding differences for the change in the standard molal Gibbs free energy of this reaction (δ $\Delta\overline{G}_r^\circ$) are also listed in table 7. The values of (δ log K_w) and (δ $\Delta\overline{G}_r^\circ$) in table 7 can be compared with estimated uncertainties in log K_w ($\pm$log K_w) and $\Delta\overline{G}_r^\circ$ ($\pm\Delta\overline{G}_r^\circ$) reported by Sweeton, Mesmer, and Baes (1974). The experimental values of log K_w at 1 bar and vapor-liquid saturation

TABLE 7

Predicted and experimental values of log K_w at 1 bar and vapor-liquid saturation pressures of H_2O at temperatures >75°C

T (°C)	log K_w [a]	δlog K_w [b]	$\pm$log K_w [c]	$\Delta\overline{G}_r^\circ$ [a,d]	$\delta\Delta\overline{G}_r^\circ$ [b,e]	$\pm\Delta\overline{G}_r^\circ$ [c,e]
0	-14.939	-0.002	0.009	18.672	+2	9
25	-13.995	+0.002	0.009	19.093	-3	9
50	-13.272	0.000	0.006	19.624	0	12
75	-12.706	-0.003	0.006	20.241	+4	12
100	-12.261	-0.003	0.009	20.934	+5	12
125	-11.912	-0.002	0.009	21.702	+2	18
150	-11.645	+0.003	0.012	22.547	-6	21
175	-11.451	+0.010	0.012	23.482	-22	24
200	-11.309	+0.007	0.012	24.484	-16	24
225	-11.225	+0.003	0.012	25.586	-8	27
250	-11.198	+0.002	0.015	26.805	-4	36
275	-11.230	+0.006	0.027	28.167	-16	69
300	-11.331	+0.030	0.045	29.717	-79	117
325	-11.526			31.546		
350	-11.879			33.870		
360	-12.096			35.043		

[a] Predicted values from the revised HKF model. [b] Experimental values reported by Sweeton, Mesmer and Baes (1974), minus corresponding values from the revised HKF model. [c] Estimated uncertainties in the experimental values reported by Sweeton, Mesmer and Baes (1974). [d] kcal mole^{-1}. [e] cal mole^{-1}.

pressures given by Sweeton, Mesmer, and Baes (1974) were generated by simultaneously regressing (1) potentiometric data for temperatures from 0° to 300°C and ionic strengths from 0.02 to 3.0, (2) values of $\Delta\overline{H}_r^\circ$ determined from calorimetric data at temperatures from 0° to 55°C, and (3) values of log K_w calculated from conductance data at temperatures from 51° to 271°C. The regression calculations were carried out with an empirical equation to describe the temperature dependence of log K_w, together with a semiempirical expansion of the Debye-Hückel equation to include higher order terms in temperature and ionic strength. The resulting estimated uncertainties in log K_w ($\pm$log K_w) represent ± 3 standard deviations from the regression values. Values of $\Delta\overline{G}_r^\circ$ and log K_w predicted in the present study are also given in table 7. The values of $\Delta\overline{G}_r^\circ$ were calculated from $\Delta\overline{G}^\circ_{H_2O}$ obtained from the equation of state for H_2O developed by Haar, Gallagher, and Kell (1980) using predicted values of $\Delta\overline{G}^\circ_{OH^-}$ generated from eqs (49) and (A-5) in app. A using the equation of state coefficients for OH^- given in table 3.

It can be seen by comparison of the values of δ log K_w and $\delta\ \Delta\overline{G}_r^\circ$, respectively, with those of $\pm$log K_w and $\pm\Delta\overline{G}_r^\circ$ in table 7, that the differences between the experimental and predicted values of log K_w and $\Delta\overline{G}_r^\circ$ are less than the estimated uncertainties in the corresponding experimental values at all temperatures. In the temperature range where extensive experimental data are available (0°–275°C), the maximum values of $\pm$log K_w and $\pm\Delta\overline{G}_r^\circ$ are 0.027 log units and ± 69 cal mole^{-1}. In contrast the maximum values of δ log K_w are $\delta\ \Delta\overline{G}_r^\circ$ are 0.010 log units and -22 cal mole^{-1}. For the same temperature range, the average values of $\pm$log K_w and $\pm\Delta\overline{G}_r^\circ$ are 0.012 log units and 22.8 cal mole^{-1}, which are larger than the average absolute values of δ log K_w (0.004 log units) and $\delta\Delta\overline{G}_r^\circ$(7.3 cal mole^{-1}) by a factor of three.

The remarkably close agreement of the independently predicted values of log K_w shown in table 7 with the corresponding experimental values leaves little doubt that the revised HKF model permits highly accurate predictions of the standard partial molal properties of aqueous species to temperatures of at least 300°C at vapor-liquid saturation pressures for H_2O. The agreement is particularly impressive in view of the fact that the revised equation of state coefficients for OH^- were obtained by regression of experimental values of $\overline{V}^\circ$, $\overline{\kappa}^\circ$, and $\overline{C}_P^\circ$ for aqueous electrolytes at 1 bar and temperatures below 100°C (see above). Because electrostatic solvation contributions to the standard partial molal properties of aqueous species predominate at high temperatures and low pressures, the close agreement of the predicted and experimental values of log K_w at temperatures above 200°C also strongly supports the revised interpretation of the effective electrostatic radii ($r_{e,j}$) of aqueous ions (eqs 34 and 35) and the predictive accuracy of the equation representing g as a function of temperature and the density of H_2O (eq 36A, B, and C).

In contrast to the close agreement of the predicted and experimental values of log K_w at vapor-liquid saturation pressures for H_2O, com-

parison of predicted and experimental values of log K_w at high pressures reveals somewhat larger discrepancies. Predicted values of log K_w at high pressures calculated in the manner described above are shown in table 8. These predicted values of log K_w were used to calculate the values of (δ log K_w) shown in table 8 using experimental values of log K_w reported by Linov and Kyrukov (1972) at the corresponding pressures and temperatures. The precision of the potentiometric data reported by Linov and Kryukov (1972) is estimated in the present study to be ±1 mV. An uncertainty of ±1 mV in the potentiometric data corresponds to pressure-independent uncertainties in the experimental values of log K_w at 18°, 25°, 50°, and 75°C, respectively, of ±0.017, ±0.017, ±0.016, and ±0.014. It can be seen in table 9 that for pressures greater than 1 kb most of the absolute values of δ log K_w are larger than these uncertainties. A probably explanation for the larger values of δ log K_w at these high pressures is given below.

Linov and Kryukov (1972) generated values of the logarithm of the ratio of the dissociation constant of H_2O at a given pressure (P) to that at the reference pressure (P_r) (log ($K_{w,P}/K_{w,P_r}$)) by extrapolation of potentiometric data ($E_P - E_{P_r}$) to infinite dilution using the relation.

$$\log\left(\frac{K_{w,P}}{K_{w,P_r}}\right) = \frac{-F(E_P - E_{P_r})}{2.303RT} + \log\left(\frac{\gamma_{H^+,P}\,\gamma_{OH^-,P}}{\gamma_{H^+,P_r}\,\gamma_{OH^-,P_r}}\right), \qquad (50)$$

TABLE 8

Predicted and experimental values of log K_w at temperatures from 18° to 75°C and pressures from 1 to 5 kb

P (KB)	18 °C log K_w [a]	18 °C δlog K_w [b]	25 °C log K_w [a]	25 °C δlog K_w [b]
1	-13.864	-0.009	-13.639	-0.016
2	-13.544	-0.012	-13.325	-0.049
3	-13.261	-0.013	-13.042	-0.093
4	-13.002	-0.041	-12.784	-0.132
5	-12.762	-0.087	-12.542	-0.183
P (KB)	50 °C log K_w [a]	50 °C δlog K_w [b]	75 °C log K_w [a]	75 °C δlog K_w [b]
1	-12.943	-0.059	-12.390	-0.015
2	-12.644	-0.113	-12.099	-0.048
3	-12.370	-0.162	-11.832	-0.080
4	-12.115	-0.209	-11.582	-0.117
5	-11.873	-0.267	-11.344	-0.165

[a] Predicted value from the revised HKF model. [b] Experimental values reported by Linov and Kryukov (1972) minus corresponding values predicted from the revised HKF model.

TABLE 9.

Conventional standard partial molal volumes ($\overline{V}_j^\circ$) of aqueous cations in cm^3 $mole^{-1}$ at vapor-liquid saturation pressures for H_2O and temperatures from 0° to 350°C. The values shown in this table were computed from eqs (A-1) in app. A and (B-1), (B-9), and (B-10) in app. B, using coefficients taken from table 3 together with values of ϵ given in table H-2 and those of Q in table H-3, g in table H-8, and $(\partial g/\partial P)_T$ in table H-9 of app. H

T(°C)	Li^+	Na^+	K^+	Rb^+	Cs^+	NH_4^+	Mg^{++}	Ca^{++}	Sr^{++}	Ba^{++}
0	-0.48	-3.43	7.45	13.34	19.30	17.39	-21.50	-19.20	-17.85	-15.41
25	-0.88	-1.11	9.06	14.32	21.42	18.13	-21.55	-18.06	-17.41	-12.60
50	-1.25	-0.13	9.76	14.73	22.38	18.42	-22.16	-17.98	-17.63	-11.64
75	-1.68	0.29	10.07	14.90	22.90	18.50	-23.21	-18.50	-18.27	-11.52
100	-2.25	0.37	10.17	14.92	23.19	18.45	-24.79	-19.56	-19.35	-12.02
125	-3.03	0.17	10.09	14.82	23.31	18.28	-27.09	-21.26	-20.98	-13.12
150	-4.13	-0.32	9.83	14.59	23.30	17.96	-30.43	-23.83	-23.40	-14.99
175	-5.96	-1.35	9.25	14.13	23.11	17.36	-36.26	-28.38	-27.60	-18.42
200	-7.87	-2.52	8.57	13.57	22.84	16.66	-41.91	-32.97	-31.88	-22.03
225	-10.45	-4.22	7.55	12.76	22.37	15.65	-49.29	-39.15	-37.65	-27.03
250	-13.98	-6.69	6.03	11.53	21.61	14.15	-58.67	-47.35	-45.40	-33.93
275	-18.87	-10.37	3.65	9.61	20.37	11.85	-70.03	-58.15	-55.83	-43.55
300	-25.79	-16.20	-0.37	6.31	18.15	7.96	-81.34	-71.68	-69.60	-57.19
325	-34.52	-26.05	-8.16	-0.27	13.52	0.41	-74.59	-80.87	-82.47	-74.11
350	-9.41	-32.02	-23.48	-15.04	1.68	-15.01	203.25	57.43	18.73	-20.10

where F represents Faraday's constant, E_P and E_{P_r} denote the emf of the cell at the pressure of interest and the reference pressure, respectively, and $\gamma_{H^+,P}$, γ_{H^+,P_r}, $\gamma_{OH^-,P}$, and γ_{OH^-,P_r} stand for the activity coefficients of the H^+ and OH^- at the subscripted pressures. Despite the fact that Linov and Kryukov's (1972) potentiometric measurements were made at ionic strengths of 0.10 to 0.11, they used the Debye-Hückel limiting law to predict the values of the second term on the right side of eq (50). An extended form of the Debye-Hückel equation would be more appropriate for these ionic strengths. Regression of the potentiometric data of Linov and Kryukov (1972) using the extended Debye-Hückel equation given by Helgeson, Kirkham, and Flowers (1981) yields experimental values of log K_w at high pressures which are much closer to those predicted in the present study. Similar regression of the potentiometric data specifying the predicted values of log K_w in table 8 yields results to within ±1 mV of Linov and Kryukov's data.

If the high pressure discrepancies discussed above are not in fact a consequence of errors in Linov and Kryukov's (1972) method of extrapolation of their experimental data to infinite dilution, then the values of δ log K_w in table 8 would indicate that the pressure terms in the revised HKF model are in error. This does not seem likely in view of the success of the model in representing both the pressure and temperature dependence of the standard partial molal properties of a large number of aqueous electrolytes.

Standard partial molal properties of aqueous electrolytes.—Predictions of a given standard partial molal property of different aqueous electrolytes ($\overline{\Xi}_k^\circ$) from the revised HKF model suggest that the shape of the P-T-$\overline{\Xi}_k^\circ$ surface for any one electrolyte is similar to those for all the others. As a consequence, the configurations of the isobars and isotherms for the calculated values of $\overline{V}^\circ$, $-\overline{\kappa}^\circ$, $\overline{E}_x^\circ$, $\overline{C}_P^\circ$, $\overline{S}^\circ$, $\Delta\overline{H}^\circ$, and $\Delta\overline{G}^\circ$ for NaCl in figures 27, 28, and 29 can be regarded as representative of aqueous electrolytes in general. The shapes of the curves in these figures arise not only from the pressure and temperature dependence of the nonsolvation ($\Delta\overline{\Xi}_n^\circ$) and solvation ($\Delta\overline{\Xi}_s^\circ$) contributions to the properties but also from the relative magnitude of these contributions as a function of pressure and temperature.

It can be seen in figure 27 that the curve representing $\overline{V}_{NaCl}^\circ$ at vapor-liquid saturation pressures for H_2O (labeled P_{SAT}) exhibits a

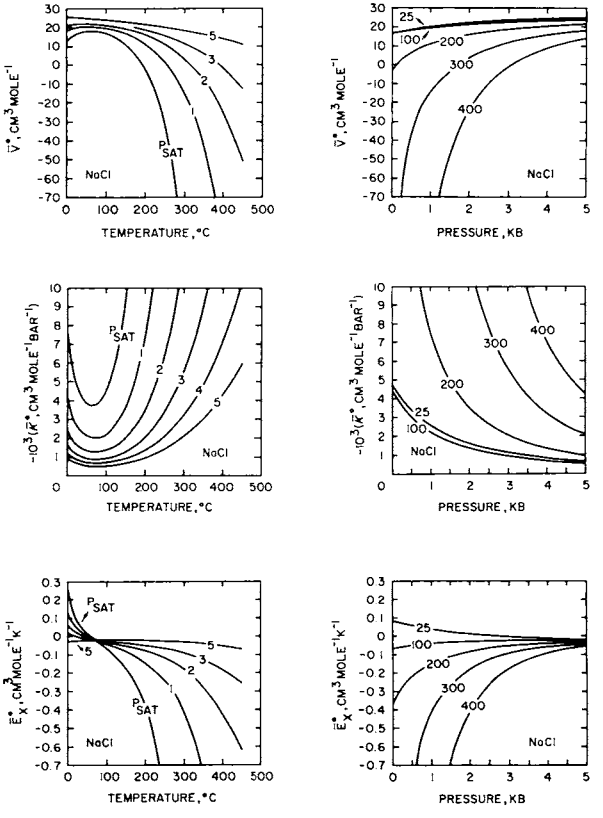

Fig. 27. Standard partial molal volume ($\overline{V}_k^\circ$), isothermal compressibility ($\overline{\kappa}_k^\circ$), and expansibility ($\overline{E}_{x,k}^\circ$) of NaCl computed from the revised HKF model as a function of pressure and temperature.

maximum at ~60°C ($T_{max,\bar{V}^\circ}$). Consequently, the P_{SAT} curve for $\bar{E}_x^\circ{}_{,NaCl}$ (fig. 27) passes through zero at the inflection point where $T = T_{max,\bar{V}^\circ}$. If $T < T_{max,\bar{V}^\circ}$, then $\bar{E}_x^\circ{}_{NaCl} > 0$, but if $T > T_{max,\bar{V}^\circ}$, then $\bar{E}_{x,NaCl}^\circ < 0$. In contrast, the P_{SAT} curve for $-\bar{\kappa}_{NaCl}^\circ$ (fig. 27) passes through a minimum at $T = T_{max,\mathring{\bar{V}}}$. The shapes of the P_{SAT} curves for $\bar{V}_{NaCl}^\circ$, $\bar{E}_{x,NaCl}^\circ$, and $-\bar{\kappa}_{NaCl}^\circ$ in figure 27 arise from the fact that the asymptotic temperature dependence of the nonsolvation contributions ($\Delta\bar{V}_{n,k}^\circ$, $-\Delta\bar{\kappa}_{n,k}^\circ$, and $\Delta\bar{E}_{x,n,k}^\circ$) opposes that of the solvation contributions ($\Delta\bar{V}_{s,k}^\circ$, $-\Delta\bar{\kappa}_{s,k}^\circ$, and $\Delta\bar{E}_{x,s,k}^\circ$). For $T < T_{max,\mathring{\bar{V}}}$ and $T \rightarrow \Theta = 228$ K, the nonsolvation contributions dictate the shapes of the P_{SAT} curves because $\bar{V}_k^\circ \rightarrow \Delta\bar{V}_{n,k}^\circ \rightarrow -\infty$, $-\bar{\kappa}_k^\circ \rightarrow -\Delta\bar{\kappa}_{n,k}^\circ \rightarrow \infty$, and $\bar{E}_{x,k}^\circ \rightarrow \Delta\bar{E}_{x,n,k}^\circ \rightarrow \infty$. However, for $T > T_{max,\bar{V}^\circ}$ and $T \rightarrow T_{c,H_2O}$, the solvation contributions control the shapes of the P_{SAT} curves because $\bar{V}_k^\circ \rightarrow \Delta\bar{V}_{s,k}^\circ \rightarrow -\infty$, $-\bar{\kappa}_k^\circ \rightarrow -\bar{\kappa}_{s,k}^\circ \rightarrow \infty$, and $\bar{E}_{x,k}^\circ \rightarrow \Delta\bar{E}_{x,s,k}^\circ \rightarrow \infty$. The configurations of the isotherms for $\bar{V}_{NaCl}$, $\bar{E}_{x,NaCl}^\circ$, and $-\bar{\kappa}_{NaCl}^\circ$ in figure 27

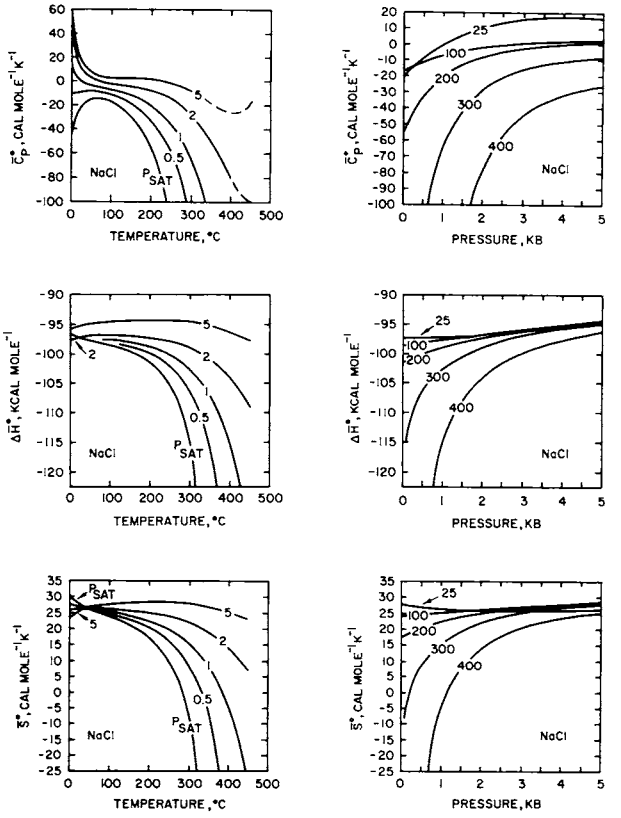

Fig. 28. Standard partial molal isobaric heat capacity ($\bar{C}_{P,k}^\circ$), entropy ($\bar{S}_k^\circ$) and apparent enthalpy of formation ($\Delta\bar{H}_k^\circ$) of NaCl computed from the revised HKF model as a function of pressure and temperature.

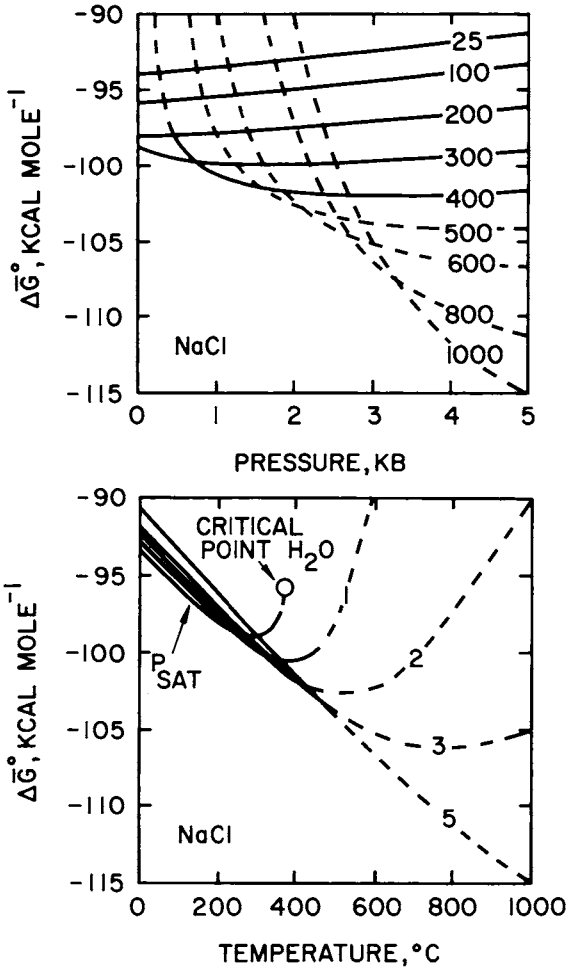

Fig. 29. Apparent standard partial molal Gibbs free energy of formation ($\Delta\bar{G}_k^\circ$) of NaCl computed from the revised HKF model as a function of pressure and temperature. The curves are dashed at pressures and temperatures where extrapolated values of g were used (see text and fig. 26).

are controlled in a similar manner. For $T > T_{max,\bar{V}^\circ}$, the shapes of the isotherms are a function primarily of $\Delta\bar{V}^\circ_{s,k}$, $-\Delta\bar{\kappa}^\circ_{s,k}$, and $\Delta\bar{E}^\circ_{x,s,k}$, which decrease asymptotically and approach relatively small values with increasing pressure. Because $\Delta\bar{V}^\circ_{c,k}$, $-\Delta\bar{\kappa}^\circ_{n,k}$, and $\Delta\bar{E}^\circ_{x,n,k}$ also decrease asymptotically and approach relatively small values with increasing pressure, the isotherms are asymptotic for $T < T_{max,\bar{V}^\circ}$. It follows that with increasing pressure, $-\bar{\kappa}^\circ_k$ and $\bar{E}^\circ_{x,k}$ approach relatively small values at all temperatures. However, as $\Delta\bar{V}^\circ_{s,k}$ and $\Delta\bar{V}^\circ_{c,k}$ become relatively small at

high pressures, $\overline{V}_k^\circ$ approaches a nearly constant value, which is approximately equal to the intrinsic standard partial molal volume ($\overline{V}_{i,k}^\circ$). Note that the curvature of the isobars for $\overline{V}_{NaCL,}^\circ$, $\overline{E}_{x,NaCl}^\circ$, and $-\overline{\kappa}_{NaCl}^\circ$ in figure 27 decreases with increasing pressure.

It can be seen by comparison of figures 27 and 28, that the configurations of the isotherms and isobars for $\overline{C}_{P,NaCl}^\circ$, $\overline{S}_{NaCl}^\circ$, and $\Delta\overline{H}_{NaCl}^\circ$ are similar to those of the curves representing the volumetric properties. These similarities occur because the pressure and temperature dependence and relative magnitude of the nonsolvation and solvation contributions to these properties are closely analogous to those of the volumetric properties. The curves for $\overline{C}_{P,NaCl}^\circ$ in figure 28 are dashed where uncertainties in the calculated values of the Born function X and $\Delta\overline{C}_{P,s,NaCl}^\circ$ become relatively high. The large changes in the predicted values of $\overline{C}_{P,NaCl}^\circ$ at pressures above 0.5 kb and temperatures below ~100°C in figure 28 are controlled by $\Delta\overline{C}_{P,n,NaCl}^\circ$. Currently there are no available experimental heat capacity data for NaCl or other aqueous electrolytes at $P > 0.5$ kb and $T < 100°C$ that can be used to confirm the predictions shown for these temperatures and pressures in figure 28. Nevertheless, they seem reasonable to us because $(\partial\overline{C}_P^\circ/\partial P)_T = -T(\partial^2\overline{V}_k^\circ/\partial T^2)_P$ and the predicted values of $\overline{V}_k^\circ$ for NaCl are in close agreement with experimental values of $\overline{V}_{NaCl}^\circ$ in this pressure and temperature region (see figs. 13 and 18).

As described above, estimated values of $\Delta\overline{G}_k^\circ$ can be calculated from the revised HKF model to temperatures of 1000°C using the values of ϵ and g shown in table 6 and figure 26, respectively. High-temperature values of $\Delta\overline{G}_k^\circ$ for NaCl estimated in this manner are represented by the dashed curves in figure 29. The P_{SAT} curve and the 1 kb isobar for $\Delta\overline{G}_{NaCl}^\circ$ minimize at temperatures corresponding to $\overline{S}_{NaCl}^\circ = 0$ for these pressures in figure 28. Similarly, the 200°, 300°, and 400°C isotherms for $\Delta\overline{G}_{NaCl}^\circ$ shown in figure 29 exhibit minima at pressures where the corresponding isotherms representing $\overline{V}_{NaCl}^\circ$ in figure 27 intersect $\overline{V}_{NaCl}^\circ = 0$. Note that if $\overline{S}_{k,P,,T,}^\circ$ and $\overline{V}_{k,P,,T,}^\circ$ are positive, the isobars and isotherms for $\Delta\overline{G}_k^\circ$ of other electrolytes should exhibit minima similar to those of NaCl because $\overline{S}_k^\circ$ and $\overline{V}_k^\circ$ are highly negative for all electrolytes in the critical region of H_2O.

Excluding the term for the solvation contribution to $\Delta\overline{G}_k^\circ$ ($\Delta\overline{G}_{k,s}^\circ$), the sum of the remaining terms in the revised equation for $\Delta\overline{G}_k^\circ$ (eqs 49 and A-7 in app. A) describes a quasi-planar P-T-$\Delta\overline{G}_k^\circ$ surface. In contrast, $\Delta\overline{G}_{k,s}^\circ$ becomes increasingly less negative as termperatures and pressures approach the critical region of H_2O, which leads to increasing curvature of the isobars and isotherms in the critical region. The similarity between the P-T-$\overline{\Xi}_k^\circ$ surfaces for NaCl (figs. 27, 28, and 29) and other aqueous electrolytes is a consequence of the common effect for all electrolytes of the structural and electrostatic properties of H_2O on the pressure and temperature dependence of $\Delta\overline{\Xi}_{n,k}^\circ$, and $\Delta\overline{\Xi}_{s,k}^\circ$, respectivley. The equation of state and Born coefficients for aqueous electrolytes in the revised HKF model can be regarded conceptually as scaling parame-

ters that relate the P-T-$\overline{\Xi}_k^\circ$ surfaces to these solvent properties. Differences between values of a given standard partial molal property $\overline{\Xi}_k^\circ$ for NaCl and other aqueous electrolytes are caused primarily by the effects of ion size and charge on values of $\overline{\Xi}_j^\circ$. Predicted values of $\overline{\Xi}_j^\circ$ from the revised HKF model for aqueous ions of differing size and charge are considered below.

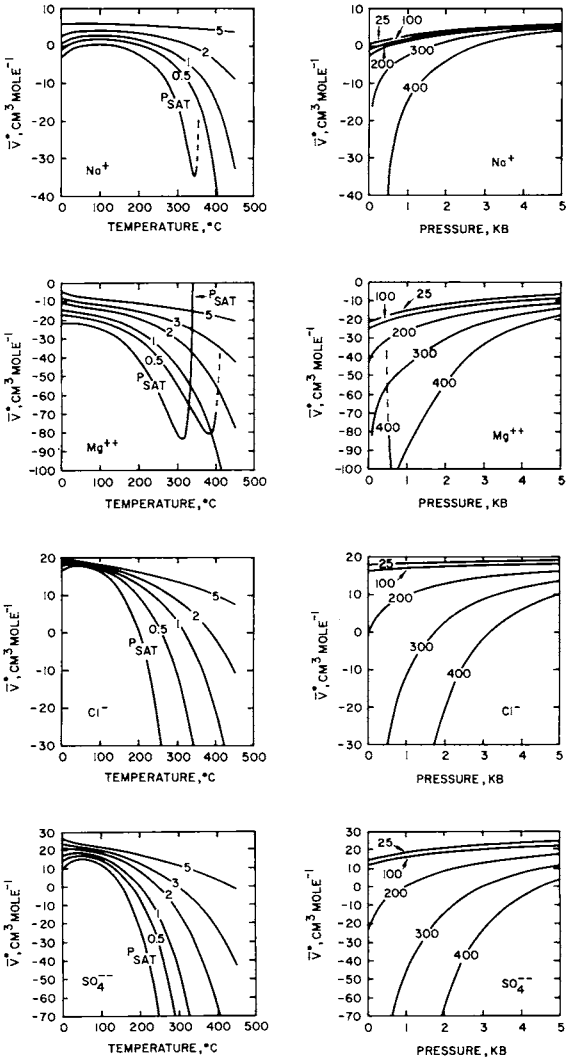

Fig. 30. Conventional standard partial molal molal volumes ($\overline{V}_j^\circ$) of Na^+, Mg^{++}, Cl^-, and SO_4^{--} as functions of pressure and temperature computed from the revised HKF model.

Conventional standard partial molal properties of aqueous ions.— Prediction of $\overline{V}_j^\circ$, $\overline{C}_{P,j}^\circ$, $\overline{S}_j^\circ$ and $\Delta\overline{G}_j^\circ$ from the revised HKF model generated the curves shown for Na^+, Mg^{++}, Cl^-, and SO_4^{--} in figures 30 through 33. Comparison of the predicted values of $\overline{\Xi}_j^\circ$ for these ions with corresponding values predicted for the other ions listed in table 3 suggests that the configurations of the curves in figures 30 through 33

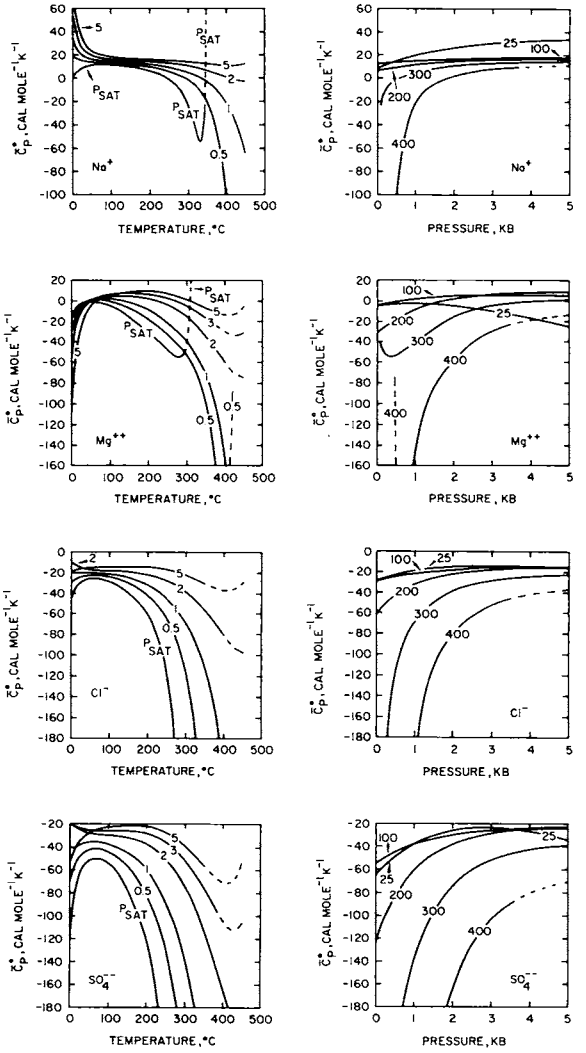

Fig. 31. Conventional standard partial molal isobaric heat capacities ($\overline{C}_P^\circ$) of Na^+, Mg^{++}, Cl^-, and SO_4^{--} as functions of pressure and temperature computed from the revised HKF model.

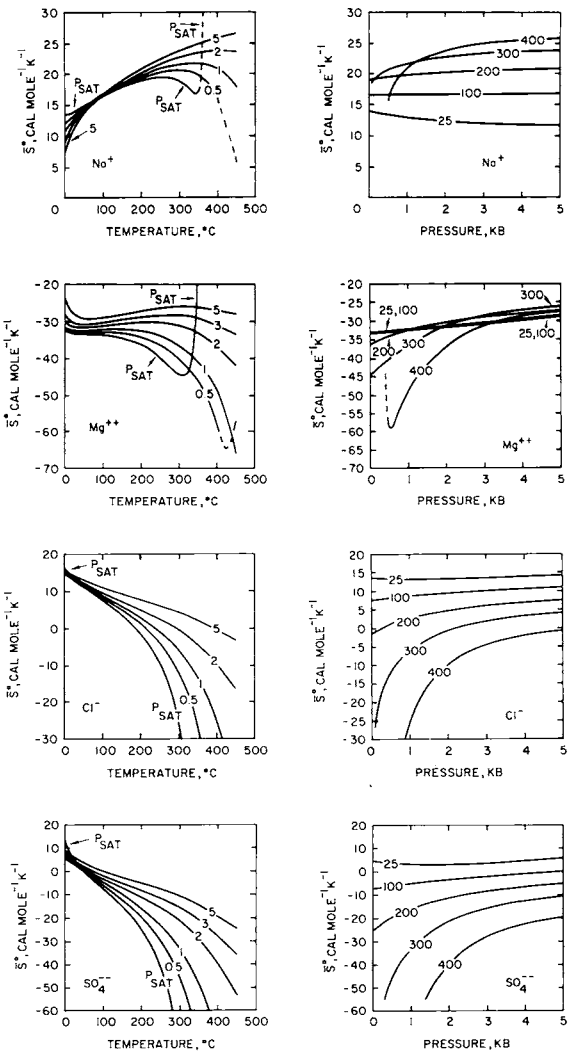

Fig. 32. Conventional standard partial molal entropies ($\bar{S}_j^\circ$) of Na^+, Mg^{++}, Cl^-, and SO_4^{--} as functions of pressure and temperature computed from the revised HKF model.

are representative of those for ions of the same charge. Calculated values of $\bar{V}_j^\circ$, $\bar{C}_{pj}^\circ$, $\bar{S}_j^\circ$ and $\Delta\bar{G}_j^\circ$ are given in tables 9 through 16 for aqueous ions at H_2O vapor-liquid saturation pressures and temperatures from 0° to 350°C.

It can be seen by inspection of figures 27 through 33 that for a given $\bar{\Xi}^\circ$, the P-T-$\bar{\Xi}^\circ$ surfaces for aqueous ions and electrolytes generally have the same shapes. In the low-temperature region where nonsolva-

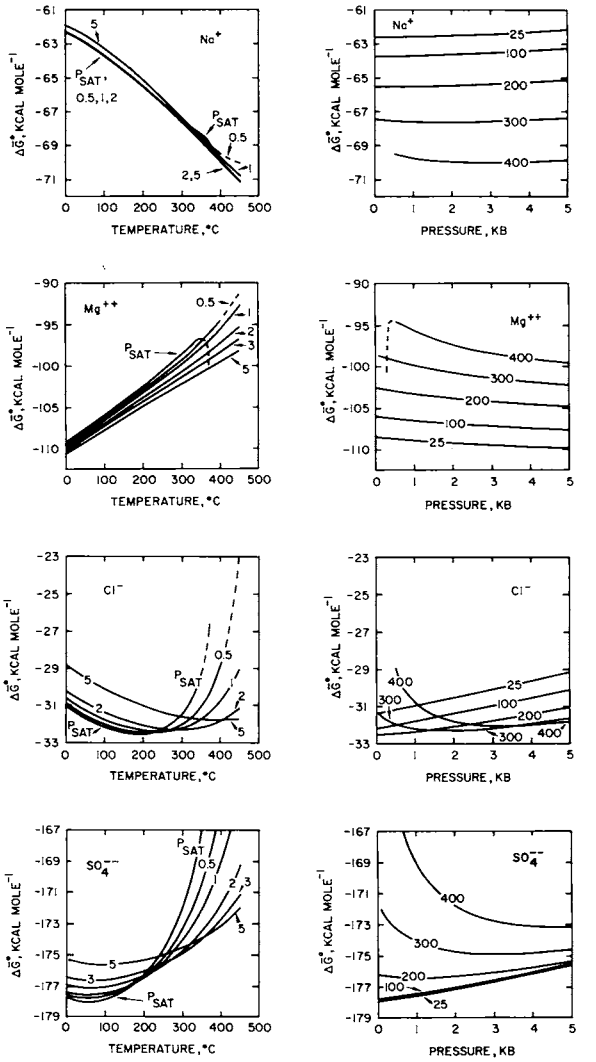

Fig. 33. Conventional apparent standard partial molal Gibbs free energies of formation ($\Delta\overline{G}_j^\circ$) of Na^+, Mg^{++}, Cl^-, and SO_4^{--} as functions of pressure and temperature computed from the revised HKF model.

tion contributions dominate the values of $\overline{\Xi}_k^\circ$ and $\overline{\Xi}_j^\circ$(see above), these similarities occur solely as a consequence of the fact that the equations for the nonsolvation contributions for aqueous electrolytes and ions differ only by pressure- and temperature-independent equation of state coefficients which are additive (see eq 49). At high temperatures where solvation contributions predominate, corresponding isobars and

TABLE 10

Conventional standard partial molal volumes ($\overline{V}_j^\circ$) of aqueous anions in cm^3 $mole^{-1}$ at vapor-liquid saturation pressures for H_2O and temperatures from 0° to 350°C—see caption of table 9

T(°C)	F^-	Cl^-	Br^-	I^-	OH^-	HCO_3^-	NO_3^-	HS^-	SO_4^{--}
0	-2.04	16.31	22.72	33.09	-6.74	21.73	23.84	17.62	9.12
25	-1.32	17.79	24.85	36.31	-4.18	24.60	29.00	20.21	13.88
50	-1.65	17.94	25.34	37.35	-3.61	25.47	31.02	20.89	14.93
75	-2.66	17.36	25.00	37.36	-4.06	25.38	31.68	20.64	14.09
100	-4.36	16.14	23.97	36.62	-5.36	24.57	31.46	19.63	11.69
125	-6.94	14.15	22.16	35.09	-7.62	22.99	30.43	17.80	7.51
150	-10.78	11.10	19.33	32.56	-11.14	20.41	28.44	14.90	1.00
175	-17.07	6.15	14.69	28.33	-17.06	16.14	24.96	10.08	-9.85
200	-24.59	-0.19	8.65	22.71	-24.27	10.48	20.10	3.86	-23.42
225	-35.54	-9.69	-0.48	14.10	-34.90	1.84	12.52	-5.51	-43.60
250	-52.03	-24.54	-14.87	0.40	-51.09	-11.90	0.21	-20.23	-74.80
275	-78.60	-49.63	-39.38	-23.19	-77.49	-35.53	-21.34	-45.16	-126.62
300	-126.57	-97.71	-86.80	-69.38	-125.86	-81.79	-64.28	-93.08	-223.90
325	-231.43	-212.33	-201.28	-182.48	-233.89	-194.99	-171.59	-207.71	-449.05
350	-550.48	-639.18	-638.08	-625.58	-581.04	-637.60	-607.03	-637.02	-1236.1

TABLE 11

Conventional standard partial molal isobaric heat capacities ($\overline{C}_{P,j}^\circ$) of aqueous cations in cal $mole^{-1}$ K^{-1} at vapor-liquid saturation pressures for H_2O and temperatures from 0° to 350°C. The values shown in this table were computed from eqs (A-4) in app. A and (B-2), (B-4), (B-9), (B-10), and (B-11) in app. B using coefficients taken from table 3 together with values of ϵ given in table H-2, and those of Y in table H-4, X in table H-6, g in table H-8, $(\partial g/\partial T)_P$ in table H-10, and $(\partial^2 g/\partial T^2)_P$ in table H-12 in app. H

T(°C)	Na^+	K^+	Rb^+	Cs^+	NH_4^+	Mg^{++}	Ca^{++}	Sr^{++}	Ba^{++}
0	0.38	-3.24	-13.86	-22.83	15.62	-22.70	-15.14	-18.95	-22.53
25	9.06	1.98	-2.98	-6.29	15.74	-5.34	-7.53	-10.05	-12.30
50	11.40	3.39	0.32	-1.10	15.53	-1.88	-6.80	-8.77	-10.38
75	11.99	3.75	1.58	1.08	15.19	-2.46	-8.18	-9.77	-10.89
100	11.80	3.65	2.02	2.08	14.73	-5.10	-10.78	-12.01	-12.64
125	11.06	3.23	1.99	2.49	14.12	-9.59	-14.68	-15.51	-15.56
150	9.70	2.44	1.57	2.50	13.25	-16.58	-20.48	-20.79	-20.06
175	8.08	1.46	0.93	2.26	12.24	-23.59	-26.51	-26.37	-24.96
200	6.06	0.18	0.01	1.77	10.97	-30.71	-33.05	-32.58	-30.59
225	3.12	-1.74	-1.48	0.87	9.10	-39.12	-41.40	-40.69	-38.20
250	-1.36	-4.82	-3.94	-0.75	6.14	-48.15	-52.02	-51.45	-48.84
275	-8.89	-10.33	-8.46	-3.84	0.87	-54.86	-65.33	-66.08	-64.65
300	-23.20	-21.86	-18.18	-10.70	-10.19	-40.24	-76.13	-82.88	-88.19
325	-49.18	-50.22	-43.42	-29.58	-37.84	178.65	5.47	-36.70	-85.70
350	151.48	-69.52	-90.92	-86.41	-67.50	4657.3	2616.7	2061.7	1341.9

TABLE 12

Conventional standard partial molal isobaric heat capacities ($\bar{C}_{P,j}^{\circ}$) of aqueous anions in cal mole^{-1} K^{-1} at vapor-liquid saturation pressures for H_2O and temperatures from 0° to 350°C—see caption of table 11

T(°C)	F^-	Cl^-	Br^-	I^-	OH^-	NO_3^-	HS^-	SO_4^{--}
0	-49.26	-46.29	-50.41	-42.87	-63.05	-36.11	-39.98	-117.07
25	-27.23	-29.44	-30.42	-28.25	-32.79	-16.40	-22.17	-64.38
50	-22.62	-26.04	-25.91	-25.35	-25.43	-11.63	-18.44	-51.85
75	-23.03	-26.53	-25.81	-25.84	-24.54	-11.06	-18.76	-50.67
100	-25.95	-28.99	-27.86	-28.05	-26.68	-12.47	-21.12	-54.88
125	-31.09	-33.23	-31.71	-31.83	-31.23	-15.45	-25.25	-63.45
150	-39.16	-39.83	-37.89	-37.71	-38.76	-20.39	-31.76	-77.49
175	-49.33	-48.67	-46.32	-45.77	-48.52	-27.45	-40.51	-96.08
200	-63.20	-61.44	-58.69	-57.69	-62.13	-38.19	-53.19	-122.56
225	-84.78	-82.08	-78.86	-77.21	-83.57	-56.07	-73.74	-164.92
250	-121.00	-118.25	-114.48	-111.92	-120.00	-88.30	-109.80	-238.14
275	-189.74	-190.03	-185.68	-181.79	-189.98	-153.95	-181.49	-381.31
300	-345.84	-362.04	-357.63	-351.88	-351.06	-315.68	-353.58	-718.27
325	-808.70	-925.33	-927.89	-923.80	-841.42	-869.55	-918.77	-1787.1
350	-2960.8	-4596.9	-4771.4	-4915.2	-3370.8	-4907.3	-4631.3	-8131.2

TABLE 13

Conventional standard partial molal entropies ($\bar{S}_j^{\circ}$) of aqueous cations in cal mole^{-1} K^{-1} at vapor-liquid saturation pressures for H_2O and temperatures from 0° to 350°C. The values shown in this table were computed from eqs (A-5) in app. A and (B-2), (B-9), and (B-10) in app. B, using coefficients taken from table 3 together with values of ϵ given in table H-2 and those of Y in table H-4, g in table H-8, and $(\partial g/\partial T)_P$ in table H-10 in app. H

T(°C)	Na^+	K^+	Rb^+	Cs^+	NH_4^+	Mg^{++}	Ca^{++}	Sr^{++}	Ba^{++}
0	13.51	24.21	29.44	32.93	25.22	-31.95	-12.60	-6.33	3.72
25	14.00	24.20	28.80	31.80	26.60	-33.00	-13.50	-7.50	2.30
50	14.84	24.43	28.71	31.53	27.86	-33.25	-14.06	-8.23	1.41
75	15.72	24.70	28.79	31.54	29.01	-33.40	-14.60	-8.92	0.63
100	16.55	24.96	28.92	31.66	30.05	-33.65	-15.25	-9.66	-0.18
125	17.29	25.18	29.05	31.81	30.98	-34.11	-16.07	-10.54	-1.08
150	17.93	25.36	29.16	31.96	31.82	-34.88	-17.12	-11.63	-2.15
175	18.63	25.57	29.31	32.14	32.64	-34.91	-17.64	-12.24	-2.83
200	19.02	25.62	29.34	32.26	33.28	-36.34	-19.21	-13.81	-4.31
225	19.28	25.59	29.31	32.33	33.81	-38.06	-21.06	-15.62	-6.01
250	19.37	25.46	29.20	32.35	34.21	-40.05	-23.21	-17.75	-8.02
275	19.23	25.17	28.97	32.28	34.44	-42.22	-25.70	-20.24	-10.43
300	18.73	24.62	28.51	32.04	34.38	-44.15	-28.47	-23.14	-13.38
325	17.67	23.52	27.58	31.47	33.78	-43.14	-30.38	-25.71	-16.65
350	17.25	21.62	25.74	30.07	32.32	-8.27	-13.62	-13.72	-10.69

TABLE 14

Conventional standard partial molal entropies ($\bar{S}_j^\circ$) of aqueous anions in cal mole^{-1} K^{-1} at vapor-liquid saturation pressures for H_2O and temperatures from 0° to 350°C—see caption of table 13

T(°C)	F^-	Cl^-	Br^-	I^-	OH^-	NO_3^-	HS^-	SO_4^{--}
0	-0.08	16.74	23.14	28.46	1.30	37.21	18.84	11.92
25	-3.20	13.60	19.80	25.50	-2.60	35.10	16.30	4.50
50	-5.16	11.41	17.58	23.38	-4.88	34.02	14.71	-0.06
75	-6.84	9.46	15.67	21.48	-6.72	33.19	13.34	-3.84
100	-8.52	7.55	13.82	19.63	-8.48	32.38	11.97	-7.47
125	-10.35	5.55	11.90	17.70	-10.34	31.49	10.48	-11.27
150	-12.46	3.35	9.80	15.60	-12.44	30.41	8.76	-15.51
175	-14.25	1.28	7.81	13.57	-14.25	29.32	7.15	-19.33
200	-17.22	-1.64	5.03	10.82	-17.18	27.59	4.68	-25.12
225	-20.87	-5.19	1.63	7.49	-20.77	25.29	1.55	-32.22
250	-25.58	-9.78	-2.80	3.15	-25.42	22.02	-2.63	-41.44
275	-32.07	-16.23	-9.07	-2.99	-31.90	17.02	-8.68	-54.37
300	-42.03	-26.47	-19.13	-12.88	-41.94	8.45	-18.55	-74.76
325	-60.08	-46.28	-38.85	-32.42	-60.50	-9.47	-38.03	-113.48
350	-102.84	-102.89	-96.64	-91.01	-106.82	-66.33	-94.62	-218.04

TABLE 15

Conventional apparent standard partial molal Gibbs free energies of formation ($-\Delta\bar{G}_j^\circ$) of aqueous cations in kcal mole^{-1} at vapor-liquid saturation pressures for H_2O and temperatures from 0° to 350°C. The values shown in this table were computed from eqs (49), (A-7) in app. A, and (B-9) in app. B using coefficients taken from table 3 together with values of ϵ given in table H-2 and those of Y_{P_r,T_r} in table H-1 and g in table H-8

T(°C)	Na^+	K^+	Rb^+	Cs^+	NH_4^+	Mg^{++}	Ca^{++}	Sr^{++}	Ba^{++}
0	62.26	66.92	67.06	68.93	18.35	109.32	132.45	134.94	132.95
25	62.60	67.53	67.79	69.73	19.00	108.50	132.12	134.76	133.02
50	62.96	68.13	68.50	70.52	19.68	107.67	131.77	134.57	133.07
75	63.35	68.75	69.22	71.31	20.39	106.84	131.41	134.35	133.09
100	63.75	69.37	69.94	72.10	21.13	106.00	131.04	134.12	133.10
125	64.17	70.00	70.67	72.89	21.89	105.16	130.65	133.87	133.09
150	64.61	70.63	71.40	73.69	22.68	104.30	130.24	133.60	133.05
175	65.07	71.26	72.12	74.49	23.48	103.40	129.79	133.28	132.97
200	65.54	71.90	72.85	75.29	24.30	102.52	129.33	132.96	132.89
225	66.02	72.54	73.58	76.09	25.14	101.60	128.84	132.60	132.76
250	66.50	73.17	74.31	76.89	25.98	100.64	128.30	132.20	132.60
275	66.99	73.80	75.03	77.69	26.83	99.65	127.72	131.75	132.39
300	67.47	74.43	75.75	78.48	27.69	98.61	127.08	131.25	132.12
325	67.95	75.03	76.45	79.26	28.54	97.58	126.40	130.70	131.80
350	68.41	75.62	77.12	80.03	29.37	96.74	125.79	130.18	131.47

TABLE 16

Conventional apparent standard partial molal Gibbs free energies of formation ($-\Delta\overline{G}_j^\circ$) of aqueous anions in kcal mole^{-1} at vapor-liquid saturation pressures for H_2O and temperatures from 0° to 350°C—see caption of table 15

T(°C)	F^-	Cl^-	Br^-	I^-	OH^-	NO_3^-	HS^-	SO_4^{--}
0	67.37	31.02	24.34	11.74	37.62	25.60	3.31	177.74
25	67.32	31.39	24.87	12.41	37.59	26.50	2.88	177.93
50	67.22	31.71	25.33	13.02	37.50	27.37	2.49	177.99
75	67.07	31.97	25.75	13.58	37.35	28.21	2.14	177.94
100	66.88	32.18	26.12	14.10	37.16	29.03	1.83	177.79
125	66.64	32.34	26.44	14.56	36.93	29.82	1.54	177.56
150	66.36	32.45	26.71	14.98	36.65	30.60	1.30	177.23
175	66.01	32.50	26.92	15.33	36.30	31.34	1.12	176.77
200	65.62	32.50	27.08	15.63	35.91	32.04	0.97	176.22
225	65.15	32.41	27.16	15.86	35.45	32.70	0.89	175.51
250	64.59	32.24	27.15	15.99	34.89	33.29	0.89	174.62
275	63.91	31.93	27.02	16.00	34.20	33.79	1.02	173.48
300	63.05	31.46	26.72	15.85	33.36	34.15	1.30	171.99
325	61.95	30.70	26.14	15.41	32.25	34.26	1.86	169.97
350	60.39	29.39	25.00	14.41	30.66	33.84	2.96	166.90

isotherms for anions and electrolytes are also similar in shape. However, the curves for cations exhibit minima (figs. 30, 31, and 32) and maxima (fig. 33) which do not appear in the corresponding curves for anions and electrolytes. This difference between the shapes of the curves for cations and anions is a consequence of the different effect of the absolute standard partial molal solvation contribution of the hydrogen ion ($\Delta\overline{\Xi}^{\circ\,abs}_{s,H^+}$) to $\Delta\overline{\Xi}^\circ_{s,j}$ (eq 2) for cations and anions.

The P-T-$\Delta\overline{\Xi}^{\circ\,abs}_{s,j}$ surfaces of aqueous ions and the P-T-$\Delta\overline{\Xi}^\circ_{s,k}$ surfaces for aqueous electrolytes all resemble one another because the equations for $\Delta\overline{\Xi}^{\circ\,abs}_{s,j}$ and $\Delta\overline{\Xi}^\circ_{s,k}$ have the same general functional dependence on the electrostatic properties of H_2O and the solvent parameter g. The similarity in the shapes of the corresponding P-T-$\Delta\overline{\Xi}^\circ_s$ surfaces for anions and electrolytes follows from the fact that the P-T-$\Delta\overline{\Xi}^{\circ\,abs}_{s,j}$ surfaces for anions represent the addition of the P-T-$\Delta\overline{\Xi}^{\circ\,abs}_{s,j}$ and P-T-$|Z_j|\Delta\overline{\Xi}^{\circ\,abs}_{s,H^+}$ surfaces. In contrast, because values of $\Delta\overline{\Xi}^\circ_{sj}$ for cations are obtained by subtracting $Z_j\Delta\overline{\Xi}^{\circ\,abs}_{s,H^+}$ from $\Delta\overline{\Xi}^{\circ\,abs}_{s,j}$, the P-T-$\Delta\overline{\Xi}^\circ_{s,j}$ surfaces for cations resemble corresponding surfaces for electrolytes only if the P-T-$Z_j\Delta\overline{\Xi}^{\circ\,abs}_{s,H^+}$ and P-T-$\Delta\overline{\Xi}^{\circ\,abs}_{s,j}$ surfaces do not intersect.

In the pressure and temperature region where the effective electrostatic radii of aqueous ions ($r_{e,j}$) are constants (see fig. 19), predicted values of $Z_j\Delta\overline{\Xi}^{\circ\,abs}_{s,H^+}$ are smaller than the corresponding values of $\Delta\overline{\Xi}^{\circ\,abs}_{e,j}$ for all the ions other than H^+ shown in table 3. However, as a consequence of the decrease in values of $r_{e,j}$ as pressures and temperatures approach the critical region of H_2O, the predicted values of $Z_j\Delta\overline{\Xi}^{\circ\,abs}_{s,H^+}$ become larger than the corresponding values of $\Delta\overline{\Xi}^{\circ\,abs}_{s,j}$ for other cations. This change in relative magnitude causes isobars and isotherms for $Z_j\Delta\overline{\Xi}^{\circ\,abs}_{s,H^+}$

to intersect corresponding curved for $\Delta\overline{\Xi}^{\circ\,abs}_{e,j}$ of other cations, which leads to the minima in the curves for $\overline{V}^{\circ}_j$, $\overline{C}^{\circ}_{P,j}$ and $\overline{S}^{\circ}_j$(figs. 30, 31, and 32) and the maxima in the curves for $\Delta\overline{G}^{\circ}_j$ (fig. 33).

Limit calculations for $\overline{V}^{\circ}$, $\overline{C}^{\circ}_P$, and $\overline{S}^{\circ}$ from the revised HKF model indicate that as pressures and temperatures approach the critical point of H_2O, these properties approach ∞ for cations and $-\infty$ for anions and electrolytes. However, the limit calculations for cations and anions require extrapolated values of the solvent function g, which cannot be relied on near the critical point of H_2O (see above). Consequently, the different predicted limits for cations and anions could be the result of extrapolation errors in g (eq 36A, B, and C). Nevertheless, comparison of the P_{SAT} curves for Na^+ and Mg^{++} with those of Cl^- and SO_4^{--} in figure 33 suggests that as temperature and pressure approach those of the critical point, $\Delta\overline{G}^{\circ}_j$ for cations becomes increasingly more negative, but $\Delta\overline{G}^{\circ}_j$ for anions becomes increasingly less negative. These differences in $\Delta\overline{G}^{\circ}_j$ for cations and anions could have a significant effect on geochemical processes at temperatures and pressures in the critical region.

CONCLUDING REMARKS

Revision of the HKF model has greatly improved the accuracy of predicted standard partial molal thermodynamic properties of aqueous species, especially at high temperatures and low pressures. The revised HKF model is consistent with recent theoretical considerations of the structural and electrostatic properties of H_2O, as well as with experimental standard partial molal volumes and heat capacities of aqueous electrolytes at pressures and temperatures approaching the critical point of H_2O. Many geochemical processes occur in this pressure/temperature region where the thermodynamic properties of aqueous species change dramatically. Changes in $\Delta\overline{G}^{\circ}$ for aqueous species at temperatures above 300°C and pressures below 1 kb predicted from the revised HKF model should affect substantially calculation of the relative stabilities of minerals in geothermal systems. The revisions to the HKF model have been incorporated in a revised version of computer program SUPCRT, which will be available together with a new data file from the Laboratory of Theoretical Geochemistry (otherwise known as Prediction Central) at the University of California, Berkeley.

The revisions of the HKF model summarized above for the standard partial molal properties of aqueous ions and electrolytes can also be applied to the corresponding properties of aqueous complexes, as well as the relative partial molal properties of aqueous species. Accurate extension of the HKF model to pressures and temperatures beyond the limits of the present study can be made from experimental values of the standard partial molal properties of any single electrolyte for which experimental data are available. Experimental measurements of the calorimetric and volumetric properties of aqueous electrolyte solutions can now be made at supercritical temperatures. As more high-temperature data become available, it should be possible to

extend the revised HKF model into and perhaps through and beyond the critical region for H_2O.

ACKNOWLEDGMENTS

The research reported above represents the senior author's Ph.D. dissertation at the University of California, Berkeley. The research was supported by the National Science Foundation (NSF grants EAR, 77-14492 and EAR 81-15859), the Department of Energy (DOE contract DE-AT03-83ER-13100 and DOE grant DE-FG03-85ER-13419), and the Committee on Research at the University of California, Berkeley. We are indebted to Annemarie Meike, Ken Jackson, Everett Shock, Dimitri Sverjensky, Peter Lichtner, Eric Oelkers, William Murphy, and Barbara Ransom for helpful discussions and suggestions during the course of this study. Everett Shock's assistance in regressing experimental data for Rb^+ and HS^- is greatly appreciated. Thanks are also due Robert Wood and Jeffrey Gates for providing us with experimental data in advance of publication. George Brimhall and Leo Brewer reviewed an earlier version of this paper. Finally, we would like to express our gratitude to Gregory Anderson, Dimitri Sverjensky, Robert Wood, and George Flowers for their helpful reviews of the manuscript and to Joachim Hampel, Mike Salas, and Joan Bossart for outstanding technical assistance.

APPENDIX A

Summary of Equations for the Standard Partial Molal Properties ($\bar{\Xi}^\circ$) of Aqueous Ions and Electrolytes

It follows from $\bar{\Xi}^\circ = \Delta\bar{\Xi}^\circ_n + \Delta\bar{\Xi}^\circ_s$ and the equations given in apps. F and G that the following relations can be written:

Volume ($\bar{V}^\circ$)

$$\bar{V}^\circ = \Delta\bar{V}^\circ_n + \Delta\bar{V}^\circ_s$$

$$= a_1 + \frac{a_2}{\Psi + P} + \frac{a_3}{T - \Theta} + \frac{a_4}{(\Psi + P)(T - \Theta)} - \omega Q + \left[\frac{1}{\epsilon} - 1\right]\left[\frac{\partial \omega}{\partial P}\right]_T \quad ; \qquad \text{(A-1)}$$

Isothermal Compressibility ($\bar{\kappa}^\circ$)

$$\bar{\kappa}^\circ \equiv -\left[\frac{\partial \bar{V}^\circ}{\partial P}\right]_T = \Delta\bar{\kappa}^\circ_n + \Delta\bar{\kappa}^\circ_s$$

$$= \left[a_2 + \frac{a_4}{T - \Theta}\right]\left[\frac{1}{\Psi + P}\right]^2 + \omega N + 2Q\left[\frac{\partial \omega}{\partial P}\right]_T - \left[\frac{1}{\epsilon} - 1\right]\left[\frac{\partial^2 \omega}{\partial P^2}\right]_T \quad ; \qquad \text{(A-2)}$$

Expansibility ($\bar{E}_x^\circ$)

$$\bar{E}_x^\circ \equiv \left[\frac{\partial \bar{V}^\circ}{\partial T}\right]_P = \Delta\bar{E}_{x,n}^\circ + \Delta\bar{E}_{x,s}^\circ$$

$$= -\left[a_3 + \frac{a_4}{\Psi + P}\right]\left[\frac{1}{T-\Theta}\right]^2 - \omega U - Q\left[\frac{\partial \omega}{\partial T}\right]_P - Y\left[\frac{\partial \omega}{\partial P}\right]_T$$

$$+ \left[\frac{1}{\epsilon} - 1\right]\left[\partial\left[\frac{\partial \omega}{\partial P}\right]_T / \partial T\right]_P \quad ; \qquad \text{(A-3)}$$

Isobaric Heat Capacity ($\bar{C}_P^\circ$)

$$\bar{C}_P^\circ = \Delta\bar{C}_{P,n}^\circ + \Delta\bar{C}_{P,s}^\circ$$

$$= c_1 + \frac{c_2}{(T-\Theta)^2} - \left[\frac{2T}{(T-\Theta)^3}\right]\left[a_3(P - P_r) + a_4 \ln\left[\frac{\Psi + P}{\Psi + P_r}\right]\right]$$

$$+ \omega TX + 2TY\left[\frac{\partial \omega}{\partial T}\right]_P - T\left[\frac{1}{\epsilon} - 1\right]\left[\frac{\partial^2 \omega}{\partial T^2}\right]_P \quad ; \qquad \text{(A-4)}$$

Entropy ($\bar{S}^\circ$)

$$\bar{S}^\circ = \bar{S}_{P_r,T_r}^\circ + (\Delta\bar{S}_n^\circ - \Delta\bar{S}_{n,P_r,T_r}^\circ) + (\Delta\bar{S}_s^\circ - \Delta\bar{S}_{s,P_r,T_r}^\circ)$$

$$\bar{S}^\circ = \bar{S}_{P_r,T_r}^\circ + c_1 \ln\left[\frac{T}{T_r}\right] - \frac{c_2}{\Theta}\left[\left[\frac{1}{T-\Theta}\right] - \left[\frac{1}{T_r - \Theta}\right] + \frac{1}{\Theta}\ln\left[\frac{T_r(T-\Theta)}{T(T_r-\Theta)}\right]\right]$$

$$+ \left[\frac{1}{T-\Theta}\right]^2\left[a_3(P - P_r) + a_4 \ln\left[\frac{\Psi + P}{\Psi + P_r}\right]\right]$$

$$+ \omega Y - \left[\frac{1}{\epsilon} - 1\right]\left[\frac{\partial \omega}{\partial T}\right]_P - \omega_{P_r,T_r} Y_{P_r,T_r} \quad ; \qquad \text{(A-5)}$$

Enthalpy ($\bar{H}^\circ$) change from P, T to P_r, T_r

$$\bar{H}^\circ - \bar{H}^\circ_{P_r,T_r} = (\Delta\bar{H}^\circ_n - \Delta\bar{H}^\circ_{n,P_r,T_r}) + (\Delta\bar{H}^\circ_s - \Delta\bar{H}^\circ_{s,P_r,T_r})$$

$$= c_1(T - T_r) - c_2\left[\left[\frac{1}{T-\Theta}\right] - \left[\frac{1}{T_r-\Theta}\right]\right] + a_1(P - P_r) + a_2 \ln\left[\frac{\Psi+P}{\Psi+P_r}\right]$$

$$+ \left[\frac{2T-\Theta}{(T-\Theta)^2}\right]\left[a_3(P - P_r) + a_4 \ln\left[\frac{\Psi+P}{\Psi+P_r}\right]\right] + \omega\left[\frac{1}{\epsilon} - 1\right] + \omega TY$$

$$- T\left[\frac{1}{\epsilon} - 1\right]\left[\frac{\partial\omega}{\partial T}\right]_P - \omega_{P_r,T_r}\left[\frac{1}{\epsilon_{P_r,T_r}} - 1\right] - \omega_{P_r,T_r}T_r Y_{P_r,T_r} \; ; \qquad \text{(A-6)}$$

Gibbs Free Energy ($\bar{G}^\circ$) change from P, T to P_r, T_r

$$\bar{G}^\circ - \bar{G}^\circ_{P_r,T_r} = -\bar{S}^\circ_{P_r,T_r}(T - T_r) + (\Delta\bar{G}^\circ_n - \Delta\bar{G}^\circ_{n,P_r,T_r}) + \Delta\bar{S}^\circ_{n,P_r,T_r}(T - T_r)$$

$$+ (\Delta\bar{G}^\circ_s - \Delta\bar{G}^\circ_{s,P_r,T_r}) + \Delta\bar{S}^\circ_{s,P_r,T_r}(T - T_r)$$

$$= -\bar{S}^\circ_{P_r,T_r}(T - T_r) - c_1\left[T\ln\left[\frac{T}{T_r}\right] - T + T_r\right] + a_1(P - P_r) + a_2\ln\left[\frac{\Psi+P}{\Psi+P_r}\right]$$

$$- c_2\left\{\left[\left[\frac{1}{T-\Theta}\right] - \left[\frac{1}{T_r-\Theta}\right]\right]\left[\frac{\Theta-T}{\Theta}\right] - \frac{T}{\Theta^2}\ln\left[\frac{T_r(T-\Theta)}{T(T_r-\Theta)}\right]\right\}$$

$$+ \left[\frac{1}{T-\Theta}\right]\left[a_3(P - P_r) + a_4\ln\left[\frac{\Psi+P}{\Psi+P_r}\right]\right] + \omega\left[\frac{1}{\epsilon} - 1\right]$$

$$- \omega_{P_r,T_r}\left[\frac{1}{\epsilon_{P_r,T_r}} - 1\right] + \omega_{P_r,T_r}Y_{P_r,T_r}(T - T_r) \; . \qquad \text{(A-7)}$$

The various parameters and coefficients that appear in these equations are described in the text (see SUMMARY OF THE REVISED EQUATIONS OF STATE, p. 55).

APPENDIX B

Summary of Equations for the Born Coefficients of Aqueous Electrolytes (ω_k) and Aqueous Ions (ω_j) and their Pressure and Temperature Derivatives

It follows from eqs (14), (15), (34) and (35) given in the text that

$$\left(\frac{\partial \omega}{\partial P}\right)_T = \left(\frac{\partial g}{\partial P}\right)_T X_1 \quad , \tag{B-1}$$

$$\left(\frac{\partial \omega}{\partial T}\right)_P = \left(\frac{\partial g}{\partial T}\right)_P X_1 \quad , \tag{B-2}$$

$$\left(\frac{\partial^2 \omega}{\partial P^2}\right)_T = \left(\frac{\partial g}{\partial P}\right)_T^2 X_2 + \left(\frac{\partial^2 g}{\partial P^2}\right)_T X_1 \quad , \tag{B-3}$$

$$\left(\frac{\partial^2 \omega}{\partial T^2}\right)_P = \left(\frac{\partial g}{\partial T}\right)_P^2 X_2 + \left(\frac{\partial^2 g}{\partial T^2}\right)_P X_1 \quad , \tag{B-4}$$

and

$$\left(\partial \left(\frac{\partial \omega}{\partial P}\right)_T / \partial T\right)_P = \left(\frac{\partial g}{\partial P}\right)_T \left(\frac{\partial g}{\partial T}\right)_P X_2 + \left(\partial \left(\frac{\partial g}{\partial P}\right)_T / \partial T\right)_P X_1 \quad , \tag{B-5}$$

where for the kth aqueous electrolyte ($\omega = \omega_k$)

$$\omega_k = \eta \sum_j \nu_{j,k} Z_j^2 \left[r_{x,j} + \left| Z_j \right| (k_Z + g) \right]^{-1} \quad , \tag{B-6}$$

$$X_1 \equiv -\eta \sum_j \nu_{j,k} \left| Z_j^3 \right| \left[r_{x,j} + \left| Z_j \right| (k_Z + g) \right]^{-2} \quad , \tag{B-7}$$

$$X_2 \equiv 2\eta \sum_j \nu_{j,k} Z_j^4 \left[r_{x,j} + \left| Z_j \right| (k_Z + g) \right]^{-3} \quad , \tag{B-8}$$

and for the jth aqueous ion ($\omega = \omega_j$)

$$\omega_j = \eta \left[Z_j^2 \left[r_{x,j} + \left| Z_j \right| (k_Z + g) \right]^{-1} - Z_j (3.082 + g)^{-1} \right] \quad , \tag{B-9}$$

$$X_1 \equiv -\eta \left[\left| Z_j^3 \right| \left[r_{x,j} + \left| Z_j \right| (k_Z + g) \right]^{-2} - Z_j (3.082 + g)^{-2} \right] \quad , \tag{B-10}$$

$$X_2 \equiv 2\eta \left[Z_j^4 \left[r_{x,j} + \left| Z_j \right| (k_Z + g) \right]^{-3} - Z_j (3.082 + g)^{-3} \right] \quad , \tag{B-11}$$

where $\eta = 1.66027 \times 10^5$ Å cal mole^{-1}, $\nu_{j,k}$ represents the stoichiometric number of moles of the jth ion in one mole of the kth electrolyte, Z_j and $r_{x,j}$ correspond to the charge and the crystallographic radius of the ion, k_Z is equal to 0.94 Å for cations (k_+) and 0.0 Å for anions (k_-), and $3.082 = r_{x,H^+} + 0.94$ (see caption of table 3).

APPENDIX C

Summary of Equations and Coefficients for the Function g and its Pressure and Temperature Derivatives

$$g = 0.5\left[-b + \sqrt{b^2 - 4c}\right] \tag{C-1a}$$

where

$$b = 3.72 - 2\eta\left[\sum_{i=-1}^{4}\sum_{j=0}^{4-i} a_{ij}\,\mathrm{T}^i\,\rho^j\right]^{-1} \tag{C-1b}$$

and

$$c = 3.4571 - 3.72\eta\left[\sum_{i=-1}^{4}\sum_{j=0}^{4-i} a_{ij}\,\mathrm{T}^i\,\rho^j\right]^{-1} \tag{C-1c}$$

It follows that

$$\left[\frac{\partial g}{\partial \mathrm{P}}\right]_{\mathrm{T}} = \frac{\beta}{\mathrm{X}_1}\sum_{i=-1}^{4}\sum_{j=0}^{4-i} j\,a_{ij}\,\mathrm{T}^i\,\rho^j \quad , \tag{C-2}$$

$$\left[\frac{\partial g}{\partial \mathrm{T}}\right]_{\mathrm{P}} = \mathrm{X}_1^{-1}\sum_{i=-1}^{4}\sum_{j=0}^{4-i} a_{ij}\,\mathrm{T}^i\,\rho^j(i\mathrm{T}^{-1} - j\,\alpha) \quad , \tag{C-3}$$

$$\left[\frac{\partial^2 g}{\partial \mathrm{P}^2}\right]_{\mathrm{T}} = \left[\frac{\partial g}{\partial \mathrm{P}}\right]_{\mathrm{T}}\left[\left[\frac{\partial \ln\beta}{\partial \mathrm{P}}\right]_{\mathrm{T}} - \frac{\mathrm{X}_2}{\mathrm{X}_1}\left[\frac{\partial g}{\partial \mathrm{P}}\right]_{\mathrm{T}}\right] + \frac{\beta^2}{\mathrm{X}_1}\sum_{i=-1}^{4}\sum_{j=0}^{4-i} j^2\,a_{ij}\,\mathrm{T}^i\,\rho^j \quad , \tag{C-4}$$

$$\left[\frac{\partial^2 g}{\partial \mathrm{T}^2}\right]_{\mathrm{P}} = -\frac{\mathrm{X}_2}{\mathrm{X}_1}\left[\frac{\partial g}{\partial \mathrm{T}}\right]_{\mathrm{P}}^2 + \mathrm{X}_1^{-1}\sum_{i=-1}^{4}\sum_{j=0}^{4-i} a_{ij}\,\mathrm{T}^i\,\rho^j\left[j\alpha(j\alpha - 2i\mathrm{T}^{-1}) + i(i-1)\mathrm{T}^{-2} - j\left[\frac{\partial \alpha}{\partial \mathrm{T}}\right]_{\mathrm{P}}\right] \quad , \tag{C-5}$$

and

$$\left[\partial\left[\frac{\partial g}{\partial \mathrm{P}}\right]_{\mathrm{T}} / \partial \mathrm{T}\right]_{\mathrm{P}} = \left[\frac{\partial g}{\partial \mathrm{P}}\right]_{\mathrm{T}}\left[\left[\frac{\partial \ln\beta}{\partial \mathrm{T}}\right]_{\mathrm{P}} - \frac{\mathrm{X}_2}{\mathrm{X}_1}\left[\frac{\partial g}{\partial \mathrm{T}}\right]_{\mathrm{P}}\right] + \frac{\beta}{\mathrm{X}_1}\sum_{i=-1}^{4}\sum_{j=0}^{4-i} j\,a_{ij}\,\mathrm{T}^i\,\rho^j(i\mathrm{T}^{-1} - j\,\alpha) \quad , \tag{C-6}$$

where

$$X_1 \equiv -\eta\left[(1.91 + g)^{-2} + (1.81 + g)^{-2}\right] \tag{C-7}$$

and

$$X_2 \equiv 2\eta\left[(1.91 + g)^{-3} + (1.81 + g)^{-3}\right] \tag{C-8}$$

where η is equal to 1.66027×10^5 Å cal mole^{-1}, ρ represents the density in gm cm^{-3} of H_2O, $\beta = (\partial\rho/\partial P)_T/\rho$, $\alpha = -(\partial\rho/\partial T)_P/\rho$, and a_{ij} represents the coefficients given in Table C-1 below. The values of ρ, β, and α used in the present study were calculated from the equation of state for H_2O given by Haar, Gallagher, and Kell (1980).

TABLE C-1

Coefficients for computing values of the solvent function g and its pressure and temperature derivatives from eqs. (C-1) through (C-6).

$a(i,j)$	Value	$a(i,j)$	Value
a(-1,0)	-3.447160509×10^9	a(1,0)	-3.260300052×10^4
a(-1,1)	6.814704812×10^9	a(1,1)	5.606615908×10^4
a(-1,2)	-1.761045616×10^9	a(1,2)	-2.868203067×10^4
a(-1,3)	-4.230074117×10^9	a(1,3)	3.794138977×10^3
a(-1,4)	3.256835062×10^9	a(2,0)	2.716227245×10
a(-1,5)	-6.583330861×10^8	a(2,1)	-3.368176788×10
a(0,0)	1.806233478×10^7	a(2,2)	9.804290400
a(0,1)	-3.606097634×10^7	a(3,0)	$-1.060481048 \times 10^{-2}$
a(0,2)	2.102834814×10^7	a(3,1)	$6.934581461 \times 10^{-3}$
a(0,3)	-1.133277153×10^6	a(4,0)	$1.576972120 \times 10^{-6}$
a(0,4)	-1.416255412×10^6		

Upper limit of the shaded region in figure 19 at $164° \leq t \leq 450°$.

$$P = d_1t^3 + d_2t^2 + d_3t + d_4 + d_5\ln(t - 163) \tag{C-9}$$

Lower limit of the shaded region in figure 19 at $350° < t \leq 450°$.

$$P = d_6 + d_7t + \frac{d_8}{t^2} \tag{C-10}$$

where t stands for temperature in °C and

$d_1 = 5.37268 \times 10^{-5}$
$d_2 = -6.65484 \times 10^{-2}$
$d_3 = 3.03872 \times 10$
$d_4 = -3.39717 \times 10^3$
$d_5 = 7.72626 \times 10$
$d_6 = 7217.$
$d_7 = -8.1886$
$d_8 = -5.127 \times 10^8$

APPENDIX D

Summary of Equations for the Born Functions Y, Q, N, X and U

$$Y \equiv -\left[\frac{\partial(1/\epsilon)}{\partial T}\right]_P = \frac{1}{\epsilon^2}\left[\frac{\partial \epsilon}{\partial T}\right]_P , \tag{D-1}$$

$$Q \equiv -\left[\frac{\partial(1/\epsilon)}{\partial P}\right]_T = \frac{1}{\epsilon^2}\left[\frac{\partial \epsilon}{\partial P}\right]_T , \tag{D-2}$$

$$N \equiv \left[\frac{\partial Q}{\partial P}\right]_T = \frac{1}{\epsilon^2}\left[\left[\frac{\partial^2 \epsilon}{\partial P^2}\right]_T - \frac{2}{\epsilon}\left[\frac{\partial \epsilon}{\partial P}\right]_T^2\right] , \tag{D-3}$$

$$X \equiv \left[\frac{\partial Y}{\partial T}\right]_P = \frac{1}{\epsilon^2}\left[\left[\frac{\partial^2 \epsilon}{\partial T^2}\right]_P - \frac{2}{\epsilon}\left[\frac{\partial \epsilon}{\partial T}\right]_P^2\right] , \tag{D-4}$$

and

$$U \equiv \left[\frac{\partial Q}{\partial T}\right]_P = \frac{1}{\epsilon^2}\left[\left[\partial\left[\frac{\partial \epsilon}{\partial P}\right]_T / \partial T\right]_P - \frac{2}{\epsilon}\left[\frac{\partial \epsilon}{\partial T}\right]_P\left[\frac{\partial \epsilon}{\partial P}\right]_T\right] , \tag{D-5}$$

where ϵ represents the dielectric constant of H_2O (see app. E).

APPENDIX E

Summary of Equations and Coefficients for the Dielectric Constant of H_2O (ϵ) *and its Pressure and Temperature Derivatives*

TABLE E-1

Coefficients for computing values of the dielectric constant of H_2O (ϵ) and its pressure and temperature derivatives from eqs. (E-1) through (E-6) (Helgeson and Kirkham, 1976).

$e(i,j)$	Value	$e(i,j)$	Value
$e(0,1)$	4.39109592×10^2	$e(1,3)$	$-6.13941874 \times 10^{-2}$
$e(0,2)$	-2.18995148×10^2	$e(2,0)$	$4.61662109 \times 10^{-3}$
$e(0,3)$	1.82898246×10	$e(2,1)$	$-1.35650709 \times 10^{-3}$
$e(0,4)$	1.54886800×10^2	$e(2,2)$	$1.60491325 \times 10^{-4}$
$e(0,5)$	-6.13542375×10	$e(3,0)$	$-4.03643333 \times 10^{-6}$
$e(1,0)$	-2.33277456	$e(3,1)$	$5.94046919 \times 10^{-7}$
$e(1,1)$	1.00498361	$e(4,0)$	$1.31604037 \times 10^{-9}$
$e(1,2)$	$-2.08896146 \times 10^{-1}$		

$$\epsilon = \sum_{i=0}^{4} \sum_{j=0}^{4-i} e_{ij} T^i \rho^j \quad , \tag{E-1}$$

$$\left[\frac{\partial \epsilon}{\partial P}\right]_T = \beta \sum_{i=0}^{4} \sum_{j=0}^{4-i} j\, e_{ij} T^i \rho^j \quad , \tag{E-2}$$

$$\left[\frac{\partial \epsilon}{\partial T}\right]_P = \sum_{i=0}^{4} \sum_{j=0}^{4-i} e_{ij} T^i \rho^j (iT^{-1} - j\alpha) \quad , \tag{E-3}$$

$$\left[\frac{\partial^2 \epsilon}{\partial P^2}\right]_T = \left[\frac{\partial \epsilon}{\partial P}\right]_T \left[\frac{\partial \ln \beta}{\partial P}\right]_T + \beta^2 \sum_{i=0}^{4} \sum_{j=0}^{4-i} j^2 e_{ij} T^i \rho^j \quad , \tag{E-4}$$

$$\left[\frac{\partial^2 \epsilon}{\partial T^2}\right]_P = \sum_{i=0}^{4} \sum_{j=0}^{4-i} e_i j\, T^i \rho^j \left[j\alpha(j\alpha - 2iT^{-1}) + i(i-1)T^{-2} - j\left[\frac{\partial \alpha}{\partial T}\right]_P\right] \quad , \tag{E-5}$$

and

$$\left[\partial \left[\frac{\partial \epsilon}{\partial P}\right]_T / \partial T\right]_P = \left[\frac{\partial \epsilon}{\partial P}\right]_T \left[\frac{\partial \ln \beta}{\partial T}\right]_P + \beta \sum_{i=0}^{4} \sum_{j=0}^{4-i} j\, e_{ij} T^i \rho^j (iT^{-1} - j\alpha) \quad , \tag{E-6}$$

where ρ represents the density in gm cm^{-3} of H_2O, $\beta = (\partial \rho / \partial P)_T / \rho$, $\alpha = -(\partial \rho / \partial T)_P / \rho$ and e_{ij} represents the coefficients given in Table E-1. Equations (E-1) through (E-2) and the coefficients in table E-1 were taken from Helgeson and Kirkham (1974). The values of ρ, β and α used in this study were calculated from the equation of state for H_2O given by Haar, Gallagher, and Kell (1980). At temperatures below 100°C and pressures above 1 kb, the equations and coefficients given by Bradley and Pitzer (1979) were used instead of equations (E-1) through (E-6) to compute extrapolated values of the dielectric constant and its pressure and temperature derivatives.

APPENDIX F

Summary of Equations for the Standard Partial Molal Nonsolvation Properties ($\Delta\bar{\Xi}_n^\circ$) of Aqueous Ions and Electrolytes

It follows from eqs (8), (22), (23), (24), (28a, b, and c), (30), and (31) in the text and thermodynamic relations given below that we can write the following relations:

Volume ($\Delta\bar{V}_n^\circ$)

$$\Delta\bar{V}_n^\circ = a_1 + \frac{a_2}{\Psi + P} + \frac{a_3}{T - \Theta} + \frac{a_4}{(\Psi + P)(T - \Theta)} \quad ; \tag{F-1}$$

Isothermal Compressibility ($\Delta\bar{\kappa}_n^\circ$)

$$\Delta\bar{\kappa}_n^\circ \equiv -\left[\frac{\partial\Delta\bar{V}_n^\circ}{\partial P}\right]_T = \left[a_2 + \frac{a_4}{T-\Theta}\right]\left[\frac{1}{\Psi+P}\right]^2 ; \qquad \text{(F-2)}$$

Expansibility ($\Delta\bar{E}_{x,n}^\circ$)

$$\Delta\bar{E}_{x,n}^\circ \equiv \left[\frac{\partial\Delta\bar{V}_n^\circ}{\partial T}\right]_P = -\left[a_3 + \frac{a_4}{\Psi+P}\right]\left[\frac{1}{T-\Theta}\right]^2 ; \qquad \text{(F-3)}$$

Isobaric Heat Capacity ($\Delta\bar{C}_{P,n}^\circ$)

$$\Delta\bar{C}_{P,n}^\circ = \Delta\bar{C}_{P_r,n}^\circ - T\int_{P_r}^{P}\left[\frac{\partial\Delta\bar{E}_{x,n}^\circ}{\partial T}\right]_P dP$$

$$= c_1 + \frac{c_2}{(T-\Theta)^2} - \left[\frac{2T}{(T-\Theta)^3}\right]\left[a_3(P-P_r) + a_4 \ln\left[\frac{\Psi+P}{\Psi+P_r}\right]\right] ; \qquad \text{(F-4)}$$

Entropy ($\Delta\bar{S}_n^\circ$) change from P, T to P_r, T_r

$$\Delta\bar{S}_n^\circ - \Delta\bar{S}_{n,P_r,T_r}^\circ = \int_{T_r}^{T}\frac{\Delta\bar{C}_{P_r,n}^\circ}{T}dT - \int_{P_r}^{P}\Delta\bar{E}_{x,n}^\circ\, dP$$

$$= c_1 \ln\left[\frac{T}{T_r}\right] - \frac{c_2}{\Theta}\left[\left[\frac{1}{T-\Theta}\right] - \left[\frac{1}{T_r-\Theta}\right] + \frac{1}{\Theta}\ln\left[\frac{T_r(T-\Theta)}{T(T_r-\Theta)}\right]\right]$$

$$+ \left[\frac{1}{T-\Theta}\right]^2\left[a_3(P-P_r) + a_4 \ln\left[\frac{\Psi+P}{\Psi+P_r}\right]\right] ; \qquad \text{(F-5)}$$

Enthalpy ($\Delta\bar{H}_n^\circ$) change from P, T to P_r, T_r

$$\Delta\bar{H}_n^\circ - \Delta\bar{H}_{n,P_r,T_r}^\circ = \int_{T_r}^{T} \Delta\bar{C}_{P_r,n}^\circ \, dT + \int_{P_r}^{P} \Delta\bar{V}_n^\circ \, dP - T\int_{P_r}^{P} \Delta\bar{E}_{x,n}^\circ \, dP$$

$$= c_1(T - T_r) - c_2\left[\left(\frac{1}{T-\Theta}\right) - \left(\frac{1}{T_r-\Theta}\right)\right]$$

$$+ a_1(P - P_r) + a_2 \ln\left(\frac{\Psi + P}{\Psi + P_r}\right)$$

$$+ \left(\frac{2T-\Theta}{(T-\Theta)^2}\right)\left[a_3(P - P_r) + a_4 \ln\left(\frac{\Psi + P}{\Psi + P_r}\right)\right] ; \qquad \text{(F-6)}$$

Gibbs Free Energy ($\Delta\bar{G}_n^\circ$) change from P, T to P_r, T_r

$$\Delta\bar{G}_n^\circ - \Delta\bar{G}_{n,P_r,T_r}^\circ = -\Delta\bar{S}_{n,P_r,T_r}^\circ(T - T_r) + (\Delta\bar{H}_n^\circ - \Delta\bar{H}_{n,P_r,T_r}^\circ) - T(\Delta\bar{S}_n^\circ - \Delta\bar{S}_{n,P_r,T_r}^\circ)$$

$$= -\Delta\bar{S}_{n,P_r,T_r}^\circ(T - T_r) - c_1\left[T \ln\left(\frac{T}{T_r}\right) - T + T_r\right]$$

$$+ a_1(P - P_r) + a_2 \ln\left(\frac{\Psi + P}{\Psi + P_r}\right)$$

$$- c_2\left\{\left[\left(\frac{1}{T-\Theta}\right) - \left(\frac{1}{T_r-\Theta}\right)\right]\left(\frac{\Theta - T}{\Theta}\right) - \frac{T}{\Theta^2} \ln\left(\frac{T_r(T-\Theta)}{T(T_r-\Theta)}\right)\right\}$$

$$+ \left(\frac{1}{T-\Theta}\right)\left[a_3(P - P_r) + a_4 \ln\left(\frac{\Psi + P}{\Psi + P_r}\right)\right] \qquad \text{(F-7)}$$

APPENDIX G

Summary of Equations for the Standard Partial Molal Solvation Properties ($\Delta\bar{\Xi}_s^\circ$) of Aqueous Ions and Electrolytes

It follows from eqs (9), (15), (16), (34) and (35) in the text, equations in app. D, and thermodynamic relations given below that we can write the following relations:

Volume ($\Delta\bar{V}_s^\circ$)

$$\Delta\bar{V}_s^\circ = \left[\frac{\partial \Delta\bar{G}_s^\circ}{\partial P}\right]_T = -\omega Q + \left[\frac{1}{\epsilon} - 1\right]\left[\frac{\partial \omega}{\partial P}\right]_T ; \tag{G-1}$$

Isothermal Compressibility ($\Delta\bar{\kappa}_s^\circ$)

$$\Delta\bar{\kappa}_s^\circ \equiv -\left[\frac{\partial \Delta\bar{V}_s^\circ}{\partial P}\right]_T = \omega N + 2Q\left[\frac{\partial \omega}{\partial P}\right]_T - \left[\frac{1}{\epsilon} - 1\right]\left[\frac{\partial^2 \omega}{\partial P^2}\right]_T ; \tag{G-2}$$

Expansibility ($\Delta\bar{E}_{x,s}^\circ$)

$$\Delta\bar{E}_{x,s}^\circ \equiv \left[\frac{\partial \Delta\bar{V}_s^\circ}{\partial T}\right]_P = -\omega U - Q\left[\frac{\partial \omega}{\partial T}\right]_P - Y\left[\frac{\partial \omega}{\partial P}\right]_T$$

$$+ \left[\frac{1}{\epsilon} - 1\right]\left[\partial\left[\frac{\partial \omega}{\partial P}\right]_T / \partial T\right]_P ; \tag{G-3}$$

Isobaric Heat Capacity ($\Delta\bar{C}_{P,s}^\circ$)

$$\Delta\bar{C}_{P,s}^\circ = T\left[\frac{\partial \Delta\bar{S}_s^\circ}{\partial T}\right]_P = \omega TX + 2TY\left[\frac{\partial \omega}{\partial T}\right]_P - T\left[\frac{1}{\epsilon} - 1\right]\left[\frac{\partial^2 \omega}{\partial T^2}\right]_P ; \tag{G-4}$$

Entropy ($\Delta\bar{S}_s^\circ$)

$$\Delta\bar{S}_s^\circ = -\left[\frac{\partial \Delta\bar{G}_s^\circ}{\partial T}\right]_P = \omega Y - \left[\frac{1}{\epsilon} - 1\right]\left[\frac{\partial \omega}{\partial T}\right]_P ; \tag{G-5}$$

Enthalpy ($\Delta\bar{H}_s^\circ$)

$$\Delta\bar{H}_s^\circ = \Delta\bar{G}_s^\circ + T\Delta\bar{S}_s^\circ = \omega\left[\frac{1}{\epsilon} - 1\right] + \omega TY - T\left[\frac{1}{\epsilon} - 1\right]\left[\frac{\partial\omega}{\partial T}\right]_P . \quad \text{(G-6)}$$

Gibbs Free Energy ($\Delta\bar{G}_s^\circ$)

$$\Delta\bar{G}_s^\circ = \omega\left[\frac{1}{\epsilon} - 1\right] . \quad \text{(G-7)}$$

APPENDIX H

TABLE H-1

Summary of the dielectric constant (eq E-1 in app. E) and Born functions (eqs D-1 through D-5 in app. D) at 1 bar and for temperatures from 0° to 95°C and vapor-liquid saturation pressures for H_2O at temperatures > 95°C.

T (°C)	ϵ	$10^7 Q^a$	$10^5 Y^b$	$10^{10} N^c$	$10^7 X^d$	$10^9 U^e$
0	87.79	5.41	-5.01	-1.80	-3.47	0.19
5	85.87	5.44	-5.18	-1.74	-3.30	1.06
10	83.98	5.51	-5.34	-1.72	-3.19	1.76
15	82.11	5.61	-5.50	-1.73	-3.13	2.36
20	80.27	5.75	-5.65	-1.76	-3.10	2.89
25	78.47	5.90	-5.81	-1.82	-3.09	3.38
30	76.69	6.08	-5.96	-1.89	-3.10	3.85
35	74.96	6.29	-6.12	-1.98	-3.13	4.31
40	73.26	6.51	-6.28	-2.08	-3.16	4.77
45	71.59	6.76	-6.43	-2.20	-3.20	5.23
50	69.96	7.04	-6.60	-2.34	-3.26	5.71
55	68.36	7.33	-6.76	-2.49	-3.31	6.20
60	66.80	7.66	-6.93	-2.66	-3.37	6.71
65	65.27	8.01	-7.10	-2.85	-3.44	7.25
70	63.78	8.38	-7.27	-3.06	-3.51	7.82
75	62.31	8.79	-7.45	-3.30	-3.58	8.42
80	60.88	9.23	-7.63	-3.56	-3.66	9.07
85	59.49	9.70	-7.81	-3.85	-3.75	9.75
90	58.12	10.20	-8.00	-4.17	-3.83	10.48
95	56.78	10.75	-8.20	-4.53	-3.93	11.27
100	55.48	11.33	-8.40	-4.93	-4.03	12.11
105	54.20	11.96	-8.60	-5.37	-4.13	13.02
110	52.95	12.63	-8.81	-5.86	-4.25	14.00
115	51.73	13.36	-9.02	-6.40	-4.37	15.05
120	50.54	14.13	-9.25	-7.01	-4.49	16.19
125	49.37	14.97	-9.47	-7.69	-4.63	17.43
130	48.23	15.87	-9.71	-8.44	-4.78	18.77
135	47.11	16.84	-9.95	-9.29	-4.94	20.23
140	46.02	17.89	-10.20	-10.23	-5.12	21.82
145	44.96	19.02	-10.46	-11.30	-5.30	23.56
150	43.91	20.24	-10.73	-12.49	-5.51	25.46

^{a} bar $^{-1}$. ^{b} K^{-1}. ^{c} bar $^{-2}$. ^{d} K^{-2}. ^{e} K^{-1} bar $^{-1}$.

TABLE H-2

Dielectric constant of H_2O (ϵ) as a function of temperature and pressure. The values shown for pressures above 1 kb and temperatures < 100° C were generated by extrapolating equations given by Bradley and Pitzer (1979). All of the others were calculated with the aid of app. E. SAT refers to vapor-liquid saturation pressures for H_2O.

T	PRESSURE, KB									
(°C)	SAT	0.25	0.5	0.75	1	1.5	2	3	4	5
0	87.79	88.80	89.76	90.67	91.54	93.44	95.11	98.21	101.0	103.7
25	78.46	79.35	80.19	81.00	81.76	83.40	84.87	87.58	90.02	92.24
50	69.96	70.79	71.59	72.35	73.07	74.58	75.94	78.40	80.59	82.57
75	62.31	63.14	63.92	64.66	65.36	66.82	68.10	70.40	72.42	74.22
100	55.48	56.31	57.10	57.84	58.54	59.83	61.02	63.11	64.90.	66.46
125	49.37	50.24	51.04	51.80	52.51	53.81	54.99	57.05	58.81	60.34
150	43.91	44.82	45.67	46.45	47.18	48.50	49.68	51.74	53.47	54.97
175	39.02	39.99	40.89	41.71	42.46	43.82	45.02	47.07	48.78	50.24
200	34.61	35.65	36.62	37.49	38.28	39.68	40.90	42.96	44.65	46.08
225	30.58	31.71	32.77	33.71	34.55	36.00	37.25	39.32	41.00	42.39
250	26.87	28.09	29.29	30.30	31.20	32.72	34.00	36.09	37.75	39.11
275	23.37	24.71	26.08	27.21	28.17	29.77	31.09	33.20	34.84	36.16
300	19.99	21.47	23.10	24.36	25.40	27.10	28.46	30.58	32.21	33.50
325	16.59	18.25	20.27	21.71	22.86	24.65	26.06	28.21	29.82	31.07
350	12.87	14.80	17.55	19.22	20.49	22.41	23.87	26.04	27.62	28.84
375		10.17	14.86	16.87	18.28	20.33	21.84	24.03	25.60	26.77
400			12.14	14.61	16.20	18.40	19.96	22.18	23.73	24.87
425			9.38	12.46	14.25	16.60	18.22	20.46	21.99	23.10
450			6.80	10.44	12.43	14.93	16.61	18.88	20.40	21.48

TABLE H-3

$(Q \text{ in } bar^{-1}) \times 10^6$ as a function of pressure and temperature computed from eq. (D-2) in app. D—see caption of table H-2.

T	PRESSURE, KB									
(°C)	SAT	0.25	0.5	0.75	1	1.5	2	3	4	5
0	0.54	0.50	0.46	0.43	0.40	0.39	0.36	0.31	0.27	0.23
25	0.59	0.55	0.51	0.48	0.45	0.44	0.40	0.33	0.29	0.25
50	0.70	0.65	0.61	0.57	0.53	0.50	0.45	0.38	0.32	0.28
75	0.88	0.80	0.74	0.69	0.64	0.60	0.53	0.43	0.36	0.31
100	1.13	1.02	0.93	0.86	0.80	0.69	0.61	0.49	0.40	0.33
125	1.50	1.33	1.20	1.09	1.00	0.85	0.74	0.58	0.47	0.39
150	2.02	1.76	1.56	1.39	1.26	1.06	0.91	0.70	0.56	0.46
175	2.80	2.37	2.05	1.80	1.61	1.32	1.12	0.84	0.66	0.54
200	3.98	3.26	2.73	2.35	2.07	1.65	1.37	1.00	0.78	0.62
225	5.84	4.58	3.70	3.10	2.67	2.07	1.68	1.19	0.91	0.71
250	8.99	6.67	5.10	4.13	3.46	2.59	2.05	1.41	1.05	0.81
275	14.80	10.16	7.21	5.57	4.53	3.25	2.51	1.67	1.21	0.92
300	27.10	16.66	10.52	7.65	5.97	4.09	3.06	1.96	1.39	1.03
325	60.09	30.96	16.05	10.73	7.98	5.16	3.74	2.30	1.58	1.15
350	209.6	74.92	26.04	15.44	10.80	6.54	4.56	2.69	1.80	1.29
375		496.9	46.15	22.93	14.84	8.33	5.59	3.15	2.05	1.43
400			92.53	35.29	20.71	10.67	6.85	3.69	2.34	1.59
425			212.6	56.21	29.36	13.73	8.43	4.33	2.67	1.77
450			469.8	91.50	42.04	17.74	10.40	5.10	3.05	1.98

TABLE H-4

$(-Y \text{ in } K^{-1}) \times 10^5$ as a function of pressure and temperature computed from eq. (D-1) in app. D—see caption of table H-2.

T	PRESSURE, KB									
(°C)	SAT	0.25	0.5	0.75	1	1.5	2	3	4	5
0	5.01	5.00	4.98	4.96	4.93	4.92	4.86	4.77	4.70	4.65
25	5.81	5.73	5.65	5.58	5.52	5.40	5.30	5.14	5.01	4.91
50	6.60	6.46	6.34	6.23	6.13	5.94	5.80	5.57	5.39	5.26
75	7.45	7.25	7.08	6.93	6.79	6.53	6.34	6.04	5.82	5.65
100	8.40	8.12	7.88	7.67	7.48	7.17	6.91	6.49	6.17	5.91
125	9.47	9.08	8.75	8.47	8.22	7.81	7.48	6.97	6.59	6.30
150	10.73	10.17	9.71	9.33	9.00	8.47	8.05	7.44	7.00	6.67
175	12.25	11.44	10.80	10.28	9.84	9.16	8.64	7.90	7.39	7.02
200	14.18	12.99	12.07	11.35	10.77	9.90	9.25	8.37	7.78	7.37
225	16.77	14.97	13.60	12.60	11.83	10.70	9.91	8.85	8.19	7.73
250	20.51	17.66	15.55	14.12	13.07	11.61	10.62	9.38	8.62	8.12
275	26.40	21.57	18.13	16.02	14.57	12.66	11.44	9.96	9.10	8.56
300	36.91	27.81	21.69	18.47	16.42	13.90	12.38	10.63	9.65	9.06
325	60.06	39.37	26.91	21.73	18.76	15.39	13.49	11.40	10.29	9.64
350	141.4	67.94	35.05	26.18	21.76	17.20	14.80	12.30	11.03	10.31
375		258.8	48.81	32.39	25.64	19.39	16.35	13.34	11.88	11.06
400			74.49	41.23	30.68	22.03	18.16	14.50	12.80	11.87
425			125.0	53.90	37.16	25.15	20.20	15.75	13.75	12.68
450			197.3	71.47	45.35	28.72	22.40	16.98	14.62	13.39

TABLE H-5

$(-N \text{ in } bar^{-2}) \times 10^{10}$ as a function of pressure and temperature computed from eq. (D-3) in app. D—see caption of table H-2.

T	PRESSURE, KB									
(°C)	SAT	0.25	0.5	0.75	1	1.5	2	3	4	5
0	1.80	1.49	1.36	1.30	1.27	0.70	0.61	0.46	0.36	0.29
25	1.82	1.54	1.37	1.25	1.16	0.85	0.72	0.54	0.42	0.33
50	2.34	1.96	1.69	1.50	1.35	1.08	0.90	0.66	0.49	0.38
75	3.30	2.71	2.29	1.98	1.74	1.42	1.16	0.82	0.60	0.46
100	4.93	3.95	3.26	2.75	2.37	1.84	1.48	1.03	0.77	0.59
125	7.69	5.96	4.78	3.95	3.33	2.49	1.95	1.31	0.94	0.72
150	12.49	9.29	7.20	5.79	4.77	3.43	2.61	1.68	1.18	0.88
175	21.19	14.96	11.11	8.63	6.93	4.78	3.53	2.17	1.48	1.08
200	37.86	25.01	17.56	13.08	10.17	6.70	4.78	2.81	1.86	1.32
225	72.26	43.79	28.52	20.18	15.10	9.43	6.47	3.62	2.32	1.62
250	150.9	81.59	47.92	31.74	22.66	13.29	8.76	4.65	2.89	1.97
275	359.2	166.1	84.08	51.11	34.46	18.79	11.84	5.95	3.57	2.38
300	1052.	387.7	156.2	84.64	53.18	26.65	15.97	7.57	4.39	2.87
325	4484.	1144.	312.9	145.0	83.44	37.91	21.50	9.58	5.38	3.44
350	46960	5556.	695.5	258.5	133.3	54.12	28.92	12.08	6.55	4.10
375			1781.	481.9	217.1	77.51	38.84	15.19	7.95	4.87
400			5459.	939.6	359.4	111.3	52.12	19.04	9.63	5.78
425			(18998)	(1892)	(601)	(160)	(70)	(24)	(12)	(7)
450				(3782)	(1005)	(229)	(93)	(30)	(14)	(8)

TABLE H-6

(-X in K^{-2}) x 10^7 as a function of pressure and temperature computed from eq. (D-4) in app. D—see caption of table H-2.

T	PRESSURE, KB									
(°C)	SAT	0.25	0.5	0.75	1	1.5	2	3	4	5
0	3.48	3.05	2.71	2.45	2.27	1.83	1.62	1.29	1.02	0.81
25	3.09	2.87	2.68	2.53	2.40	2.06	1.89	1.62	1.41	1.25
50	3.26	3.03	2.84	2.68	2.54	2.26	2.08	1.81	1.62	1.48
75	3.58	3.30	3.07	2.87	2.70	2.45	2.25	1.96	1.76	1.62
100	4.03	3.64	3.33	3.07	2.86	2.52	2.27	1.93	1.73	1.62
125	4.63	4.08	3.65	3.30	3.03	2.60	2.29	1.89	1.66	1.51
150	5.51	4.68	4.07	3.60	3.24	2.70	2.33	1.86	1.60	1.44
175	6.85	5.57	4.67	4.02	3.53	2.84	2.39	1.86	1.56	1.40
200	9.01	6.93	5.54	4.61	3.95	3.06	2.52	1.90	1.58	1.41
225	12.70	9.09	6.86	5.48	4.55	3.40	2.72	2.00	1.66	1.49
250	19.48	12.71	8.86	6.74	5.41	3.88	3.04	2.20	1.82	1.64
275	33.51	19.22	11.97	8.56	6.62	4.54	3.48	2.48	2.06	1.86
300	68.62	32.46	17.00	11.22	8.29	5.43	4.08	2.87	2.37	2.15
325	193.1	65.85	25.55	15.10	10.55	6.56	4.82	3.34	2.76	2.50
350	1193.	198.5	41.20	20.84	13.60	7.96	5.71	3.88	3.17	2.85
375			72.76	29.42	17.63	9.63	6.70	4.42	3.55	3.16
400			141.7	42.15	22.84	11.50	7.71	4.86	3.79	3.30
425			(269)	(60)	(29)	(13)	(9)	(5)	(4)	(3)
450				(80)	(36)	(15)	(9)	(5)	(3)	(2)

TABLE H-7

(U in $bar^{-1}K^{-1}$) x 10^9 as a function of pressure and temperature computed from eq. (D-5) in app. D—see caption of table H-2.

T	PRESSURE, KB									
(°C)	SAT	0.25	0.5	0.75	1	1.5	2	3	4	5
0	0.19	0.51	0.74	1.01	1.34	1.23	1.05	0.78	0.60	0.48
25	3.38	3.09	2.86	2.71	2.61	2.23	1.90	1.42	1.10	0.88
50	5.71	5.07	4.56	4.15	3.83	3.18	2.68	1.99	1.53	1.22
75	8.43	7.34	6.48	5.80	5.25	4.23	3.52	2.55	1.94	1.53
100	12.11	10.31	8.94	7.87	7.01	5.72	4.80	3.62	2.88	2.38
125	17.43	14.43	12.23	10.55	9.24	7.33	6.01	4.32	3.30	2.62
150	25.46	20.34	16.73	14.11	12.12	9.31	7.44	5.13	3.78	2.90
175	38.17	29.13	23.08	18.90	15.86	11.76	9.14	6.04	4.30	3.20
200	59.54	42.81	32.29	25.51	20.81	14.80	11.16	7.05	4.85	3.50
225	98.23	65.35	46.14	34.83	27.47	18.62	13.57	8.18	5.43	3.80
250	175.7	105.3	67.89	48.35	36.60	23.46	16.48	9.45	6.05	4.10
275	354.1	183.9	103.9	68.59	49.38	29.69	20.02	10.89	6.72	4.40
300	863.9	362.9	167.4	99.93	67.65	37.79	24.39	12.57	7.47	4.72
325	2984.	884.5	288.6	150.2	94.30	48.46	29.84	14.56	8.34	5.10
350	23935	3377.	544.6	234.1	133.9	62.60	36.71	16.96	9.38	5.54
375			1159.	378.7	193.3	81.46	45.40	19.90	10.7	6.11
400			2844.	634.0	283.1	106.6	56.42	23.51	12.2	6.83
425			(7407)	(1080)	(417)	(140)	(70)	(28)	(14)	(8)
450				(1787)	(609)	(183)	(88)	(33)	(17)	(9)

TABLE H-8

(g in Å) × 10^4 as a function of pressure and temperature computed from eq. (C-1a, b, and c) using coefficients taken from C-1 in app. C. The values in parentheses are more uncertain. SAT refers to vapor-liquid saturation pressures for H_2O. Because positive values of g are generated by eq. (C-1a, b, and c) in app. C for SAT and 250 bars at 175°C, 1.5 kb at 300°, 325°, and 350°C, 1.75 kb at temperatures ≥ 350°C, and 2 kb at temperatures ≥ 425°C, these values were replaced in the table by zero (see text).

T	PRESSURE, KB								
(°C)	SAT	0.25	0.5	0.75	1	1.25	1.5	1.75	2
150	0.00	0.00	0.00	0.00	0.00	0.00	0.00	0.00	0.00
175	0.00	0.00	0.00	0.00	0.00	0.00	0.00	0.00	0.00
200	-1.45	-0.85	-0.09	0.00	0.00	0.00	0.00	0.00	0.00
225	-4.72	-2.93	-1.34	-0.34	0.00	0.00	0.00	0.00	0.00
250	-10.75	-6.52	-3.19	-1.25	-0.29	0.00	0.00	0.00	0.00
275	-22.60	-13.41	-6.43	-2.68	-0.81	-0.07	0.00	0.00	0.00
300	-46.51	-27.31	-12.52	-5.28	-1.75	-0.24	0.00	0.00	0.00
325	-97.58	-56.63	-23.98	-10.09	-3.57	-0.69	0.00	0.00	0.00
350	-228.48	-126.72	-45.27	-18.65	-6.96	-1.74	0.00	0.00	0.00
375		(-417)	-84.82	-33.17	-12.81	-3.82	-0.11	0.00	0.00
400			(-160)	-56.40	-22.08	-7.41	-1.12	0.00	0.00
425			(-315)	(-91)	-35.50	-12.90	-3.02	0.00	0.00
450			(-636)	(-139)	-52.92	-20.37	-5.96	0.00	0.00

TABLE H-9

$(\partial g / \partial P)_T$, in (Å bar^{-1}) × 10^7 as a function of pressure and temperature computed from eq. (C-2) using coefficients taken from table C-1 in app. C—see caption of table H-8.

T	PRESSURE, KB								
(°C)	SAT	0.25	0.5	0.75	1	1.25	1.5	1.75	2
150	0.00	0.00	0.00	0.00	0.00	0.00	0.00	0.00	0.00
175	-1.27	1.27	0.00	0.00	0.00	0.00	0.00	0.00	0.00
200	1.43	3.18	2.69	0.00	0.00	0.00	0.00	0.00	0.00
225	8.05	7.43	5.20	2.85	0.00	0.00	0.00	0.00	0.00
250	23.78	16.74	10.24	5.55	2.32	0.00	0.00	0.00	0.00
275	61.79	37.31	20.28	10.60	4.81	1.46	0.00	0.00	0.00
300	161.72	84.96	40.20	20.00	9.28	3.44	0.53	0.00	0.00
325	486.83	210.67	80.05	37.14	17.22	6.96	1.78	0.00	0.00
350	2333.1	673.13	162.53	67.63	30.73	13.05	4.16	0.06	0.00
375		(6835)	346.47	120.73	52.60	22.94	8.35	1.22	0.00
400			(815)	211.43	85.99	37.82	15.06	3.65	0.00
425			(2224)	(363)	133.48	58.37	24.72	7.75	-0.90
450				(602)	194.73	83.83	37.18	13.68	1.07

TABLE H-10

$(\partial g / \partial T)_P$, in (Å K^{-1}) × 10^6 as a function of pressure and temperature computed from eq. (C-4) using coefficients taken from table C-1 in app. C—see caption of table H-8.

T	PRESSURE, KB								
(°C)	SAT	0.25	0.5	0.75	1	1.25	1.5	1.75	2
150	0.00	0.00	0.00	0.00	0.00	0.00	0.00	0.00	0.00
175	-7.12	-5.76	0.00	0.00	0.00	0.00	0.00	0.00	0.00
200	-9.97	-6.79	-4.56	0.00	0.00	0.00	0.00	0.00	0.00
225	-17.59	-10.50	-5.80	-3.15	0.00	0.00	0.00	0.00	0.00
250	-34.61	-19.32	-9.47	-4.35	-1.70	0.00	0.00	0.00	0.00
275	-71.28	-38.16	-17.43	-7.53	-2.68	-0.40	0.00	0.00	0.00
300	-154.15	-78.10	-32.91	-13.97	-5.14	-1.07	0.59	0.00	0.00
325	-377.37	-170.23	-61.58	-25.51	-9.88	-2.75	0.25	0.00	0.00
350	-1373.0	-451.61	-114.08	-44.49	-17.82	-5.94	-0.72	1.09	0.00
375		(-3191)	-213.26	-73.49	-29.61	-11.01	-2.62	0.73	0.00
400			(-418)	-114.41	-45.09	-17.98	-5.64	-0.20	0.00
425			(-886)	(-166)	-62.25	-26.06	-9.62	-1.82	1.23
450				(-218)	-75.92	-33.27	-13.88	-4.01	0.56

TABLE H-11

$(\partial^2 g / \partial P^2)_T$, in (Å bar^{-2}) × 10^9 as a function of pressure and temperature computed from eq. (C-4) using coefficients taken from table C-1 in app. C—see caption of table H-8.

T	PRESSURE, KB								
(°C)	SAT	0.25	0.5	0.75	1	1.25	1.5	1.75	2
150	0.00	0.00	0.00	0.00	0.00	0.00	0.00	0.00	0.00
175	1.85	0.44	0.00	0.00	0.00	0.00	0.00	0.00	0.00
200	1.58	0.14	-0.43	0.00	0.00	0.00	0.00	0.00	0.00
225	0.42	-0.72	-0.97	-0.89	0.00	0.00	0.00	0.00	0.00
250	-3.64	-3.01	-2.22	-1.56	-1.04	0.00	0.00	0.00	0.00
275	-17.98	-9.26	-4.99	-2.96	-1.76	-0.96	0.00	0.00	0.00
300	-77.63	-28.42	-11.24	-5.72	-3.13	-1.66	-0.73	0.00	0.00
325	-440.26	-103.80	-26.14	-11.10	-5.58	-2.90	-1.37	0.00	0.00
350	-6146.4	-623.66	-65.25	-21.68	-9.82	-4.93	-2.43	-0.96	0.00
375			-184.89	-42.86	-16.94	-8.08	-4.04	-1.86	0.00
400			(-636)	-86.08	-28.51	-12.70	-6.32	-3.13	0.00
425			(-2656)	(-175)	-46.42	-19.01	-9.29	-4.79	-2.35
450				(-349)	-71.98	-26.76	-12.76	-6.76	-3.63

TABLE H-12

$(\partial^2 g / \partial T^2)_P$, in (Å K^{-2}) × 10^8 as a function of pressure and temperature computed from eq. (C-5) using coefficients taken from table C-1 in app. C—see caption of table H-8.

T	PRESSURE, KB								
(°C)	SAT	0.25	0.5	0.75	1	1.25	1.5	1.75	2
150	0.00	0.00	0.00	0.00	0.00	0.00	0.00	0.00	0.00
175	-5.54	-0.63	0.00	0.00	0.00	0.00	0.00	0.00	0.00
200	-19.39	-8.39	-1.68	0.00	0.00	0.00	0.00	0.00	0.00
225	-46.86	-22.87	-8.92	-2.01	0.00	0.00	0.00	0.00	0.00
250	-103.97	-50.74	-21.66	-8.08	-1.81	0.00	0.00	0.00	0.00
275	-234.06	-106.70	-44.11	-18.22	-6.41	-1.25	0.00	0.00	0.00
300	-590.95	-230.44	-83.37	-34.55	-13.81	-4.39	-0.51	0.00	0.00
325	-2020.8	-571.48	-152.70	-59.33	-24.77	-9.41	-2.38	0.00	0.00
350	-16074.	-2149.2	-281.25	-94.30	-39.17	-16.34	-5.56	-0.58	0.00
375			-546.99	-139.15	-55.11	-24.29	-9.82	-2.47	0.00
400			(-1191)	-187.67	-67.48	-30.97	-14.24	-5.10	0.00
425			(-2727)	(-218)	(-66)	-32.37	-17.11	-7.78	-1.73
450				(-175)	(-37)	(-23)	(-16)	-9.43	-3.58

TABLE H-13

$(\partial(\partial g/\partial P)_T/\partial T)_P$ in (Å $bar^{-1}K^{-1}$) × 10^8 as a function of pressure and temperature computed from eq. (C-4) using coefficients taken from table C-1 in app. C—see caption of table H-8.

T	PRESSURE, KB								
(°C)	SAT	0.25	0.5	0.75	1	1.25	1.5	1.75	2
150	0.00	0.00	0.00	0.00	0.00	0.00	0.00	0.00	0.00
175	0.62	0.49	0.00	0.00	0.00	0.00	0.00	0.00	0.00
200	1.60	1.11	0.70	0.00	0.00	0.00	0.00	0.00	0.00
225	3.94	2.46	1.40	0.78	0.00	0.00	0.00	0.00	0.00
250	9.65	5.38	2.79	1.45	0.74	0.00	0.00	0.00	0.00
275	24.88	12.01	5.55	2.72	1.31	0.59	0.00	0.00	0.00
300	74.33	28.91	11.02	5.02	2.36	1.04	0.36	0.00	0.00
325	311.50	83.37	22.26	9.05	4.13	1.85	0.68	0.00	0.00
350	3195.6	383.47	47.21	15.94	6.87	3.11	1.27	0.28	0.00
375			110.34	27.52	10.84	4.88	2.14	0.69	0.00
400			(302)	46.57	16.06	7.07	3.26	1.28	0.00
425			(946)	(76)	21.94	9.32	4.46	2.01	0.54
450				(117)	26.60	10.83	5.42	2.72	1.04

REFERENCES

Adams, L. H., 1931, Equilibrium in binary systems under pressure. I. An experimental and thermodynamic investigation of the system, NaCl-H_2O, at 25°: Am. Chem. Soc. Jour., v. 53, p. 3769–3813.

———1932, Equilibrium in binary systems under pressure. II. The system K_2SO_4-H_2O, at 25°: Am. Chem. Soc. Jour., v. 54, p. 2229–2243.

Ahrens, L. H., 1952, The use of ionization potentials - 1. Ionic radii of the elements: Geochim. et Cosmochim. Acta, v. 2, p. 155–169.

Allred, G. C., and Woolley, E. M., 1981a, Heat capacities of aqueous HCl, NaOH, and NaCl at 283.15, 298.15 and 313.15 K: ΔC_p° for ionization of water: Jour. Chem. Thermodynamics, v. 13, p. 147–154.

————1981b, Heat capacities of aqueous acetic acid, sodium acetate, ammonia, and ammonium chloride at 283.15, 298.15, and 313.15 K: ΔC_p° for ionization of acetic acid and for dissociation of ammonium ion: Jour. Chem. Thermodynamics, v. 13, p. 154–164.

Angell, C. A., 1982, Supercooled water, *in* Franks, F., ed., Water a comprehensive treatise v. 7: New York and London, Plenum Press, p. 1–82.

————1983, Supercooled water: Ann. Rev. Physics Chemistry, v. 34, p. 593–630.

Barbero, J. A., Hepler, L. G., McCurdy, K. G., and Tremaine, P. R., 1983, Thermodynamics of aqueous carbon dioxide and sulfur dioxide: heat capacities, volumes and the temperature dependence of ionization: Canadian Jour. Chemistry, v. 61, p. 2509–2519.

Barbero, J. A., McCurdy, K. G., and Tremaine, P. R., 1982, Apparent molal heat capacities and volumes of aqueous hydrogen sulfide and sodium hydrogen sulfide near 25°C: the temperature dependence of H_2S ionization: Canadian Jour. Chemistry, v. 60, p. 1872–1880.

Berg, R. L., and Vanderzee, C. E., 1978, Thermodynamics of carbon dioxide and carbonic acid: (a) the standard enthalpies of solution of $Na_2CO_3(s)$, $NaHCO_3(s)$, and $CO_2(g)$ in water at 298.15 K; (b) the standard enthalpies of formation, standard Gibbs energies of formation, and standard entropies of $CO_2(aq)$, $HCO_3^-(aq)$, $CO_3^{2-}(aq)$, $NaHCO_3(s)$, $Na_2CO_3(s)$, $Na_2CO_3 \cdot H_2O(s)$, and $Na_2CO_3 \cdot 10H_2O(s)$: Jour. Chem. Thermodynamics, v. 10, p. 1113–1136.

Booth, F., 1951, The dielectirc constant of water and the saturation effect: Jour. Chem. Physics, v. 19, p. 391–394.

Born, Von M., 1920, Volumen und Hydratationswärme der Ionen: Zeitschr. Physik, v. 1, p. 45–48.

Bradley, D. J., and Pitzer, K. S., 1979, Thermodynamics of electrolytes. 12. Dielectric properties of water and Debye-Hückel parameters to 350°C and 1 kbar: Jour. Phys. Chemistry, v. 83, p. 1599–1603.

Busenberg, E., Plummer, L. N., and Parker, V. B., 1984, The solubility of strontianite ($SrCO_3$) in CO_2-H_2O solutions between 2 and 91°C, the association constants of $SrHCO_3^+(aq)$ and $SrCO_3^\circ(aq)$ between 5 and 80°C, and an evaluation of the thermodynamic properties of $Sr^{2+}(aq)$ and $SrCO_3(cr)$ at 25°C and 1 atm total pressure: Geochim. et Cosmochim. Acta, v. 48, p. 2021–2035.

Chen. C.-T., Chen, J. H., and Millero, F. J., 1980, Densities of NaCl, $MgCl_2$, Na_2SO_4, and $MgSO_4$ aqueous solutions at 1 atm from 0 to 50°C and from 0.001 to 1.5 m: Jour. Chem. Eng. Data, v. 25, p. 307–310.

Chen, C.-T., Emmet, R. T., and Millero, F. J., 1977, The apparent molal volumes of aqueous solutions of NaCl, KCl, $MgCl_2$, Na_2SO_4 and $MgSO_4$ from 0 to 1000 bars at 0, 25, and 50°C: Jour. Chem. Eng. Data, v. 22, p. 201–207.

Clarke, E. C. W., and Glew, D. N., 1985, Evaluation of the thermodynamic functions for aqueous sodium chloride from equilibrium and calorimetric measurements below 154°C: Jour. Phys. Chem. Ref. Data, v. 14, p. 489–610.

Cobble, J. W., and Murray, R. C., Jr., 1980, High temperature behavior of chemical species which affect boiler performance, *in* Annual Report to the Electric Power Research Institute for the period January 1, 1979, to December 31, 1979: San Diego, Calif., San Diego State Univ. Found. p. 102.

————1981, High temperature behavior of chemical species which affect boiler performance, *in* Annual Report to the Electric Power Research Institute for the period January 1, 1980 to December 31, 1980: San Diego, Calif., San Diego State Univ. Found. p. 99.

CODATA, 1978, Recommended key values for thermodynamics, 1977. Report of the CODATA Task Group on key values for thermodynamics, 1977: Jour. Chem. Thermodynamics, v. 10, p. 903–906.

Cox, J. D., Harrop, D., and Head, A. J., 1979, The standard enthalpy of formation of ammonium nitrate and of the nitrate ion: Jour. Chem. Thermodynamics, v. 11, p. 811–814.

Criss, C. M., and Cobble, J. W., 1961, The thermodynamic properties of high temperature aqueous solutions. I. Standard partial molal heat capacities of sodium chloride and barium chloride from 0 to 100°: Am. Chem. Soc. Jour., v. 83, p. 3223–3228.

Desnoyers, J. E., de Visser, C., Perron, G., and Picker, P., 1976, Reexamination of the heat capacities obtained by flow microcalorimetry. Recommendation for the use of a chemical standard: Jour. Solution Chemistry, v. 5, p. 605–616.

Dunn, L. A., 1966, Apparent molar volumes of electrolytes. Pt. 1. Some 1-1, 1-2, 2-1, 3-1 electrolytes in aqueous solution at 25°C: Faraday Soc. Trans., v. 62, p. 2348–2354.

————1968, Apparent molar volumes of electrolytes. Pt. 3. Some 1-1 and 2-1 electrolytes in aqueous solution at 0, 5, 15, 35, 45, 55 and 65°C: Faraday Soc. Trans., v. 64, p. 2951–2961.

Eigen, M., and Wicke E., 1951, Ionenhydratation und spezifische wärme wässriger elektrolytlösungen: Zeitschr. Elektrochem., v. 55, p. 354–363.

Ellis, A. J., 1966, Partial molal volumes of alkali chlorides in aqueous solution to 200°C: Chem. Soc. [London] Jour. (A), p. 1579–1584.

————1967, Partial molal volumes of $MgCl_2$, $CaCl_2$, $SrCl_2$ and $BaCl_2$ in aqueous solution to 200°C: Chem. Soc. [London] Jour. (A), p. 660–664.

————1968, Partial molal volumes in high-temperature water. Part III. Halide and oxyanion salts: Chem. Soc [London] Jour. (A), p. 1138–1143.

Ellis, A. J., and McFadden, I. M., 1972, Partial molal volumes of ions in hydrothermal solutions: Geochim. et Cosmochim. Acta, v. 36, p. 413–426.

Enea, O., Singh, P. P., Woolley, E. M., McCurdy, K. G., and Hepler, L.G., 1977, Heat capacities of aqueous nitric acid, sodium nitrate, and potassium nitrate at 298:15: ΔC_p° of ionization of water: Jour. Chem. Thermodynamics, v. 9, p. 731–734.

Fortier, J.-L., Leduc, P.-A., and Desnoyers, J. E., 1974, Thermodynamic properties of alkali halides. II. Enthalpies of dilution and heat capacities in water at 25°C: Jour. Solution Chemistry, v. 3, p. 323–349.

Frank, H. S., 1955, Thermodynamics of a fluid substance in the electrostatic field: Jour. Chem. Physics, v. 23, p. 2023–2032.

Gardner, W. L., Jekel, E. C., and Cobble, J. W., 1969, The thermodynamic properties of high temperature aqueous solutions. IX. Standard partial molal heat capacities of sodium sulfate and sulfuric acid from 0 to 100°: Jour. Phys. Chemistry, v. 73, p. 2017–2020.

Gates, J. A., ms, 1985, Thermodynamics of aqueous electrolyte solutions at high temperatures and pressures: Ph.D. thesis, Univ. Delaware, Newark, Delaware, 340 p.

Gates, J. A., Wood, R. H., and Quint, J. R., 1982, Experimental evidence for the remarkable behavior of the partial molal heat capacity at infinite dilution of aqueous electrolytes at the critical point: Jour. Phys. Chemistry, v. 86, p. 4948–4951.

Gibson, R. E., 1934, The influence of concentration on the compression of aqueous solutions of certain sulfates and a note on the representation of the compressions of aqueous solutions as a function of pressure: Am. Chem. Soc. Jour., v. 56, p. 4–14.

————1938, On the effect of pressure on the solubility of solids in liquids: Am. Jour. Sci., 5th ser., v. 35A, p. 49–69.

Grant-Taylor, D. F., 1981, Partial molal volumes of sodium chloride solutions at 200 bar, and temperatures from 175 to 350°C: Jour. Solution Chemistry, v. 10, p. 621–630.

Haar, L., Gallagher, J., and Kell, G., 1980, Thermodynamic properties of fluid water, *in* Straub, J., and Scheffler, K., eds., Proceedings of the 9th international conference on the properties of steam, Munich, 1979: Oxford, Pergamon, p. 69–82.

Helgeson, H. C., 1982, Prediction of the thermodynamic properties of electrolytes at high pressures and temperatures, *in* Rickard, D. T., and Wickman, F. E., eds., Chemistry and geochemistry of solutions at high temperatures and pressures: Oxford, Pergamon, p. 133–177.

Helgeson, H. C., and Kirkham, D. H., 1974, Theoretical prediction of the thermodynamic behavior of aqueous electrolytes at high pressures and temperatures: I. Summary of the thermodynamic/electrostatic properties of the solvent: Am. Jour. Sci., v. 274, p. 1089–1198.

———— 1976. Theoretical prediction of the thermodynamic behavior of aqueous electrolytes at high pressures and temperatures: III. Equation of state for aqueous species at infinite dilution: Am. Jour. Sci., v. 276, p. 97–240.

Helgeson, H. C., Kirkham, D. H., and Flowers, G. C., 1981, Theoretical prediction of the thermodynamic behavior of aqueous electrolytes at high pressures and temperatures: IV. Calculation of activity coefficients, osmotic coefficients, and apparenrt molal and standard and relative partial molal properties to 600°C and 5 kb: Am. Jour. Sci., v. 281, p. 1249–1516.

Hilbert, R., ms. 1979, pVT-Daten von Wasser und von wässrigen Natriumchlorid-Lösungen bis 873 K. 4000 Bar und 25 Gewichtsprozent NaCl: Ph. D. thesis, Univ. Karlsruhe, Karlsruhe, West Germany, 212 p.

Isono, T., 1980. Measurements of density, viscosity and electrolytic conductivity of concentrated aqueous electrolyte solutions. 1. LiCl, NaCl, KCl, RbCl, CsCl, $MgSO_4$, $ZnSO_4$ and $NiSO_4$: Rikagaku Kenkyusho Hokoku, v. 56, p. 103–114.

Kearns, E. R., ms. 1966, Compressibilities of some dilute aqueous solutions: Ph.D. thesis, Yale Univ., New Haven, Conn., 122 p.

Likke, S., and Bromley, L. A., 1973, Heat capacities of aqueous NaCl, KCl, $MgCl_2$ $MgSO_4$, and Na_2SO_4 solutions between 80° and 200°C: Jour. Chem. Eng. Data, v. 18, p. 189–195.

Linov, E. D., Kryukov, P. A., 1972, The ionization of water at pressures between 1 and 8000 kg/cm^2 and at temperatures 18, 25, 50 and 75°C: Akad. Nauk SSSR Izv. Sib. Otd., Ser. Khim. Nauk, no. 4, v. 10, p. 10–13.

Lo Surdo, A., Alzola, E. M., and Millero, F. J., 1982, The (p, V, T) properties of concentrated aqueous electrolytes. I. Densities and apparent molar volumes of NaCl, Na_2SO_4, $MgCl_2$, and $MgSO_4$ solutions from 0.1 mol kg^{-1} to saturation and from 273.15 to 323.15 K: Jour. Chem. Thermodynamics: v. 14, p. 649–662.

L'vov, S. N., Zarembo, V. I., and Gilyarov, V. N., 1981, High-precision study of volume properties of water solutions of sodium chloride under high parameters: Geokhimiya, v. 4, p. 505–516.

Millero, F. J., 1972, The partial molal volume of electrolytes in aqueous solutions, *in* Horne, R. A., ed., Water and aqueous solutions: New York, John Wiley & Sons, p. 519–564.

———— 1982, The effect of pressure on the solubility of minerals in water and seawater: Geochim. et Cosmochim. Acta. v. 46, p. 11–22.

Millero, F. J., and Drost-Hansen, W., 1968, Apparent molal volumes of aqueous monovalent salt solutions at various temperatures: Jour. Chem. Eng. Data, v. 13, p. 330–333.

Millero, F. J., Hoff, E. V., and Kahn, L., 1972, The effect of pressure on the ionization of water at various temperatures from molal-volume data: Jour. Solution Chemistry, v. 1, p. 309–327.

Millero, F. J., and Knox, J. H., 1973, Apparent molal volumes of aqueous NaF, Na_2SO_4 KCl, K_2SO_4, $MgCl_2$, and $MgSO_4$ solutions at 0 and 50°C: Jour. Chem. Eng. Data, v. 18, p. 407–411.

Millero, F. J., Ricco, J., and Schreiber, D. R., 1982, PVT properties of concentrated aqueous electrolytes. II. Compressibilities and apparent molar compressibilities of aqueous NaCl, Na_2SO_4, $MgCl_2$, and $MgSO_4$ from 0 to 50°C: Jour. Solution Chemistry, v. 11, p. 671–686.

Millero, F. J., Ward, G. K., Lepple, F. K., and Hoff, E. V., 1974, Isothermal compressibility of aqueous sodium chloride, magnesium chloride, sodium sulfate, and magnesium sulfate solutions from 0 to 45°C at 1 atm: Jour. Phys. Chemistry, v. 78, p. 1636–1643.

Mitchell, R. E., and Cobble, J. W., 1964, The thermodynamic properties of high temperature aqueous solutions. VII. The standard partial molar heat capacities of cesium iodide from 0 to 100°: Am. Chem. Soc. Jour., v. 86, p. 5401–5403.

Morss, L. R., and Williams, C. W., 1983, Enthalpies of formation of strontium dichloride and of the strontium ion (Sr^+) in water and in 1 mol · dm^{-3} HCl, and an assessment of enthalpies of formation of alkaline-earth dichlorides: Jour. Chem. Thermodynamics, v. 15, p. 279–285.

Ohling, W., and Schneider, G. M., 1979, Densities and isothermal compressibilities of aqueous solutions of lithium chloride and cesium bromide at 293.15 K up to 200 MPa: Jour. Chem. Thermodynamics, v. 11, p. 1203–1204.

Owen, B. B., and Kronick, P. L., 1961, Standard partial molal compressibilities by ultrasonics. II. Sodium and potassium chlorides and bromides from 0 to 30°C: Jour. Phys. Chemistry, v. 65, p. 84–87.

Pauling, L., 1927, The sizes of ions and the structure of ionic crystals: Am. Chem. Soc. Jour., v. 49, p. 765–790.

Perron, G., Desnoyers, J. E., and Millero, F. J., 1974, Apparent molal volumes and heat capacities of alkaline earth chlorides in water at 25°C: Canadian Jour. Chemistry, v. 52, p. 3738–3741.

———— 1975, Apparent molal volumes and heat capacities of some sulfates and carbonates in water at 25°C: Canadian Jour. Chemistry, v. 53, p. 1134–1138.

Perron, G., Fortier, J.-L., and Desnoyers, J. E., 1975, The apparent molar heat capacities and volumes of aqueous NaCl from 0.01 to 3 mol kg^{-1} in the temperature range 274.65 to 318.15 K: Jour. Chem. Thermodynamics, v. 7, p. 1177–1184.

Pitzer, K. S., 1983, Dielectric constant of water at very high temperature and pressure: Natl. Acad. Sci. Proc., v. 80, p. 4575–4576.

Pitzer, K. S., Peiper, J. C., and Busey, R. H., 1984, Thermodynamic properties of aqueous sodium chloride solutions: Jour. Phys. Chem. Ref. Data, v. 13, p. 1–102.

Puchkov, L. V., Styazhkin, P. S., and Fedorov, M. K., 1976, Specific heat capacities of aqueous NaCl solutions at temperatures up to 350°C and pressures up to 1000 kg/cm^2: Jour. Appl. Chemistry USSR, v. 49, p. 1268–1271.

Rogers, P. S. Z., and Pitzer, K. S., 1982, Volumetric properties of aqueous sodium chloride solutions: Jour. Phys. Chem. Ref. Data, v. 11, p. 15–81.

Roux, A. H., Perron, G., and Desnoyers, J. E., 1984, Capacités calorifiques, volumes, expansibilités et compressibilités des solutions aqueuses concentrées de LiOH, NaOH et KOH: Canadian Jour. Chemistry, v. 62, p. 878–885.

Rüterjans, H., Schreiner, F., Sage, U., and Ackermann, Th., 1969, Apparent molal heat capacities of aqueous solutions of alkali halides and alkylammonium salts: Jour. Phys. Chemistry, v. 73, p. 986–994.

Shin, C., and Criss, C. M., 1979, Standard enthalpies of formation of anhydrous and aqueous magnesium chloride at 298.15 K: Jour. Chem. Thermodynamics, v. 11, p. 663–666.

Smith-Magowan, D., and Wood, R. H., 1981, Heat capacity of aqueous sodium chloride from 320 to 600 K measured with a new flow calorimeter: Jour. Chem. Thermodynamics, v. 13, p. 1047–1073.

Sweeton, F. H., Mesmer, R. E., and Baes, C. F., Jr., 1974, Acidity measurements at elevated temperatures. VII. Dissociation of water: Jour. Solution Chemistry, v. 3, p. 191–214.

Tammann, G., 1895, Über die volumen Veranderungen bei Neutralisation verdunnter Lösungen: Zeitschr. Phys. Chemie, v. 16, p. 91–96.

Tanner, J. E., and Lamb, F. W., 1978, Specific heats of aqueous solutions of NaCl, NaBr, and KCl: Comparisons with related thermal properties: Jour. Solution Chemistry, v. 7, p. 303–316.

Tremaine, P. R., Sway, K., and Barbero, J. A., 1986, The apparent molar heat capacity of aqueous hydrochloric acid from 10 to 140°C: Jour. Solution Chemistry, v. 15, p. 1–22.

Vaslow, F., 1966, The apparent molal volumes of the alkali metal chlorides in aqueous solution and evidence for salt-induced structure transitions: Jour. Phys. Chemistry, v. 70, p. 2286–2294.

———— 1969, The apparent molal volumes of the lithium and sodium halides. Critical-type transitions in aqueous solution: Jour. Phys. Chemistry, v. 73, p. 3745–3750.

Wagman, D. D., Evans, W. H. Parker, V. B., Schumm, R. H., Halow, I., Bailey, S. M., Churney, K. L., and Nuttall, R. L., 1982, The NBS tables of chemical thermodynamic properties: selected values for inorganic and C_1 and C_2 organic substances in SI units: Jour. Phys. Chem. Ref. Data, v. 11 (Supp. 2), p. 1–392.

Wheeler, J. C., 1972, Behavior of a solute near the critical point of an almost pure solvent: Ber. Bunsen-Gesell. Phys. Chemistry, v. 76, p. 308–318.

Wood, R. H., Smith-Magowan, D., Pitzer, K. S., and Rogers, P. S. Z., 1983, Comparison of experimental values of $\bar{V}^\circ_2$, $\bar{C}^\circ_{P2}$, and $\bar{C}^\circ_{V2}$ for aqueous NaCl with predictions using the Born equation at temperatures from 300 to 573.15 K at 17.7 MPa: Jour. Phys. Chemistry, v. 87, p. 3297–3300.

Wood, R. H., Quint, J. R., and Groller, J.-P. E., 1981, Thermodynamics of a charged sphere in a compressible dielectric fluid. A modification of the Born equation to include the compressibility of the solvent: Jour. Phys. Chemistry, v. 85, p. 3944–3949.